# INVESTIGATION OF THE EFFECT OF HETEROATOM AND INTEGRATION OF BORON ON BENZODITHIOPHENE AND PYRAZINE CONTAINING CONJUGATED POLYMERS FOR PHOTOVOLTAIC APPLICATIONS

A THESIS SUBMITTED TO
THE GRADUATE SCHOOL OF NATURAL AND APPLIED SCIENCES
OF
MIDDLE EAST TECHNICAL UNIVERSITY

BY

YEŞİM ABACIOĞLU

IN PARTIAL FULFILLMENT OF THE REQUIREMENTS
FOR
THE DEGREE OF MASTER OF SCIENCE
IN
CHEMISTRY

JULY 2021

Approval of the thesis:

**INVESTIGATION OF THE EFFECT OF HETEROATOM AND INTEGRATION OF BORON ON BENZODITHIOPHENE AND PYRAZINE CONTAINING CONJUGATED POLYMERS FOR PHOTOVOLTAIC APPLICATIONS**

submitted by **YEŞİM ABACIOĞLU** in partial fulfillment of the requirements for the degree of **Master of Science** i**n Chemistry, Middle East Technical University** by,

Prof. Dr. Halil Kalıpçılar
Dean, Graduate School of **Natural and Applied Sciences** _____

Prof. Dr. Özdemir Doğan
Head of the Department, **Chemistry** _____

Prof. Dr. Ali Çırpan
Supervisor, **Chemistry, METU** _____

Dr. Sedat Sürdem
Co-Supervisor, **BOREN** _____

**Examining Committee Members:**

Prof. Dr. Levent Kamil Toppare
Chemistry, METU _____

Prof. Dr. Ali Çırpan
Chemistry, METU _____

Prof. Dr. Yasemin Arslan Udum
Technical Sciences Vocational School, Gazi University _____

Assoc. Prof. Dr. İrem Erel Göktepe
Chemistry, METU _____

Assist. Prof. Dr.Çağatay Dengiz
Chemistry, METU _____

Date: 12.07.2021

**I hereby declare that all information in this document has been obtained and presented in accordance with academic rules and ethical conduct. I also declare that, as required by these rules and conduct, I have fully cited and referenced all material and results that are not original to this work.**

Name Last name : Yeşim Abacıoğlu

Signature :

# ABSTRACT

## INVESTIGATION OF THE EFFECT OF HETEROATOM AND INTEGRATION OF BORON ON BENZODITHIOPHENE AND PYRAZINE CONTAINING CONJUGATED POLYMERS FOR PHOTOVOLTAIC APPLICATIONS

Abacıoğlu, Yeşim
Master of Science, Chemistry
Supervisor : Prof. Dr. Ali Çırpan
Co-Supervisor: Dr. Sedat Sürdem

July 2021, 93 pages

In the context of this thesis, two different subjects were investigated for photovoltaic applications of conjugated polymers; the effect of heteroatom and integration of boron. The element boron has received considerable attention in the research of alternative energy sources due to its superior properties, and incorporation of boron in conjugated systems is considered as an important strategy to achieve efficient photovoltaics. In this sense, benzodithiophene and pyrazine containing conjugated polymer was synthesized, and boron was embedded into the conjugated system using the post-polymerization borylation method which has been recently reported in the literature. Two polymers, non-borylated (**P1A**) and borylated (**P1B**) polymers were compared in terms of their electronic and optical properties for photovoltaic applications. Another concept, namely the effect of heteroatom, was investigated by altering one heteroatom on benzazole acceptor of benzodithiophene and pyrazine containing conjugated random polymers. Here, three different random polymers, benzotriazole-bearing **RP1**, benzothiadiazole-bearing **RP2**, and benzoselenadiazole-bearing **RP3**, were synthesized. For all polymers, electrochemical studies were carried out by cyclic voltammetry to calculate the HOMO and LUMO levels of the polymers, and UV-Vis Spectrophotometry analyzes were performed for optical

studies. As a result of these studies, electronic and optical properties of all polymers were investigated. In this work, photovoltaic application studies of the polymers were carried out by using Polymer:$PC_{71}BM$ blend as an active layer in the construction of the bulk heterojunction solar cells. Power conversion efficiencies and blend film morphologies were investigated. As a result, poor power conversion efficiency values of 0.30% and 0.06% were obtained for non-borylated and borylated polymers, respectively. Finally, for random polymers, the highest power conversion efficiencies were obtained as a result of several optimizations as follows: 1.68% for **RP1**, 1.15% for **RP2** and 2.14% for **RP3**.

Keywords: Organoboron compounds, Heteroatom effect, Benzodithiophene, Pyrazine, Organic photovoltaics

# ÖZ

## FOTOVOLTAİK UYGULAMALAR İÇİN BENZODİTİYOFEN VE PİRAZİN İÇEREN KONJÜGE POLİMERLERDE HETEROATOM VE BOR ENTEGRASYONU ETKİSİNİN İNCELENMESİ

Abacıoğlu, Yeşim
Yüksek Lisans, Kimya
Tez Yöneticisi: Prof. Dr. Ali Çırpan
Ortak Tez Yöneticisi: Dr. Sedat Sürdem

Temmuz 2021, 93 sayfa

Bu tez kapsamında, konjüge polimerlerin fotovoltaik uygulamaları için iki farklı konu araştırılmıştır; heteroatom ve bor entegrasyonu etkisi. Bor elementi, üstün özelliklerinden dolayı alternatif enerji kaynaklarına yönelik araştırmalarda büyük ilgi görmüştür ve bor elementinin konjuge sistemlere dahil edilmesi verimli fotovoltaikleri elde etmek için önemli bir strateji olarak görülmektedir. Bu kapsamda benzoditiyofen ve pirazin içeren konjuge bir polimer sentezlenmiş ve literatürde son zamanlarda rapor edilmiş olan post-polimerizasyon borilasyon yöntemi kullanılarak bor konjuge sisteme entegre edilmiştir. Bor içermeyen (**P1A**) ve bor içeren (**P1B**) iki polimer, fotovoltaik uygulamalar için elektronik ve optik özellikleri açısından karşılaştırılmıştır. Diğer bir kavram, yani heteroatom etkisi, bir heteroatomun benzoditiyofen ve pirazin içeren rastgele konjuge polimerlerin benzazol akseptörü üzerinde değiştirilmesiyle araştırılmıştır. Burada, benzotriazol içeren **RP1**, benzotiadiazol içeren **RP2** ve benzoselenadiazol içeren **RP3** olmak üzere üç farklı rastgele polimer sentezlenmiştir. Tüm polimerler için, polimerlerin HOMO ve LUMO seviyeleri döngüsel voltametri ile yapılan elektrokimyasal çalışmalar sonucunda hesaplanmış ve optik özellikleri incelemek için UV-Vis Spektrofotometri analizleri yapılmıştır. Yapılan bu çalışmalar sonucunda tüm polimerlerin elektronik

ve optik özellikleri araştırılmıştır. Bu tez çalışmasının amacı doğrultusunda, yığın heteroeklem güneş pillerinin yapımında aktif katman olarak polimer:$PC_{71}BM$ karışımı kullanılarak polimerlerin fotovoltaik uygulama çalışmaları yapılmıştır. Güç dönüşüm verimleri ve blend film morfolojileri araştırılmıştır. Sonuç olarak, bor içermeyen ve bor içeren polimerler için sırasıyla %0.30 eV ve %0.06 eV'lik zayıf güç dönüşüm verimi değerleri elde edilmiştir. Son olarak, rastgele polimerler için, çeşitli optimizasyonlar sonucunda en yüksek güç dönüşüm verimleri **RP1** için %1.68 eV, **RP2** için %1.15 eV ve **RP3** için %2.14 eV olmak üzere elde edilmiştir.

Anahtar Kelimeler: Organobor bileşikler, Heteroatom etkisi, Benzoditiyofen, Pirazin, Organik fotovoltaikler

To my beloved family…

## ACKNOWLEDGMENTS

I would like to express my deepest gratitude to my supervisor Prof. Dr. Ali Çırpan for his guidance, encouragements and insight throughout my research. In particular, I am sincerely grateful for being a member of his research group, and also for his efforts to create such a nice working environment and for all the opportunities.

I would like to thank National Boron Research Institute (BOREN) for the financial support during my graduate education and for the many opportunities.

I would like to thank my co-supervisor Dr. Sedat Sürdem for his support during my research on BOREN project, and for providing the resources of the institution available when needed.

I would like to thank Prof. Dr. Levent Toppare for his valuable guidance and comments on this thesis studies.

I want to express my sincere thanks to Assist Prof. Dr. Çağatay Dengiz for his great advice during my graduate studies. His timely suggestions with kindness and positive attitude motivated me at every stage of my research.

I also would like to thank Sultan Taşkaya Aslan for her guidance and help to complete my master's studies, and for imparting her knowledge and experiences.

I am extremely thankful to my dear friend and my lab mate Berrin Ayyıldız. During my master's studies and the completion of this dissertation, her kind help and co-operation along with her endless support even in the most stressful times were invaluable to me. I also want to thank her for all the things we went through and enjoy the memorable and precious times together.

I would like to thank Soner Öztürk for his efforts and help during my experimental stage performed at BOREN, and for his ideas for the realization of the project.

I also want to thank Ekin Tutmaz, Mert Can Erer and Eda Alemdar Yılmaz for photovoltaic device applications and morphological analyzes of polymers.

I am deeply indebted to these lovely people; Ali Sait Güllü, Meriç Çalışkan, Gülten Özkul Atlı and Merve Yıldırım, for their precious friendship and for all the good memories.

I am so grateful to my family, my mother, my father, my lovely grandmother, my dear aunt who raised me to become the person I am today. I am so proud to have such a perfect family who always supports me and believes in me and is always there for me whenever and wherever I need them. I cannot describe how much all those great efforts and sacrifices they made for my success mean to me. And today, I am so thankful that they are by my side, and for knowing that they will always be. I also would like to thank my grandfather who passed away during this journey, and want him to know, what I always wish him to hear, that all the things I have accomplished in my life wouldn't come true without him and I owe everything I have to him.

I would like to take this opportunity to thank Selin Taş, my sister and my true friend, who has always been there for me throughout the years. Despite the distances between us, I am so glad that this friendship worked in every possible way and we still managed to grow together. Words are not enough how much she and her endless support mean to me.

I want to thank Ogün Tarakci from the bottom of my heart, for every single thing and for constant encouragement throughout my research period. Throughout this adventure, and the ones before, I feel so lucky to have such an amazing partner in my life.

Thanks are also extended to Dilan Ece Dikbıyık, Selin Gülmez, Oğuzhan Karakurt and every other member of Çırpan and Toppare Research Group, who directly or indirectly helped throughout the finalization of this dissertation and for the pleasant working environment.

This work is partially funded by National Boron Research Institute (BOREN) under grant 2019-31-07-25-001.

## TABLE OF CONTENTS

## LIST OF TABLES

TABLES

## LIST OF FIGURES

FIGURES

## LIST OF ABBREVIATIONS

ABBREVIATIONS

| | |
|---|---|
| PV | Photovoltaic |
| OPV | Organic Photovoltaic |
| OLED | Organic Light-Emitting Diode |
| OFET | Organic Field-Effect Transistor |
| BHJ | Bulk Heterojunction |
| ITO | Indium Tin Oxide |
| HTL | Hole Transport Layer |
| ETL | Electron Transport Layer |
| PEDOT | Polyethylenedioxythiophene |
| PSS | Polystyrene Sulfonate |
| $PC_{71}BM$ | Phenyl-$C_{71}$-butyric acid methyl ester |
| WF | Work Function |
| CP | Conjugated Polymer |
| HOMO | Highest Occupied Molecular Orbital |
| LUMO | Lowest Unoccupied Molecular Orbital |
| J | Current Density |
| V | Voltage |
| $J_{SC}$ | Short Circuit Current Density |
| $V_{OC}$ | Open Circuit Voltage |

| | |
|---|---|
| $P_{max}$ | Maximum Power |
| $P_{in}$ | Incident Power |
| FF | Fill Factor |
| AM | Air Mass |
| PCE | Power Conversion Efficiency |
| EQE | External Quantum Efficiency |
| IPCE | Incident Photon-to-Current Efficiency |
| PAc | Polyacetylene |
| UV | Ultraviolet |
| Vis | Visible |
| IR | Infrared |
| NIR | Near-Infrared |
| D | Donor |
| A | Acceptor |
| CT | Charge Transfer |
| ICT | Intermolecular Charge Transfer |
| ECL | Effective Conjugation Length |
| BDT | Benzodithiophene |
| Py | Pyrazine |
| BT | Benzothiadiazole |
| BTz | Benzotriazole |
| BSe | Benzoselenadiazole |

| | |
|---|---|
| $E_g$ | Band-gap |
| $E_g^{op}$ | Optical Band-gap |
| $E_g^{el}$ | Electronic Band-gap |
| CV | Cyclic Voltammetry |
| $TBAPF_6$ | Tetrabutylammonium Hexafluorophosphate |
| ACN | Acetonitrile |
| CE | Counter Electrode |
| RE | Reference Electrode |
| WE | Working Electrode |
| NBS | *N*-Bromosuccinimide |
| DCM | Dichloromethane |
| DMF | Dimethylformamide |
| THF | Tetrahydrofuran |
| NMR | Nuclear Magnetic Resonance |
| $M_n$ | Number Average Molecular Weight |
| $M_w$ | Weight Average Molecular Weight |
| PDI | Polydispersity Index |
| GPC | Gel Permeation Chromatography |
| AFM | Atomic Force Microscopy |
| TEM | Transmission Electron Microscopy |
| TGA | Thermal Gravimetry Analysis |
| DSC | Differential Scanning Calorimetry |

| | |
|---|---|
| DPE | Diphenyl ether |
| DIO | Diiodooctane |

# CHAPTER 1

# INTRODUCTION

## 1.1 Solar Energy

Over the years, the relation between greenhouse gasses and global temperature has been known. As human population increased, these two terms remained stable for quite a long time. However, in recent years, this natural cycle has been disrupted by exceeding greenhouse gas level and increasing temperature. The reason for this change is the rapid increase in population over the last two centuries. Consequently, a significant increase in global temperature is followed by a rising level of $CO_2$ in the atmosphere.

Growing human population leads to higher energy consumption and dramatic increase in demand for electricity. Since the population is still growing fast, energy consumption is rising. Although the impacts are still under discussion, human energy consumption is driving climate change due to the use of fossil fuels as an energy source. In addition, it is known that there is an end date for the use of fossil fuels [1]. Therefore, to satisfy the growing energy demand, the need for cleaner energy resources, unlike fossil fuels, has become significantly important. Although there are many different types of renewable energy such as wind, tidal, wave, ocean, bio etc., solar energy is the best in terms of its potential. The amount of energy that can be extracted is much greater than others. In this sense, solar energy is considered as the primary available energy source due to enormous amount of solar resource on Earth's surface, along with its other advantages such as renewable, pollution-free and significantly less $CO_2$ production compared to fossil fuel resources [2].

## 1.2 Solar Cell Technology

Solar energy comes in as photons and should be converted into a form that is more useful. Solar cell is a device that receives sunlight and converts the sun's energy into electricity, and it is the most widespread solar conversion technology today. The sun will source an enormous amount of energy for at least the next ten billion years, and the proper use of this energy source depends significantly on the development of solar cell technology [2]. Therefore, understanding the fundamentals of this technology provides information needed to evaluate future photovoltaic (PV) technologies that might be developed or presented.

Photovoltaics rely on the pohotovoltaic effect, which was described by a French scientist Becquerel in 1839, as the generation of an electrical current as a function of incoming sunlight. This idea evolved over a long period of time to the first generation of solar cells in the form of inorganic silicon photovoltaics in the 1950s. The early versions of the solar cells, called first generation solar cells, were mainly crystalline silicon solar cells, which were highly expensive. In addition, there were other drawbacks, such as high material consumption and high-embodied energy. Therefore, a different class of solar cells was developed as second generation solar cells, also known as thin-film solar cells. In this case, thin film was used instead of a bulk material. Amorphous silicon solar cells were the first example of this class of PVs that can be developed at lower temperatures than crystalline solar cells. Although this new generation of solar cells solved the problems of high-embodied energy, high temperatures and high materials usage, they were unstable [2],[3].

Over time, various thin-film technologies such as cadmium telluride (CdTe), copper indium galium selenide (CIGS) and many others emerged, but all of them had a stability problems. In addition to instability, another drawback can be addressed to the toxicity of some materials that have been used in thin-film solar cells [4]. As a result, the disadvantages led to the development of another generation of solar cells, namely the third generation, which provides much lower costs, much thinner films, and much lower temperatures. In addition, there are so many alternatives in these

emerging photovoltaics in terms of infinite variations in materials, material composition, synthesis, architecture, layer stacking, etc., and consequently this new generation of solar cells offers remarkable potential [5].

In the course of the development of photovoltaics, inorganic-based ones seem to have taken the lead in photovoltaic technology in terms of high efficiency. In recent years, however, promising alternatives have gained interest. Unlike traditional semiconductors, organic materials have attracted great interest in solar cell technology due to their numerous advantages. Although inorganic analogs are efficient technologies, they employ scarce and expensive materials or energy-intensive materials such as silicon, which entails the need for purification. Some materials, such as CdTe, are toxic and it is dangerous to allow these materials into nature due to ecotoxicity and environmental impact. Eventually, inorganic-based photovoltaics have production limitations for many reasons, such as material toxicity, high installation costs due to the weight of the cells, non-flexibility, and high production costs [3].

Organic photovoltaics are a strong alternative to inorganic counterparts as they offer several advantages such as low-cost synthesis due to more abundant materials, favorable electronic properties, low production and installation costs due to their light weight, solution processability, and flexibility. Most importantly, they do not contain toxic materials. This allows the production of solar cells with a very low environmental impact [6]. Considering all these advantages, significant research has been conducted to overcome many of the problems encountered in solar conversion technologies, such as processability, stability and efficiency, especially for organic-based ones. Many enhancements have been made on these issues to achieve more efficient and compatible technologies that are advantageous in every way [7]. As can be seen in Figure 1.1., there is an increasing trend in the efficiency of these devices [8]. Recently, the power conversion efficiency of organic solar cells has reached 18.2 % which is a significant advancement. With this large and constantly developing industry of solar energy, outstanding organic-based solar cell technologies with higher efficiencies will emerge eventually.

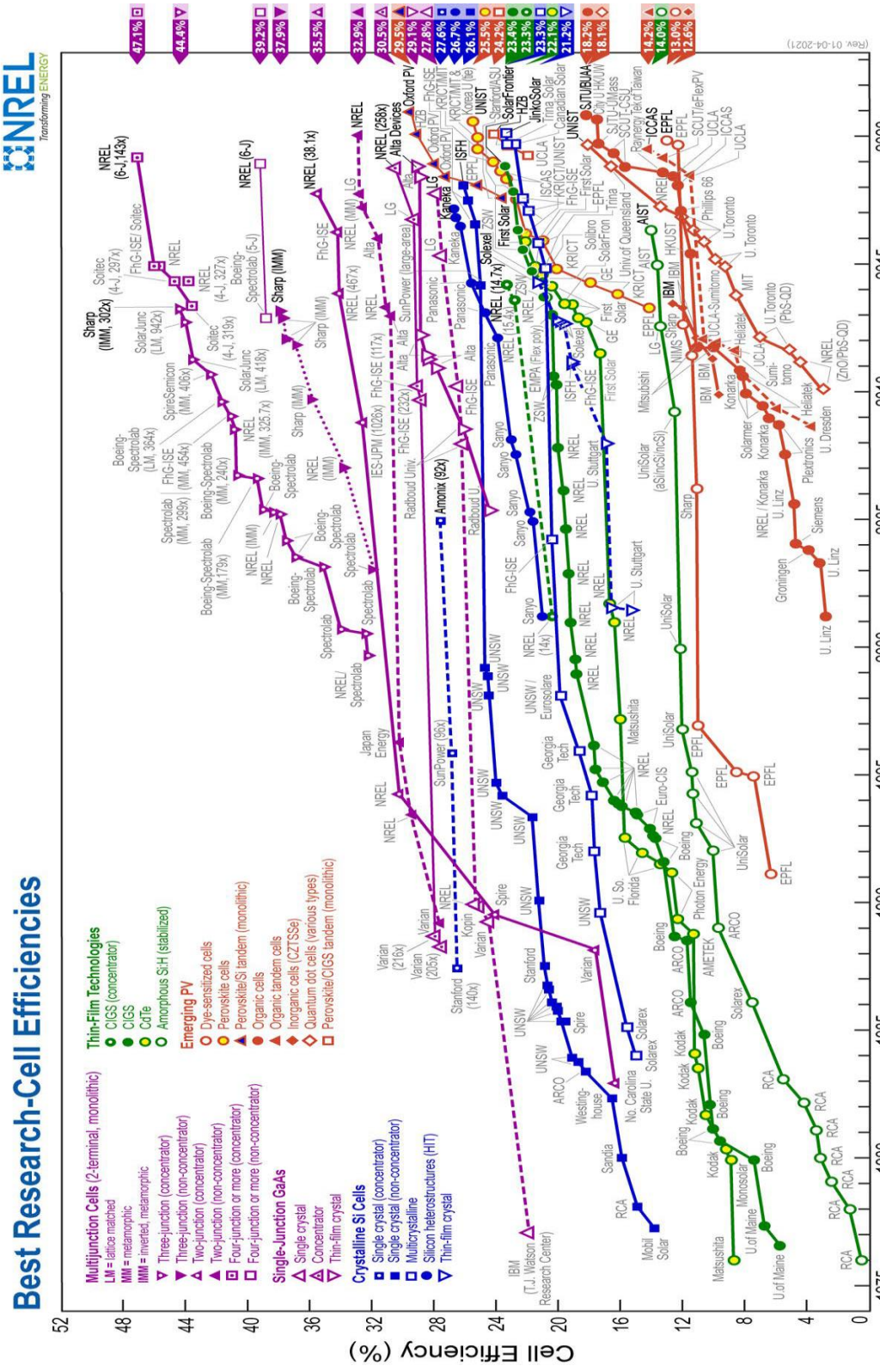


**Figure 1.1.** Solar cell efficiencies

## 1.3 Organic Photovoltaics

Organic solar cells, also called organic photovoltaics (OPVs), are a type of emerging photovoltaics that use organic materials mainly based on π-conjugated polymers and small molecules, and are of increasing interest in solar cell technology. As described in the previous section, organic photovoltaics offer several advantages which can be listed as follows:

1. The flexibility and light weight of the modules
2. Translucency
3. Easy integration into many products
4. The availability of new opportunities in the market
5. Low manufacturing cost compared to other conventional technologies
6. Short energy payback time
7. Low carbon footprint

All of these advantages listed above indicate that OPV technology is a disruptive technology that has a great potential within the solar cell industry [9]. In addition to the general information already mentioned, this section presents the device architecture and working principles of organic photovoltaics, characterizations, and important solar cell parameters that affect device performance are presented under the corresponding subtitles.

### 1.3.1 Bulk Heterojunction Device Architecture

So far, various arrangements of device architectures have been used in OPVs. The goal of these modifications was to achieve improved efficiency and stability of these devices. Some of these modifications were made to the active layer of the construction, which is the layer composed of donor and acceptor materials, and sandwiched between two electrodes. Early versions of OPV devices were built both in single layers, consisting of fine mixture of donor and acceptor molecules, and bilayer arrangements. Although these are very simple arrangements of donor and

acceptor materials, the resulting power conversion efficiencies are very low, mainly due to the short diffusion length of excitons, the electron-hole pair formed in the photoactive material, in organics [10]. Therefore, solar cells in the form of bulk-heterojunction architecture were generated to achieve better efficiencies.

Bulk heterojunction, invented by Yu et al., is the blend of donor and acceptor material with a bicontinual phase separation. This concept is the most efficient way of forming the active layer because BHJ films provide phase separation in the order of the diffusion length of excitons. In the operation of the device, explained in more detail in the following section, the absorption of photons by the photoactive material results in the formation of excitons. The electron and hole pair excitons can travel and diffuse through the material, but the distance traveled before they collapse is approximately 10 to 20 nm in organic semiconductors. In this case, in order to achieve an optimal size structure, BHJ concept can be used as an effective way in which the donor and acceptor are intermixed on the nanometer scale [10],[11]. The structure of BHJ OPVs is shown in Figure 1.2.

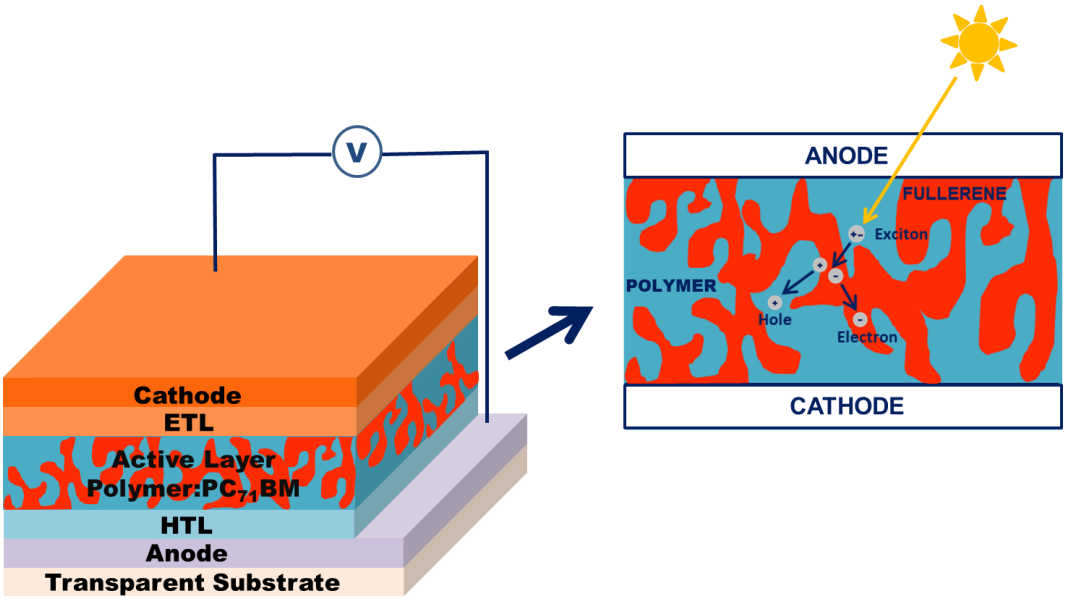


**Figure 1.2.** Device architecture of a BHJ OPV, containing blend of donor material polymer (blue) and acceptor material fullerene (red)

In the construction, the active layer is occupied at the center and surrounded by electron and hole transport layers. At the outermost, two electrodes, cathode and anode, are present. The active layer consists of a polymer as donor material and a fullerene ($C_{60}$) derivative as acceptor material, usually PCBM. In the form of bulk heterojunction, intermixing donor and acceptor materials in a solution is followed by spin coating of the mixed solution on a transparent substrate. Glass is usually preferred as a transparent substrate, and used by coating with a conductive and transparent electrode material. In general, due to its transparency and conductivity, indium tin oxide (ITO) is preferred. Since ITO enables hole collection, it is usually coated with a hole transport layer (HTL), mainly based on polyethylenedioxythiophene: polystyrene sulfonate (PEDOT:PSS). This hole transport layer facilitates charge separation and collection of holes at the anode electrode [9]. On top of the HTL, the active layer is coated with electron transport layer (ETL) and cathode electrode. Evaporated metal aluminum (Al) can be used as the cathode electrode in device fabrication by thermal evaporation process. Inorganic fluorides, such as lithium fluoride (LiF), are known to be promising materials for electron extraction and can be used as ETL to reduce the work function (WF) of the electrode for more efficient electron collection. Moreover, this interlayer between the electrode and organic active layer serves as a buffer layer to prevent cathode material Al from penetrating into the organic layer during the thermal evaporation process [12].

### 1.3.2 Working Principle of BHJ OPV Devices

The operating principle of BHJ OPV devices is simply based on four steps that are required for a cell to function properly. These steps can be introduced as follows:

1. Light absorption and exciton generation
2. Exciton diffusion
3. Charge separation
4. Charge collection

Operation of a solar cell is composed of successive events that begin with the absorption of photons in the active layer. As the donor material polymer absorbs light, excitons are generated, which are bound charges of electrons and holes. Subsequently, excitons diffuse through the phase boundary between the donor and acceptor, namely the donor-acceptor interphase. Here, the charge separation takes place and as a final step, the charges migrate through the two materials of the active layer to the electrodes [7].

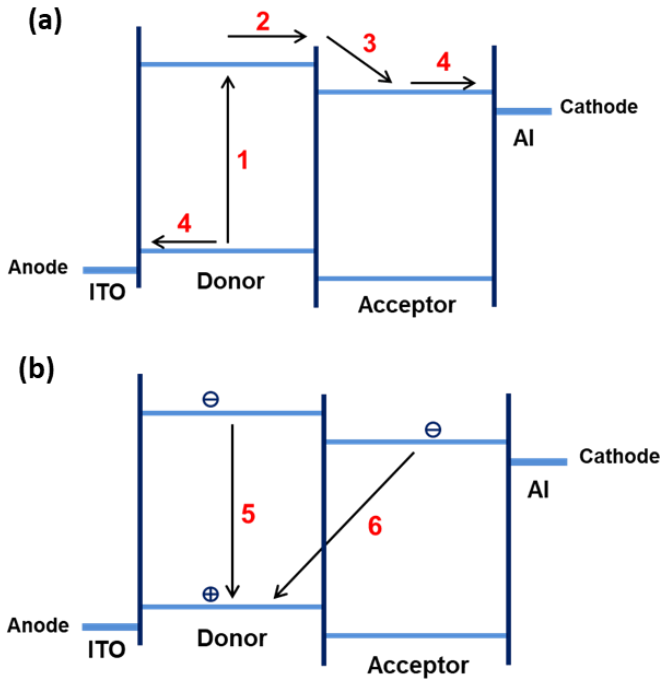


**Figure 1.3.** Schematic illustration of the working principle of BHJ OPVs on which corresponding numbers indicate (a) four stages of the operation of the cell, and (b) undesired processes in operating BHJ OPVs

A simple illustration of the operation of BHJ OPVs is shown in Figure 1.3., to better understand and visualize the mechanism. Here, consecutive events are indicated by numbers in the correct order of the operation stages. Thus, number 1 corresponds to the light absorption and exciton generation stage, followed by exciton transport to the interface between donor and acceptor material. Number 3 signifies the forward electron transfer, and 4 is the charge transport stage. As these stages take place in order, there are two undesired processes that might occur; recombination of the electrons and holes in the photoactive material, and back transfer of electrons from

the acceptor material to the donor material, polymer [9]. On the contrary of these undesired processes, to generate electricity, charge carriers must reach to the separate electrodes, which can be provided by introducing different electrode materials having distinct energy levels, and intermediate layers that facilitate the charge transportation towards the right directions [11].

### 1.3.3 Characterization of Organic Photovoltaics

The performance of a solar cell can be obtained by scanning an applied voltage across the cell and measuring the current response. The resulting data are used to plot a J-V curve, a current density vs. voltage graph, where the current is plotted against the voltage applied [13]. Figure 1.4. represents an illustration of a J-V curve, on which fundamental parameters of OPV; open circuit voltage ($V_{OC}$), short circuit current density ($J_{SC}$), maximum power ($P_{max}$), maximum voltage ($V_{max}$) and maximum current density ($J_{max}$) are shown. Next section includes a detailed explanation of these basic parameters and calculations by using these limits to extract other important characteristics of OPVs.

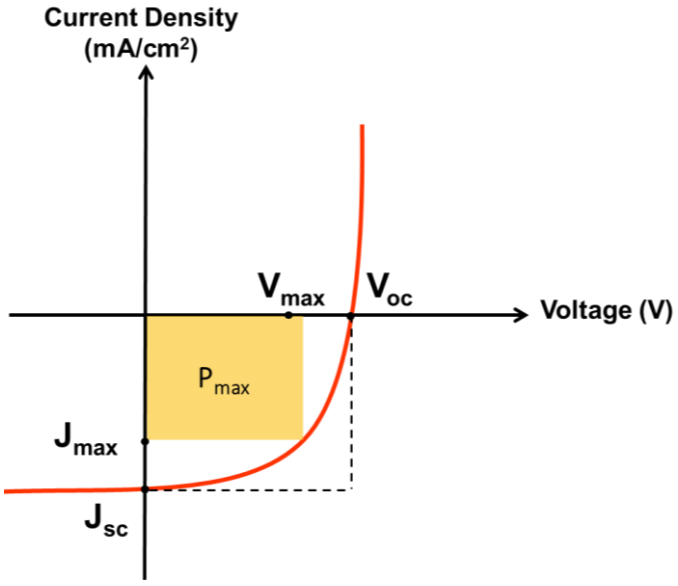


**Figure 1.4.** Schematic illustration of a J-V curve of a photovoltaic device

### 1.3.4 Parameters of Organic Photovoltaics

#### 1.3.4.1 Open Circuit Voltage

The open circuit voltage ($V_{OC}$) of a photovoltaic device is achieved when the current flowing through the system is zero. As shown on J-V curve, it is also defined as the maximum voltage a solar cell can supply. Numerous reports have shown that there is a direct relation between $V_{OC}$ value and the energy gap between HOMO and LUMO levels [14],[15]. Scharber proposed an equation by analyzing wide range of material combinations to express this relationship as below, where q is the elementary charge, and $E_{HOMO,D}$ and $E_{LUMO,A}$ values are HOMO and LUMO energy of donor and acceptor, respectively. Here the loss of $V_{OC}$ is found as 0.3 V, which is an empirical value, and this means that loss can be greater or smaller [15].

$$V_{OC} = \left(\frac{1}{q}\right)\left(\left|E_{HOMO,D}\right| - \left|E_{LUMO,A}\right| - 0.3\ V\right)$$

In OPVs, during the film preparation process, molecular interactions, crystallinity of polymers and fullerene based acceptors, and kink formations in polymer chains may introduce a disorder to the system. Blakesley found how disorder influences $V_{OC}$ value and other parameters. Accordingly, as the disorder increases, $V_{OC}$ decreases, and meanwhile, along with $V_{OC}$ value, $J_{SC}$ and FF also decrease. An important process that influences the $V_{OC}$ parameter is the recombination, which occurs before the charge collection at the corresponding electrodes. As electrons at the conduction band lose energy and stabilize back to a lower energy state in valance band, this induces recombination with the hole. This results in annihilation of carriers and cause energy loss, which eventually leads to carrier recombination $V_{OC}$ loss [16]. In addition, there are several factors affecting the $V_{OC}$, such as temperature, morphology, light intensity, electrode work function, charge transfer (CT) states, D-A interface area etc. Considering all those direct and indirect effects, it is important to develop methods to prevent the losses or to enhance $V_{OC}$, which plays a predominant role to determine the PCE [14],[15].

#### 1.3.4.2 Short Circuit Current Density

Short circuit current density ($J_{SC}$), of the solar cell is defined as the maximum current density when the external voltage equals to zero. This parameter depends on several factors, such as absorption of active layer, transportation of charge carriers through the material, band gap, and quantum efficiency for the charge separation. However, it is observed in the presence of optical losses because photons from a part of the spectrum could not be absorbed, or the absorption could not result in exciton generation [17],[11]. In addition, not all the charges generated through the absorption of photons can contribute to $J_{SC}$ due to recombination process [17].

In general, since it depends on the amount of photons absorbed, the broad absorption spectrum is favorable to harvest a large fraction of photons from the wide range of solar spectrum [11]. It is known that in combination of fullerene based acceptors, the photoactive material is the donor polymer. Thus, light absorption properties of CPs effects $J_{SC}$ value.

#### 1.3.4.3 Fill Factor

An important parameter that can be extracted from the J-V curve is the fill factor (FF), which provides information about the form of the curve. Fill factor can be simply defined as the ratio between two areas, corresponding to the maximum power generated and the theoretical maximum power that can be obtained from the cell, which is the product of open circuit voltage and short circuit current density [13]. Since the maximum power produced by the solar cell is the product of maximum power voltage and maximum power current density, the fill factor can be expressed by the following formula.

$$\mathrm{FF}\ (\%) = \frac{V_{Pmax} \times J_{Pmax}}{V_{OC} \times J_{SC}} \times 100$$

To ensure high power conversion efficiencies, the value of FF should be as high as possible, which is also close to the ideal. However, it can never be equal to the ideal

unit value, because the maximum power generated from the solar cell is always less than the theoretical one [18].

#### 1.3.4.4 Power Conversion Efficiency

The primary parameter of a solar cell is the power conversion efficiency (PCE), which indicates the overall performance of a device. It can be extracted from the J-V curve under the simulated AM1.5G illumination with 100 mW/cm$^2$ incident light intensity [19]. PCE can be calculated by the following equation, where product of $V_{OC}$, $J_{SC}$ and FF is the maximum power generated in the external circuit, and $P_{in}$ is the incoming light power.

$$\mathrm{PCE}(\%) = \frac{V_{OC} \times J_{SC} \times FF}{P_{in}} \times 100$$

#### 1.3.4.5 External Quantum Efficiency

External quantum efficiency (EQE) is the ratio between the number of collected charge carriers and number of incoming photons on the active layer of the device. This is also known as incident photon-to-current efficiency (IPCE). This parameter represents how efficiently the cell converts the incident light into electrical energy. When new material combinations are investigated, a common strategy is to optimize the architecture of the device through analysis of D-A blend ratio, thickness, and processing parameters, such as solvent systems, annealing, additive treatments etc. Therefore, EQE measurements can be used to determine an outcome for the device performance with respect to all these variables [20].

The measurement can be performed by illuminating with varying frequencies of light and recording the electrical current of the device (the number of charge carriers generated). As a result, EQE curve can be obtained as a function of wavelength, and the area under the curve corresponds to the total number of charge carriers generated by the device. Thus, integration of EQE vs. wavelength graph gives the electrical

current density. It should be mentioned that, the light absorbed by the active layer is always less than the incoming light because of losses due to the reflection of light [21]. In addition, EQE measurements are useful to investigate if there is any degradation of the device, which can be achieved a reduction in EQE over time. This indicates a deterioration of the photoconversion properties of the photoactive material. On the other hand, a change observed in the shape of a curve may stem from morphological alterations [20],[21].

## 1.4 Conjugated Polymers

Conjugated polymers (CPs) can be simply defined as polymers that contain alternating double and single bonds along the polymer chain, referred to as conjugated bonds. These polymers were used as insulators in electrical applications until the significant conductivity of polyacetylene (PAc) was discovered through a doping process. With this work, it was reported that conjugated materials can be electrically conductive under certain conditions [22]. Later, in 2000, this discovery was rewarded with a Nobel Prize jointly awarded to Alan J. Heeger, Alan G. MacDiarmid, and Hideki Shirakawa for being one of the most important discoveries to benefit mankind. Since this scientific breakthrough, conjugated polymers have become a highly interesting topic due to their tunable band gap, easy processability, high flexibility, and high electroactivity [23]. Thus, thanks to the research in this field, various conjugated polymers have been synthesized. Some of the common conjugated polymers are introduced in the following figure 1.5.

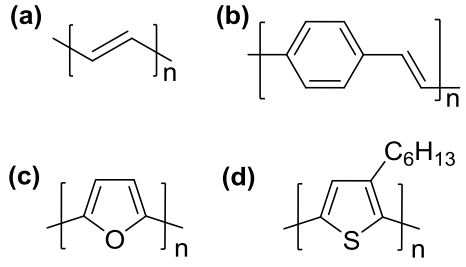


**Figure 1.5.** Structures of some common conjugated polymers; (a) polyacetylene, (b) poly(*p*-phenylenevinylene) (c) polyfuran, (d) poly(3-hexylthiophene)

Conductive polymers have paved the way for a novel field of research that is not only of theoretical importance but also has many important practical applications. As a result, three major branches have developed over time; theoretical science to understand the mechanism of electrical conductivity, polymer synthesis to produce new materials, and rapidly growing interest in many applications, especially in optoelectronics [24]. Conjugated polymers can be used in many devices, such as organic light-emitting diodes (OLEDs), organic field-effect transistors (OFETs), organic photovoltaics (OPVs), and electrochromic devices, which are important classes of future energy conversion technologies.

### 1.4.1 Polymer Synthesis

Polymers can be synthesized through polymerization reactions, which can be achieved by simply linking the monomers together to form a covalently bonded chain. Several types of polymerization reactions are present in the literature, and some of these methods, such as Stille cross-coupling, Suzuki cross-coupling, and direct arylation polymerization reactions, are known to be useful in the context of organic solar cells [25]. Stille cross-coupling method is one of the effective methods to obtain conjugated polymers. The mechanism and more detailed information about this method are explained in the following subtitle. Suzuki cross-coupling is another way to generate carbon-carbon bonds through palladium catalyst. Here, organoboron functionalized compounds, which are known to be less toxic than organostannane compounds, and organic halides are used as coupling partners. The mechanism proceed in four steps; oxidative addition, metathesis, transmetallation and reductive elimination. In this method, in addition to the analogous Stille, an additional base is required to act as an accelerator of the transmetallation step [26]. Recently, an alternative method to Suzuki and Stille has been applied to obtain donor-acceptor type conjugated polymers; direct arylation. It is an advantageous method because complicated steps in the preparation of monomers are eliminated since no stannylated or boronated reagents are required. In this case, the reaction between a

halogenated aromatic monomer and non-functionalized aromatic monomer takes place with the help of palladium catalyst [27].

#### 1.4.1.1 Stille Cross-Coupling Reaction

Stille cross-coupling reaction allows the generation of new carbon-carbon bonds by transmetallation of an organostannane compound with an organic halide in the presence of a palladium catalyst under mild conditions. Organostannane compounds are usually stable and insensitive to moisture or air, but they are also toxic substances [28]. The mechanism of Stille cross-coupling proceeds through four sequential steps; ligand dissociation, oxidative addition, transmetallation and reductive elimination. With the starting materials prepared for polymerization under the conditions of Stille cross-coupling, the coupling product continually enters the cycle leading to the formation of the polymer. In the course of the reaction, one major side reaction may occur, namely the oxidative homocoupling of the organostannane reagent [29].

### 1.4.2 Band-gap Engineering

The conductivity of the polymers are mainly depends on the presence of conjugation along the polymer chain. However, as mentioned earlier, before doping, these materials exhibited almost no conductivity. Their electrical conductivity can be significantly improved by doping. This can be accomplished either chemically when the polymer is exposed to a solution or a vapor of the dopant, or through electrochemical doping, which is possible by subjecting the polymer in a solution with an applied potential [30]. In this process, a removal of an electron from the valance band through oxidation is known as p-type doping, and an addition of an electron to the conduction band by reduction is known as n-type doping. As a result, band structure can be altered through either n-type or p-type doping, in other words, the energy level separation between the conduction band and valance band. As compared with other materials such as metals and insulators, conducting π-

conjugated polymers are in a class of semi-conductors which stand in between these two materials in terms of the band gap (Figure 1.6.).

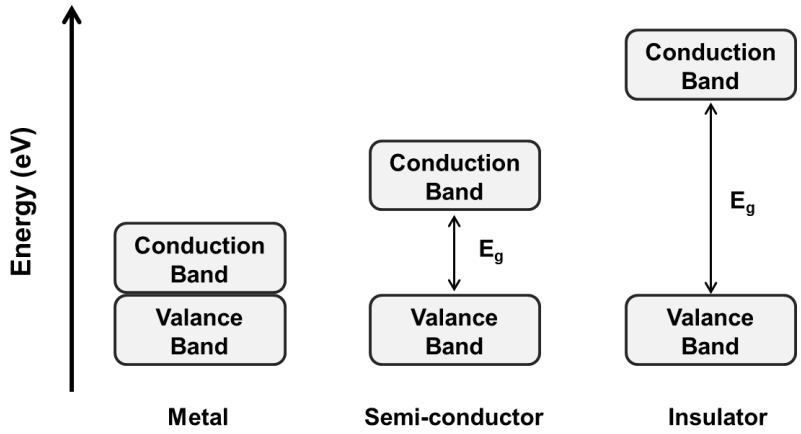


**Figure 1.6.** Representation of the energy gap ($E_g$) between HOMO and LUMO in a metal, a semi-conductor, and an insulator

The energy conversion process particularly requires the collection of the sunlight as much as possible. In this context, the amount of photons available is an important aspect due to the conversion of photons to electrons by photovoltaics. The solar spectrum covers a wide range, from UV to visible and to infrared (IR). However, the flux of photons as a function of wavelength indicates a decreasing trend towards the IR region of the spectrum. In this case, it is important to extend the absorption, to provide a better overlap with the solar spectrum [31]. Tunability of the band gap of CPs is of great importance to achieve low band gap polymers that enable maximum photon harvesting. Therefore, to cover all these broad range of solar spectrum, the use of semi-conductors with a low band gap is an effective way to achieve OPVs with high efficiencies. In addition, in excitonic devices, there are some limits to achieve a low band gap, leading to an optimum band gap. Two important characteristics a CP should have are low HOMO level to increase the $V_{OC}$ value and a LUMO level higher than fullerene based acceptor's LUMO for an efficient charge dissociation in BHJ OPV devices [31], [32]

There are several factors that affect the band gap of CPs, such as intramolecular charge transfer interactions, bond length alternation, aromaticity, effect of

substituents, length of π-conjugation, etc. The control of molecular energy level and band gap are important aspects related to the improvement of the photovoltaic properties of conjugated systems. To tailor these properties, there are promising strategies that are commonly used in the design of conjugated polymers. In the following subsections, two different approaches have been presented, namely the donor-acceptor approach and the atomistic approach.

#### 1.4.2.1 Donor-Acceptor Approach

One of the most important and commonly used strategies is the donor-acceptor (D-A) approach, which can be achieved by altering donor or acceptor units in the conjugated polymer. This concept is introduced for the first time by Wynberg and co-workers in 1992 [33]. The aim of D-A approach is to create a lower band gap through a molecular orbital hybridization, as can be seen in Figure 1.7., and also the intramolecular charge transfer interactions between the electron-rich donor and electron-deficient acceptor units [32]. The combination of high-lying HOMO levels of donor unit and low-lying LUMO levels of acceptor unit leads to a narrow band gap for a CP. Tailoring the band gap relies on the choice of donor and acceptor moieties, in other words, the electron density difference between these units along the backbone of the polymer. Thus, proper selection of these units is important to tune the band gap by achieving efficient intramolecular charge transfer interactions and high mobility [32],[34]. To illustrate, when a too strong acceptor unit presents in the CP, it may deteriorate the hole transport feature of the polymer or result in having a polymer with a remarkably low-lying LUMO.

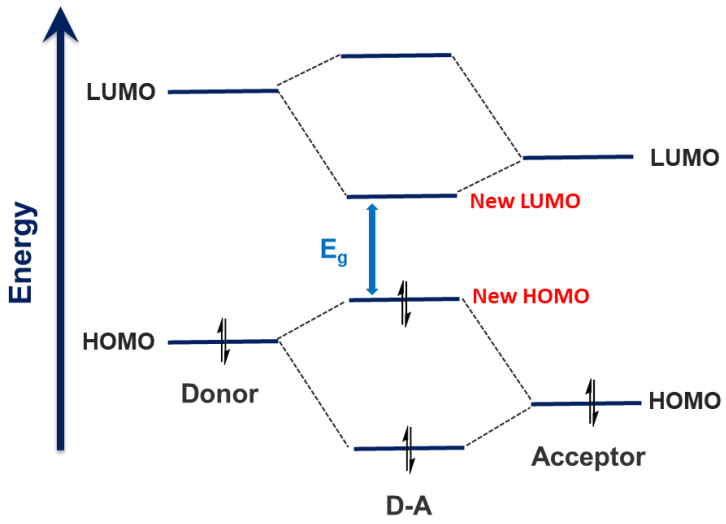


**Figure 1.7.** Molecular orbital hybridization for a D-A approach

In this approach, with the hybridized molecular orbitals through various combinations of D-A moieties, the energy levels may not be predicted simply based on HOMO and LUMO levels of the isolated monomers to be combined in the polymer. HOMO and LUMO energy levels significantly depend on the degree of electron delocalization within the effective conjugation length (ECL) of the polymer which is mainly affected by the conformation of the backbone. Hence, to be able to predict the magnitude of the energy gap, intrinsic properties of the monomers should be taken into account, such as structure, side chains, functional groups that effect the backbone conformation [32].

The D-A approach has been recently extended to design terpolymers with one donor and two acceptors (D-$A_1$)-(D-$A_2$) or two donors and one acceptor ($D_1$-A)-($D_2$-A) systems. The aim of these types of systems is to generate efficient OPVs due to large coverage of the solar spectrum and highly tunable band gap features of these materials based on the variation of the amount of each monomer unit [35].

#### 1.4.2.2 Atomistic Approach

In terms of D-A type CPs, the replacement of donor or acceptor moieties with stronger or weaker ones, as well as the change of the donor to acceptor ratio within

the scaffold have been studied in the recent years [36]. To better understand the structure-property relationship in D-A polymers for the development of high-performance materials, atomistic approach has been used as an effective strategy that can be achieved by altering the heteroatom in either donor or acceptor moieties of CPs. Recently, the role of heteroatom in controlling the electronic and optical properties along with the solid-state packing of CPs has been investigated [37]. It is well known that molecular orbitals are generated by mixing atomic orbitals. Therefore, altering a single atom on the donor or acceptor unit has a diverse effect on the electronic properties of this unit.

The recent studies of atomistic approach have been carried out to understand the basis of fundamental structure-property correlation in chalcogen derivatives [38], [39]. They have attracted a great attention to tailor the electronic and structural properties, since these characteristics have a direct impact on the solid-state packing as well as the charge transport features of the CPs. In this case, the heteroatom effect has been investigated by preparing CPs which contain mostly benzazole acceptors [36], [40].

## 1.5 Donor and Acceptor Moieties

### 1.5.1 Benzodithiophene Moiety

Benzodithiophene (BDT) molecule has been attracted a great interest as a common donor moiety in the conjugated polymers, due to its several advantages. BDT has a large, planar and symmetric conjugated structure that can form π-π stacking easily. Since this π-π stacking correlates with high charge carrier mobility, it is reasonable to expect good mobility for BDT-containing conjugated polymers [41]. Moreover, tunable solubility and electronic properties can be achieved by attaching different substituents, from the available positions of 4 and 8, to the BDT structure (Figure 1.8.).

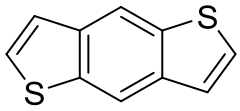


**Figure 1.8.** Structure of benzodithiophene unit

It is known that band gap of CPs can be affected by the steric hindrance between two adjacent units, and BDT has very low steric hindrance between its neighboring units. As a result, other advantageous properties of this electron-rich donor moiety, such as thermal stability, high absorption coefficient along with its previously mentioned features make BDT an ideal conjugated unit to create new photovoltaic materials [42].

### 1.5.2 Pyrazine Moiety

In the literature, incorporation of N-heterocycle acceptor moieties into CPs has been applied to achieve greater planarity, better crystallinity and low-lying energy levels of the frontier orbitals. So far, these types of conjugated systems have been reported only to a limited extent, and pyrazine (Py) core-based D-A type CPs have not been well explored. Moon et al. studied wide band gap conjugated polymers containing pyrazine units for the first time, and reported that introducing electron-deficient Py into the backbone of polymers is useful to improve planarity and optoelectronic properties of the conjugated systems [43].

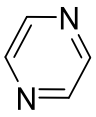


**Figure 1.9.** Structure of pyrazine unit

Among many heterocyclic compounds, Py is mostly used in conjugated systems as a π-linker or acceptor, due to its favorable charge transfer properties [44]. Therefore, the use of Py in π-conjugated systems where electron transport is necessary can be a convenient way to modify and improve their useful properties. In addition, Gong et al. reported that pyrazine-core promotes the luminescent properties, and since it is

very sensitive to acid and base, Py derivatives can serve as sensors. Besides its superior properties, another important aspect is the chelation of the nitrogen atom of Py. To utilize this moiety in conjugated structures, many derivatives of Py can be achieved by cross-coupling reactions leading to structural changes and extension of π-conjugation [43].

### 1.5.3 Benzazole Moieties

Benzazole acceptor moiteies have been widely incorporated into conjugated systems for solar cell applications due to their planar molecular structures and intrinsic properties. There are number of benzazole acceptors in the literature, which differ depending on the central heteroatom on the azole ring. In this study, benzotriazole, benzothiadiazole and benzoselenadiazole acceptor moieties were used, which are known to possess great electron-withdrawing properties (Figure 1.10.). Having a planar structure, these acceptor units provide an increase in close molecular packing and strong intermolecular interactions in the solid state, and promote enhanced charge carrier mobility.

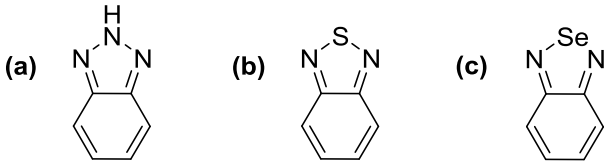


**Figure 1.10.** Structure of benzazole acceptor units; (a) benzotriazole (BTz), (b) benzothiadiazole (BT), (c) benzoselenadiazole (BSe)

When comparing electron withdrawing ability of benzazole acceptors, central atom and aromaticity of the azole ring are considerably important aspects [45]. Benzotriazole, having nitrogen (N) atom on the azole ring, is the least strong acceptor among these three benzazole units. However, it offers a tunable solubility for the conjugated polymers due to its availability for alkylation from the N position. Thus, when solubility and processability problems arise for the polymer, benzotriazole can be useful to fine-tune the solubility through the alkylation, which provides sufficient

solubility. Benzothiadiazole and benzoselenadiazole are much stronger acceptors as compared to benzotriazole counterpart of the benzazole acceptors. However, when they are compared, benzoselenadiazole is the strongest, even though sulfur and selenium have similar electronegativity [45],[46] Thus, it depends on some other factors. Due to incorporation of a larger and more polarizable Se atom, the aromaticity of the azole ring decreases and the quinoid structure can be adopted, and consequently, benzoselenadiazole becomes a relatively stronger electron acceptor than benzothiadiazole [47]. On the other hand, benzothiadiazole is one of the stable acceptor moiteies, and it can be synthesized easily.

## 1.6 Boron-Containing Conjugated Polymers

Boron-containing conjugated polymers or organoboron CPs are classified as emerging materials of great importance for the improvement of recently generated energy conversion applications. Due to the electron deficiency of boron (B), incorporation of B atoms into π-conjugated systems offers electron-accepting properties and provides unique optoelectronic behaviors along with improved performances in OLED and OPV devices [48]. In this part of the thesis, this strategy is explained in detail in the following subtitles and is supported with some examples from the literature.

### 1.6.1 Integration of Main Group Elements in Conjugated Polymers

Organic molecules containing large delocalized π-conjugated systems have been used for OPVs due to the bonding arrangement that allows easy charge transport through the organic material to enable more convenient and efficient device applications. In order to develop organic materials useful for these operations, Baumgartner et al. reported that incorporation of the main group elements into π-conjugated structures is an important strategy [49]. Moreover, Yamaguchi et al. claimed that it promotes desirable properties of these systems, such as suitable

HOMO and LUMO levels, low band gap, and high charge carrier mobility. Due to their remarkable features, incorporation of such elements B, Si, P, S and Se into the π-conjugated framework as bridging units, as shown in Figure 1.11., is an effective way to achieve unusual electronic structures and molecular arrangements [50].

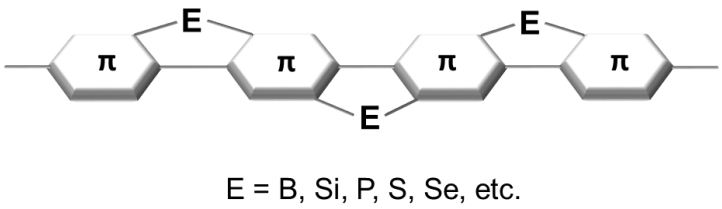


**Figure 1.11.** Schematic representation of the incorporation of main-group elements into π-conjugated framework

Among other main group elements, boron is an attractive alternative due to its unique properties stemming from the presence of vacant $p_z$ orbital. Boron contains three valence electrons occupying three $sp^2$ orbitals, resulting in the formation of three σ-bonds with three adjacent units. Because of its empty $p_z$ orbital, which is capable of participating in the π-conjugation of the aromatic system, electrons can be delocalized through the molecule by overlapping this empty $p_z$ orbital perpendicular to the aromatic plane (Figure 1.12.). This is considered a powerful strategy to successfully achieve more efficient applications of conjugated systems [51].

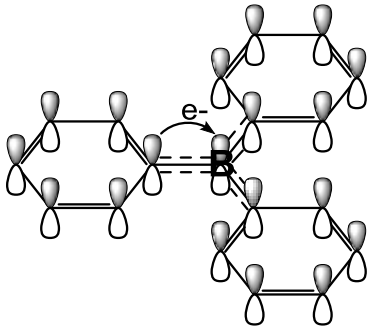


**Figure 1.12.** π-conjugation with boron

### 1.6.2 Organoboron Compounds

Organoboron compounds display new approaches like p-π* conjugation, B-N coordination bond etc. to modify the electronic structures of conjugated systems in the use of OPVs. Since these types of devices ideally need to make use of broad range of absorption spectrum, which organoboron compounds ensure, variety of organoboron compounds and their unique properties are needed to be explored [52]. Moreover, boron-bearing molecules provide rich donor-acceptor tunability, which is critical to generate OPVs with high efficiencies [48]. In terms of introducing boron into conjugated frameworks, organoboron polymers have been also investigated, and as a result, variety of functions were noted. Hence, in this context, tricoordinate and tetracoordinate complexes of boron, their characteristics, and the principle of B-N coordination bond are presented in this section.

Tricoordinated complexes of boron are generally unstable. The introduction of bulky functional groups substituted to the boron atom is required for this form, due to high reactivity of boron towards nucleophiles and water [53]. Thus, with this strategy, enhanced stability is generally observed. This is an important aspect since it is favorable to have compounds that are stable to moisture and air to better observe their electronic properties. According to the research on these compounds, Chujo and co-workers stated that tricoordinate boron generates an empty $p_z$ orbital involved in conjugation through the main chain of the polymer. Their combination with different monomers resulted in desired properties, such as strong fluorescence emission and significant bathochromic shifts in the absorption and emission spectra. The explanation for these behaviors can be attributed to the conjugative overlap of vacant $p_z$ orbital of the boron atom and π orbitals [54]. Some examples of tricoordinated boron-bearing conjugated organoboron compounds and polymers are shown in Figure 1.13..

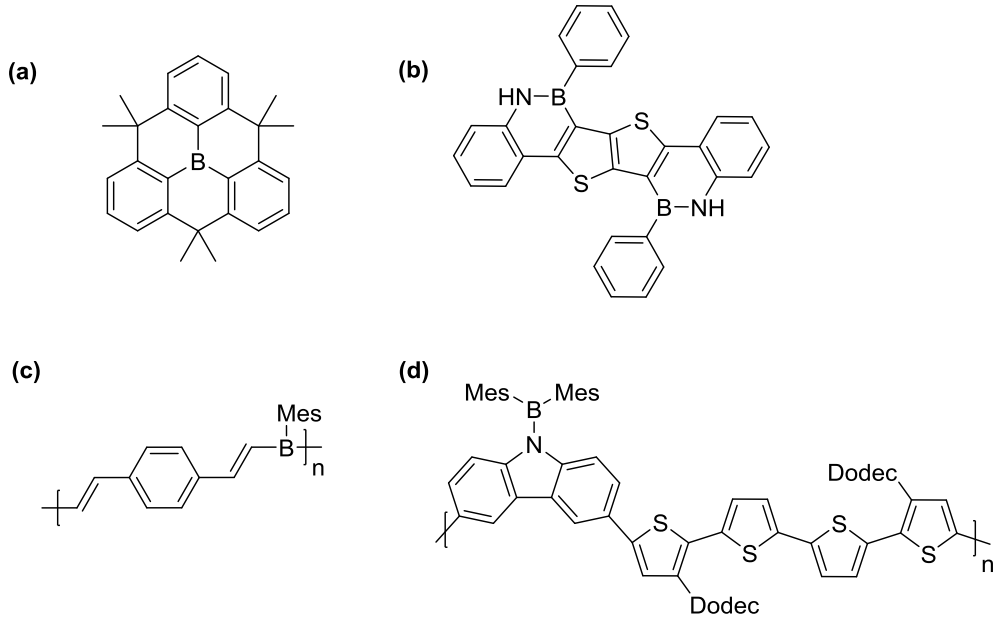


**Figure 1.13.** Some examples of tricoordinated boron-containing organoboron compounds, (a) and (b), and polymers, (c) and (d)

In addition to bathochromic shift, low-lying LUMO energy levels, and ease of reduction are observed electronic influences of tricoordinated boron. Moreover, they exhibit Lewis acid or electron-accepting properties and interact with electron-donating units, which is related to the electron deficiency of boron atom. However, substituted groups have an effect on this. To illustrate, by introducing fluoride anion into the tricoordinate boron, a decrease in electron deficiency was reported in the literature in another work by Chujo et al. [55]. This led to the restraint of donor-acceptor interactions containing tricoordinated boron. Hence, due to this tunability of optical properties, they can be used in sensor applications as well [54].

On the other hand, tetracoordinated boron exhibit great stability, and several organoboron polymers in which boron is in tetracoordinate state have been explored. Most of these structures display efficient features as luminescent materials and some were presented in the literature as efficient fluorescent dye [54],[56]. Many of the tetracoordinated compounds exhibit excellent fluorescence quantum efficiency along with tunable optoelectronic properties [53],[56]. The tetracoordinated design of organoboron compounds, of which some examples are given in Figure 1.14., are

more favorable due to its high stability. Same is valid for the tetracoordinated organoboron polymers, and the reason can be addressed to the chelate effect due to incorporation of boron into the ring system, the main chain, and electronic saturation due to Lewis acid-base interaction [56].

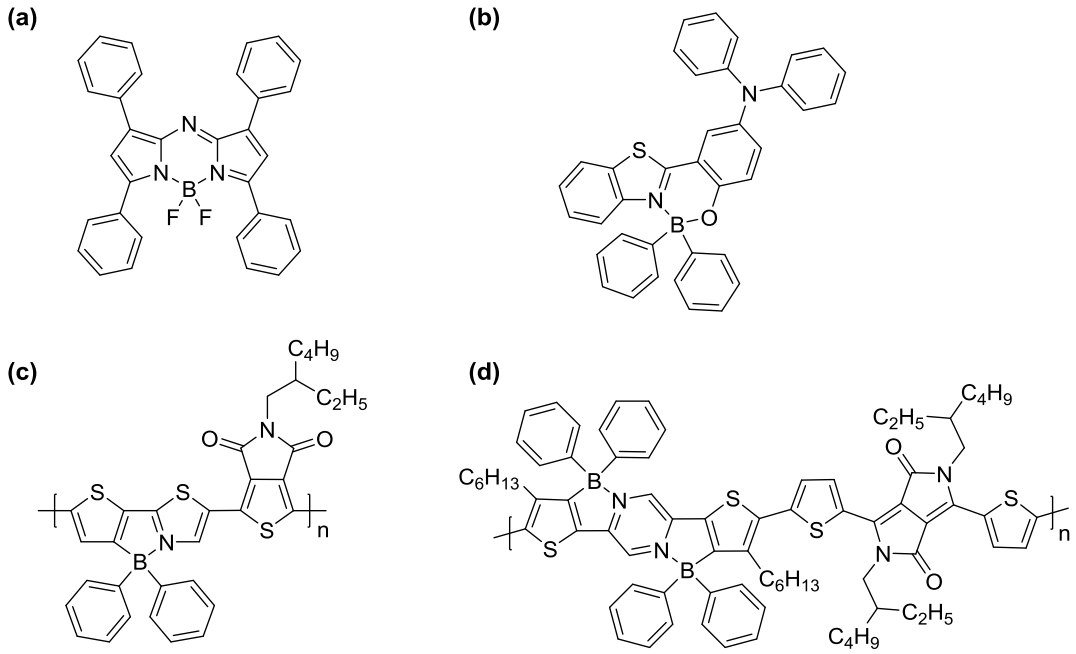


**Figure 1.14.** Some examples of tetracoordinated boron-containing organoboron compounds, (a) and (b), and polymers, (c) and (d)

In order to make it a more efficient way to maximize π-conjugation and obtain a stable boron-containing conjugated system, as mentioned, additional conjugated units can be introduced to the framework. In addition, another proper adjustment is the replacement of C-C bonds with B-N bonds to obtain favorable functions [53]. In the following subtitle, the principle of incorporating the B-N coordination bond is explained in more detail.

### 1.6.2.1 Principle of B-N Coordination Bond

The element Boron having an atomic number 5 and Nitrogen having atomic number 7 are both neighboring to the element Carbon (having an atomic number 6) in the periodic table. Thus, total number of electrons of two C atoms is equal to the sum of

B and N. Replacement of two carbons with B and N in a conjugated framework produces an isoelectronic system, and the resulting B-N embedded π-conjugated systems offers favorable properties. It is known that B atom has an empty p orbital, and N atom carry a lone pair of electrons. Therefore, B-N coordination bond can form through occupation of the empty p orbital of B atom by the lone pair electrons of the N [57].

B-N unit contains a N atom carrying a positive charge (cationic character) and a B atom with the negative charge (anionic character). As B-N unit incorporated into the π-conjugated framework, positive charge of the N atom promotes the static potential and the electron deficient nature of the system, which leads to achieve low-lying LUMO energy levels. In addition, B-N coordination adjusts the optoelectronic properties of conjugated systems, and enhances the intramolecular interactions, which is proven by a study of Liu and co-workers. As mentioned previously, bulky group substitution is often preferred to obtain rich π-conjugated and stable boron-bearing systems. However, as Dou and Liu stated, these groups prevent intramolecular interactions of the compounds in solid state and weaken the charge-transportation, and to overcome this problem, instead of B-C bond, introduction of B-N bond can be applied to the system [53],[57]. Also, replacing C-C bonds with B-N, provides great co-planarity and rigidity of the backbones. As a result, all these characteristics make π-conjugated systems containing B-N coordination bond a potentially useful designs as organic semiconductors for OPVs [57].

### 1.6.3 Post-Polymerization Borylation Method

As mentioned earlier, in the literature, there are some studies on polymers merged with boron to improve the optoelectronic properties of CPs. So far, hydroboration, haloboration and phenylboration polymerization techniques and other coupling methods have been introduced in the literature to synthesize these organoboron polymers [56]. On the other hand, there are other methods available and developing to achieve these materials successfully, such as post-polymerization borylation

method. In the literature, electrophilic C-H borylation was applied to small molecules that contain BT moiety, using $BCl_3$ to introduce boron into the structure and further treatment with diarylzinc ($Zn(aryl)_2$) or trialkyl aluminum ($Al(alkyl)_3$) to stabilize the boron unit [58]. These studies demonstrate that this method is useful to achieve highly emissive and low band gap small molecules.

According to the study of Dailey and Turner et al., this method can be extended to synthesize boron containing polymers, by controlling the percentage of boron units incorporated into the polymer through changing molar equivalents of the boron source ($BCl_3$) with respect to the repeating unit, and by further stabilization of boron with $ZnPh_2$. Here, the borylation was proven with two methods; an increase in the molecular weight due to addition of boron containing units, and bathochromic absorption speactra of borylated polymers. The resulting polymers contain a C,N chelated $BPh_2$ units on the polymer chain, and it is reported that these polymers exhibited superior EQE values and red shifts above 150 nm in the emission spectra. As a result, post-polymerization borylation method is simply a high-yielding method to introduce stable boron units into the CP main chains [59]. This method is considered as an alternative new method for the development of organoboron polymers having intrinsic properties derived from incorporation of stable boron units to utilize these materials in optoelectronic devices.

## 1.7 Aim of Study

The effect of heteroatom substitution through atomistic approach and incorporation of main gorup elements have been attracted a great attention for developing efficient materials for optoelectronic devices. In the sense of these two important contexts, the focus of this thesis study contains two subjects separately; the effect of heteroatom and integration of boron in CPs for photovoltaic applications. As mentioned in detail previously, boron has many intrinsic properties that draws attention for developing new conjugated polymers utilized for emerging photovoltaics. Recently, number of papers published has enlightened the way for the

synthesis and applications of boron-containing conjugated polymers. In order to obtain a stable organoboron polymers, new methods for the synthesis of this emerging class of polymeric materials have been reported by scientists, such as post-polymerization borylation. In this direction, benzodithiophene and pyrazine containing conjugated polymer was synthesized, and followed by incorporation of boron into the system by this recently developed method of post-polymerization borylation. The method was apllied to achieve a partially borylated polymer through adjustment of the equivalance of boron source with respect to the repeating unit of polymer by referring to the article of post-polymeriation borylation. Stabilization of boron unit was provided by substituting phenyl groups to boron unit. Accordingly, non-borylated (**P1A**) and borylated (**P1B**) polymers, shown in Figure 1.15., were synthesized and compared in terms of their electronic and optical properties for photovoltaic applications. Numerous features of the synthesized polymers **P1A** and **P1B** were investigated by applying several techniques.

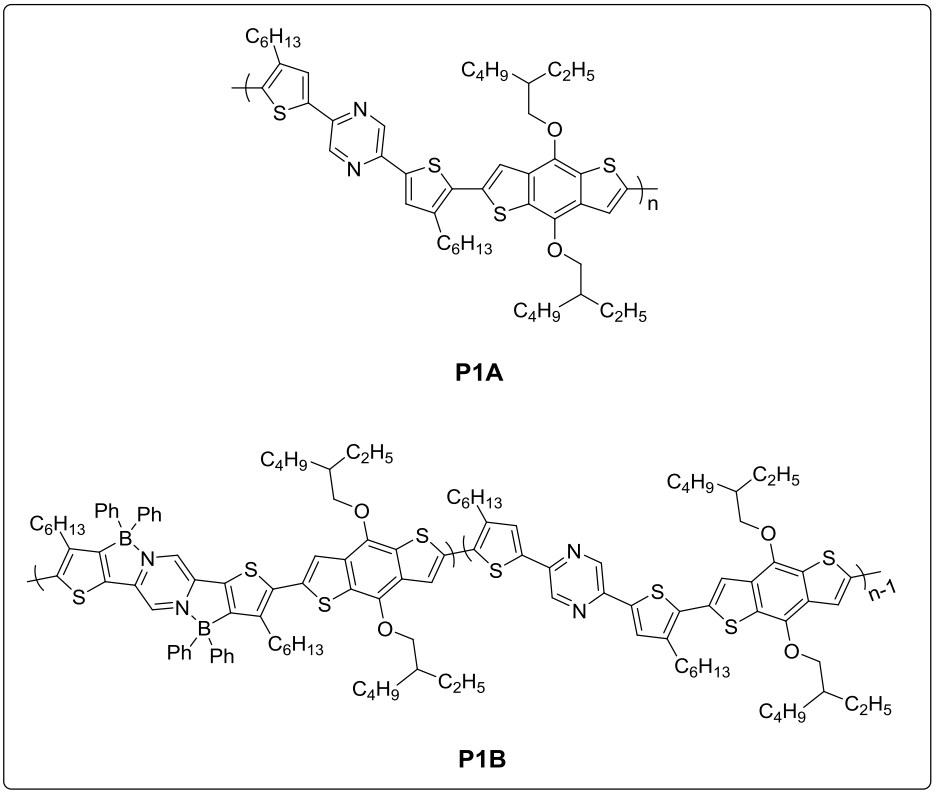


**Figure 1.15.** Structure of polymers **P1A** and **P1B**

The other concept, namely the effect of heteroatom on CPs, was investigated by altering the central heteroatom on benzazole acceptor of benzodithiophene and pyrazine containing conjugated random polymers. As stated previously, the central atom and aromaticity of the azole ring are key factors for the electron-accepting nature of benzazole moieties. Accordingly, three different random polymers, benzotriazole-containing **RP1**, benzothiadiazole-containing **RP2**, and benzoselenadiazole-containing **RP3**, were synthesized (Figure 1.16.). Optical and electrochemical studies of all three syntesized polymers were carried out to investigate the effect of heteroatom alteration in optical and electronic properties. In addition, many characterization techniques were applied to the synthesized polymers. In accordance with the aim of this study, photovoltaic application studies and blend film morphology studies of polymers were performed.

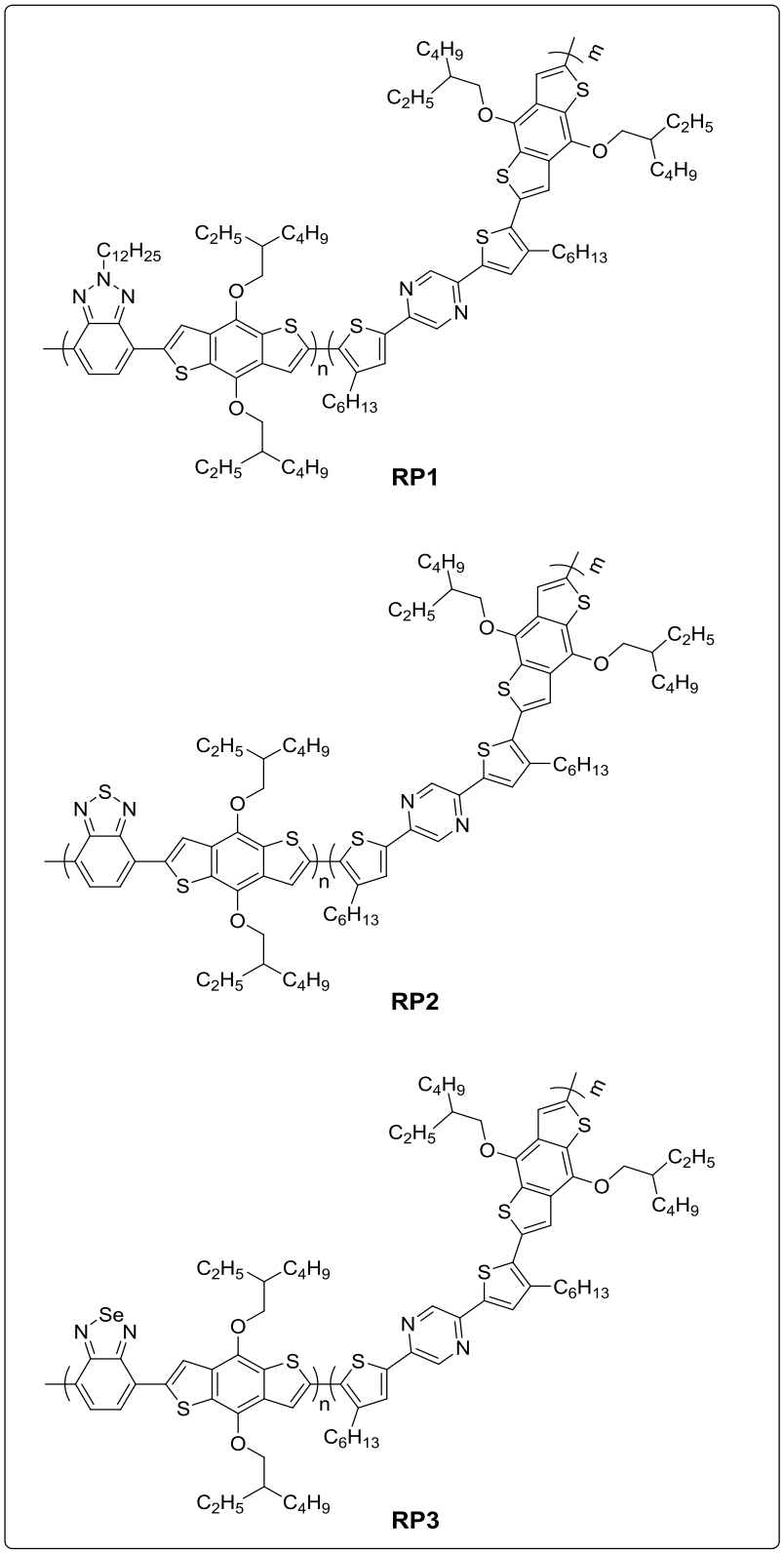


**Figure 1.16.** Structure of polymers **RP1**, **RP2**, and **RP3**

# CHAPTER 2

# EXPERIMENTAL

## 2.1 Materials and Methods

In this study, all commercially available chemicals were purchased form Sigma Aldrich, and used without further purification. Toluene solvent was distilled just before usage over benzophenone and sodium under the nitrogen atmosphere. The synthetic routes of monomers are given under the corresponding titles. For the synthesized compounds, which needed a further purification, Merck Silica Gel 60 was used as the stationary phase in column chromatography purification method. All polymers were synthesized via Stille cross-coupling reaction, and their synthesis procedures were given as well in this chapter. Synthesized organic molecules were structurally identified by Nuclear Magnetic Resonance Spectroscopy (NMR). Both $^{1}H$ and $^{13}C$ NMR of molecules were obtained in deuterated $CDCl_3$ solvent by Bruker Spectrospin Avance DPX-400 Spectrometer where tetramethyl silane (TMS) was used as an internal standard. Molecular weights and polydispersity index (PDI) of polymers were obtained by Shimadzu RID-20A Gel Permeation Chromatography (GPC), which was calibrated against polystyrene standards in chloroform solvent. Oxidation-reduction potentials, HOMO-LUMO energy levels and electronic band gaps of polymers were characterized by Cyclic Voltammetry (CV). In this method, all electrochemical measurements were carried out in three-electrode spectroelectrochemical cell, where platinum wire is the counter electrode (CE), ITO coated glass is the working electrode (WE) and Ag wire is the reference electrode (RE). For the CV measurements, all electrodes were immersed in a 0.1 M tetrabutylammonium hexafluorophosphate ($TBAPF_6$)/ acetonitrile (ACN) electrolyte solution and cyclic potential was performed with a scan rate of 100 mV/s. Gamry Instrument Reference 600 Potentiostat was connected to the three electrodes

to control the potential applied to WE with respect to RE, and to measure the current that flows between WE and CE. Optical features of polymers were determined by JASCO V-770 UV-Vis/ NIR spectrophotometer. Thermal properties of polymers were obtained by Perkin Elmer Diamond differential scanning calorimeter (DSC) and Pyris 1 TGA Thermogravimetry Analyzer (TGA). Morphology studies were carried out using Atomic Force Microscopy (AFM) and Transmission Electron Microspcopy (TEM).

### 2.1.1 OPV Device Fabrication

OPV devices were fabricated with established device architecture of ITO/PEDOT:PSS/Polymer:$PC_{71}BM$/LiF/Al. Cleaning and etching procedures were followed by oxygen plasma treatment, which was applied for 5 minutes to both regulate the work function and purify from organic impurities. Subsequently, PEDOT:PSS solution was filtered through polytetrafluoroethylene (PET) filters with a pore size of 0.45 microns and coated with spin coating at 4000 rpm, and dried at 135 ℃ for 15 minutes. Active layer solutions to be coated on PEDOT:PSS were prepared by dissolving donor-acceptor mixtures Polymer:$PC_{71}BM$ with different blend ratios in chloroform at a mixture concentration of 20 mg/mL, approximately 3 hours before coating and rotated at 35°C during this time. Active layer solutions of devices were coated without being filtered because of the solubility problem. The same solutions were coated in an open air atmosphere due to their high volatility. The active layer coated samples were taken into the vacuum evaporation system for metal evaporation on them. Lithium fluoride/aluminum (LiF/Al) metal electrode system was coated on the active layer under the nitrogen atmosphere by thermal evaporation method at a pressure of approximately $1\times 10^{-6}$ mbar. Photovoltaic characterizations of the fabricated cells were carried out under simulated AM1.5G irradiation with 100 mW/cm$^2$ light intensity using Keithley 2400 device, and as a result, J-V curves and PCE of devices were obtained.

## 2.2 Synthesis of Monomers

### 2.2.1 Synthesis of 2-tributylstannyl-4-hexylthiophene [60]

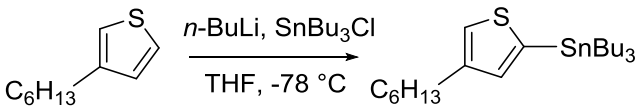


**Figure 2.1.** Synthesis of 2-tributylstannyl-4-hexylthiophene

3-Hexylthiophene (4.00 g, 23.77 mmol) was placed in a two-neck round-bottom flask and dissolved in a freshly distilled tetrahydrofuran (THF) (50 mL) under the nitrogen atmosphere. While the solution cooled to -78 ℃, *n*-BuLi (10.5 mL of a 2.5 M solution in hexane, 26.14 mmol) was added dropwise to the reaction mixture. After stirring for 1 hour, tributyltin chloride (7.5 mL, 26.14 mmol) was added dropwise. The solution was stirred overnight at room temperature and quenched with water. Reaction mixture was extracted with DCM and water. The organic layer was dried over $MgSO_4$ and filtered. The solvent was removed under vacuum for further purification (10.01 g, 92% yield).

### 2.2.2 Synthesis of 2,5-di(3-hexylthiophen-2-yl)pyrazine [61]

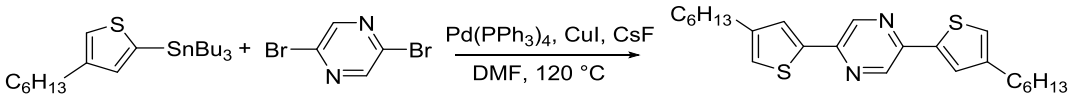


**Figure 2.2.** Synthesis of 2,5-di(3-hexylthiophen-2-yl)pyrazine

2,5-dibromopyrazine (1.00 g, 1.26 mmol), 2-tributylstannyl-4-hexylthiophene (4.61 g, 10.09 mmol), CuI (32.02 mg, 168 µmol), CsF (6.39 mg, 42 µmol) and tetrakis(triphenyphosphine) palladium(0) catalyst (437.2 mg, 378 µmol) were added in a two-neck round-bottom flask and dissolved in dry DMF (30 mL). After degassing under nitrogen atmosphere for 15 minutes, temperature was adjusted to 120 ℃, and the reaction was stirred overnight. The reaction solvent was evaporated under vacuum on the rotary evaporator and extracted with DCM and brine. Organic

layer was dried over $MgSO_4$ and filtered. Solvent was removed under vacuum and crude product was purified by silica gel column chromatography method (4 hexane: 1 DCM). The product was recrystallized with hexane for further purification and obtained as yellow crystals (1.05 g, 61% yield).

$^1$H NMR (400 MHz, $CDCl_3$) δ 8.81 (s, 2H), 7.49 (s, 2H), 7.06 (s, 2H), 2.67 – 2.61 (m, 4H), 1.71 – 1.61 (m, 4H), 1.39 – 1.29 (m, 12H), 0.90 ppm (t, *J* = 6.9 Hz, 6H). $^{13}$C NMR (101 MHz, $CDCl_3$) δ 145.98, 144.86, 140.90, 139.36, 126.61, 123.43, 31.67, 30.54, 30.43, 28.98, 22.63, 14.11 ppm.

### 2.2.3 Synthesis of 2,5-bis-(5-bromo-4-hexylthiophen-2-yl)pyrazine [61]

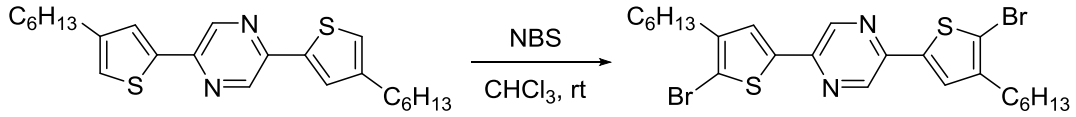


**Figure 2.3.** Synthesis of 2,5-bis-(5-bromo-4-hexylthiophen-2-yl)pyrazine

Coupling product (500 mg, 1.21 mmol) and *N*-bromosuccinimide (NBS) (474 mg, 2.67 mmol) were placed in a round bottom flask and degassed for 15 minutes under nitrogen atmosphere. Freshly distilled chloroform (35 mL) was added, and reactants were dissolved immediately. The reaction was stirred at room temperature overnight in a dark environment. The reaction mixture was extracted with DCM and water, and the organic layer was dried over $MgSO_4$ and filtered. Silica gel column chromatography method was applied (5 hexane:1 DCM), and the product was obtained as a yellow solid (455 mg, 94% yield).

$^1$H NMR (400 MHz, $CDCl_3$) δ 8.72 (s, 2H), 7.33 (s, 2H), 2.58 (t, *J* = 6.8 Hz, 4H), 1.68 – 1.53 (m, 4H), 1.43 – 1.26 (m, 12H), 0.90 ppm (t, *J* = 5.1 Hz, 6H). $^{13}$C NMR (101 MHz, $CDCl_3$) δ 143.67, 140.47, 138.73, 138.01, 125.91, 113.19, 31.33, 30.54, 29.49, 29.14, 28.75, 22.44 ppm.

### 2.2.4 Synthesis of 4,7-dibromobenzo[*c*][1,2,5]thiadiazole [62]

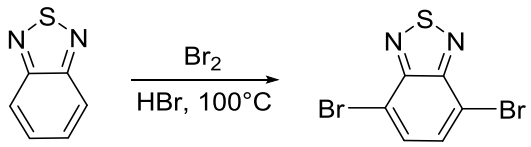


**Figure 2.4.** Synthesis of 4,7-dibromobenzo[*c*][1,2,5]thiadiazole

Benzo-1,2,5-thiadiazole (5.00 g, 36.72 mmol) was placed in a 250 mL two-neck round-bottom flask and dissolved in 65 mL hydrobromic acid. After refluxing at 100 ℃ for 1 hour, bromine (6.77 mL, 100.15 mmol), which is diluted with 45 mL hydrobromic acid, was slowly added through a liquid addition apparatus. The reaction was monitored by thin layer chromatography (TLC). After the disappearance of reactant was observed, the reaction mixture was cooled to room temperature. Afterwards, mixture was slowly poured into sodium bisulfate solution and stirred for 1 hour. The solution was filtered and the product was collected on filter paper. Solid product remaining on the filter paper was washed with water and cold diethyl ether respectively, and the desired product was obtained as a yellow solid (10.25 g, 95% yield).

$^{1}$H NMR (400 MHz, $CDCl_3$) δ 7.73 ppm (s, 1H). $^{13}$C NMR (101 MHz, $CDCl_3$) δ 152.83, 132.22, 113.78 ppm.

### 2.2.5 Synthesis of 3,6-dibromobenzene-1,2-diamine [63]

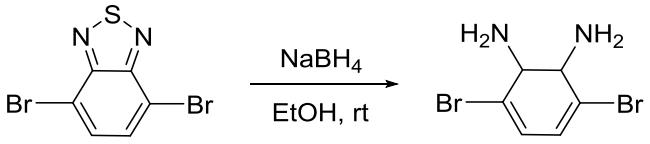


**Figure 2.5.** Synthesis of 3,6-dibromobenzene-1,2-diamine

4,7-dibromobenzo[*c*][1,2,5]thiadiazole (9.72 mg, 33.07 mmol) was dissolved in 300 mL ethanol and stirred in a 2000 mL erlenmayer flask at room temperature. After cooling to 0 ℃, sodium borohydride (18.76 g, 495.98 mmol) was added in portions

to the reaction mixture and the solution was stirred for 1 hour. The temperature was raised to 25 °C, and reaction was stirred overnight. Reaction solvent was evaporated under vacuum using a rotary evaporator. The product was extracted with water and diethyl ether. Organic phase was dired over $MgSO_4$ and filtered through filter paper. Diethyl ether was removed under reduced pressure, and the product was obtained as a yellow solid (7.9 g, 90% yield).

### 2.2.6 Synthesis of 4,7-dibromobenzo[*c*][1,2,5]selenadiazole [64]

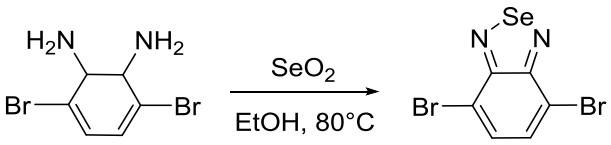


**Figure 2.6.** Synthesis of 4,7-dibromobenzo[*c*][1,2,5]selenadiazole

3,6-dibromobenzene-1,2-diamine (3.00 g, 11.20 mmol) was dissolved in 30 mL ethanol, and while it was stirred selenium dioxide (1.49 g, 13.44 mmol) was added to the reaction mixture. After addition, temperature was adjusted to 80 °Cand reaction was stirred overnight. After completion of the reaction, temperature was cooled to 0 °Cand filtered. The remaining solid on the filter paper was washed with cold ethanol and the product was obtained as a yellow solid (2.90 g, 75 % yield).

$^{1}$H NMR (400 MHz, $CDCl_3$) δ 7.65 ppm (s, 2H).

$^{13}$C NMR of this compound could not be achieved. However, GC-MS result was obtained and shown in the appendices section.

### 2.2.7 Synthesis of 4,7-dibromo-2H-benzo[*d*][1,2,3]triazole [65]

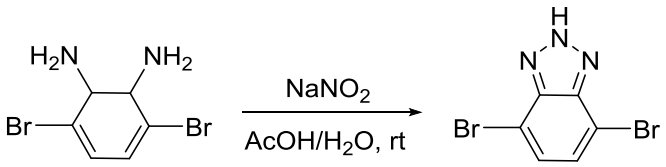


**Figure 2.7.** Synthesis of 4,7-dibromo-2H-benzo[*d*][1,2,3]triazole

3,6-dibromo-1,2-benzenediamine (7 g, 26.32 mmol) was dissolved in 75 mL acetic acid and stirred in a 250 mL erlenmayer flask. Sodium nitrate (2 g, 28.75 mmol) was dissolved in 30 mmL water and slowly added to the reaction mixture. After stirring for one hour, solution was filtered through filter paper. The remaining solid was washed with distilled water to remove acetic acid, and a solid product was obtained (6.7 g, 92% yield).

### 2.2.8 Synthesis of 4,7-dibromo-2-dodecyl-2H-benzo[*d*][1,2,3]triazole [65]

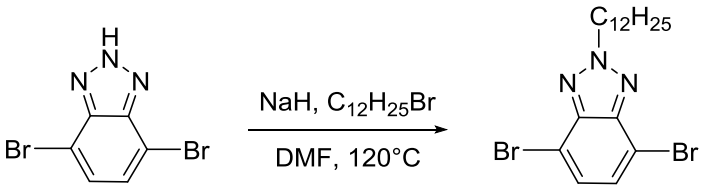


**Figure 2.8.** Synthesis of 4,7-dibromo-2-dodecyl-2H-benzo[*d*][1,2,3]triazole

The previously synthesized compound (3.0 g, 10.83 mmol) was placed in a two-neck round-bottom flask and dissolved in 20 mL dry DMF under nitrogen atmosphere. The reaction was kept stirred at room temperature, and sodium hydride (311.98 mg, 13.10 mmol) was added under the same reaction conditions. After the addition of sodium hydride was completed, temperature was adjusted to 120 ℃ and 1-bromododecane (3.25 g, 12.97 mmol) was added to the mixture, and reaction was stirred overnight. The reaction mixture was cooled at room temperature and quenched with water. Solution was extracted with chloroform and water, and the organic layer was dried over $MgSO_4$. After filtration, chloroform was removed using

a rotary evaporator. Compound was purified by silica gel column chromatography method (4 hexane: 1 chloroform), and product was obtained (1.4 g, 30% yield).

$^{1}$H NMR (400 MHz, $CDCl_3$) δ 7.44 (s, 2H), 4.77 (t, $J$ = 7.4 Hz, 2H), 2.18 – 2.10 (m, 2H), 1.24 (s, 18H), 0.87 ppm (t, $J$ = 6.8 Hz, 3H). $^{13}$C NMR (101 MHz, $CDCl_3$) δ 143.71, 129.50, 109.98, 57.49, 31.90, 30.22, 29.59, 29.34, 28.98, 26.50, 22.69, 14.13ppm (12 out of 15 signals expected).

## 2.3 Synthesis of Polymers

### 2.3.1 Synthesis of RP1

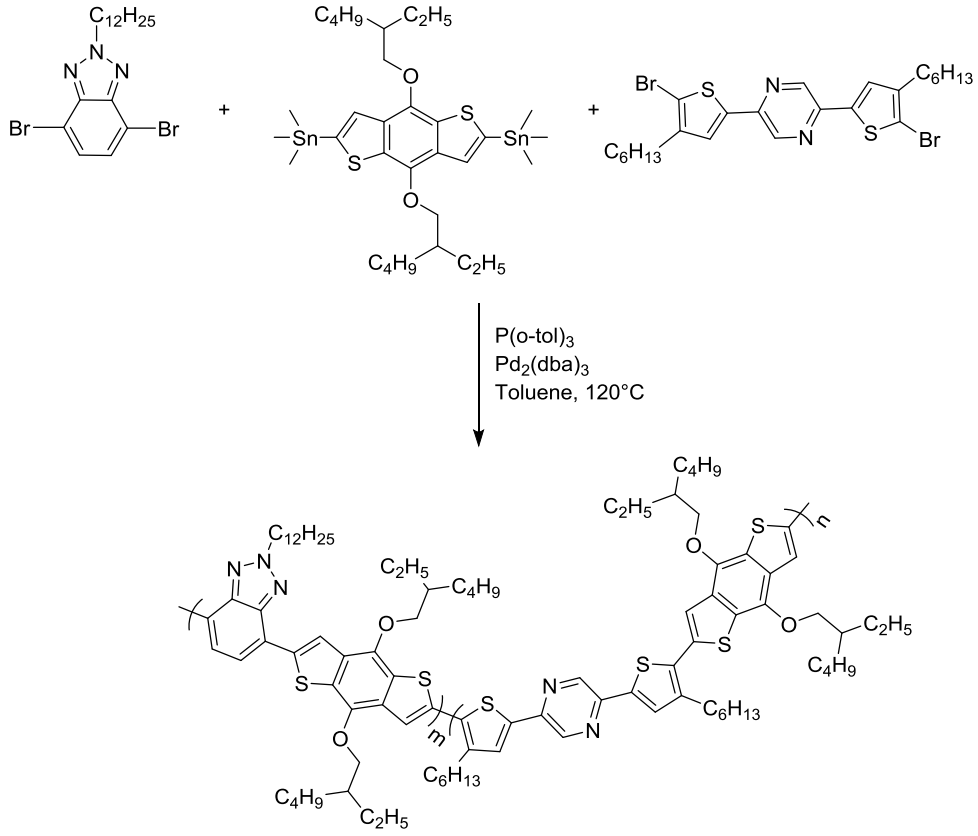


**Figure 2.9.** Synthesis of **RP1**

Benzotriazole (BTz) acceptor (150 mg, 510 µmol), pyrazine (Pz) acceptor (192 mg, 510 µmol) and benzodithiophene (BDT) donor (520 mg, 1.02 mmol) were placed in

a 100 mL Schlenk tube for polymerization reaction via Stille cross-coupling. The compounds were dissolved in freshly distilled toluene (10 mL) and degassed for 10 minutes under nitrogen atmosphere at room temperature. $P(o\text{-tolyl})_3$ (15%) and $Pd_2(dba)_3$ (5%) were then added and the reaction mixture was heated to 110 °C. After stirring for 48 hours, 2-(tributylstannyl)thiophene (251 mg, 674 µmol) was added as the first end-capper and the reaction was stirred for 3 hours. Then 2-bromo thiophene (220 mg, 1.35 mmol) was added as the second end-capper and the reaction was stirred overnight. The polymerization reaction was completed after a total of 72 hours, and the mixture was cooled to room temperature. Solution was precipitated in cold methanol (100 mL) and filtered to obtain solid product. The collected precipitate was purified over a Soxhlet extractor in methanol, acetone, and hexane respectively to remove monomers and oligomers. Finally, $CHCl_3$ was used to extract the polymer. To remove any remaining catalysts, Pd scavenger was added to the solution and stirred for one hour. Subsequently, silica gel column chromatography ($CHCl_3$) was used to get rid of any residual quadrasil. Solvent was removed under reduced pressure through a rotary evaporator. The polymer was obtained as a dark red solid (303 mg, 90% yield).

GPC results of **RP1** were obtained as; Mn = 7 kDa, Mw = 9 kDa, PDI = 1.33.

### 2.3.2 Synthesis of RP2

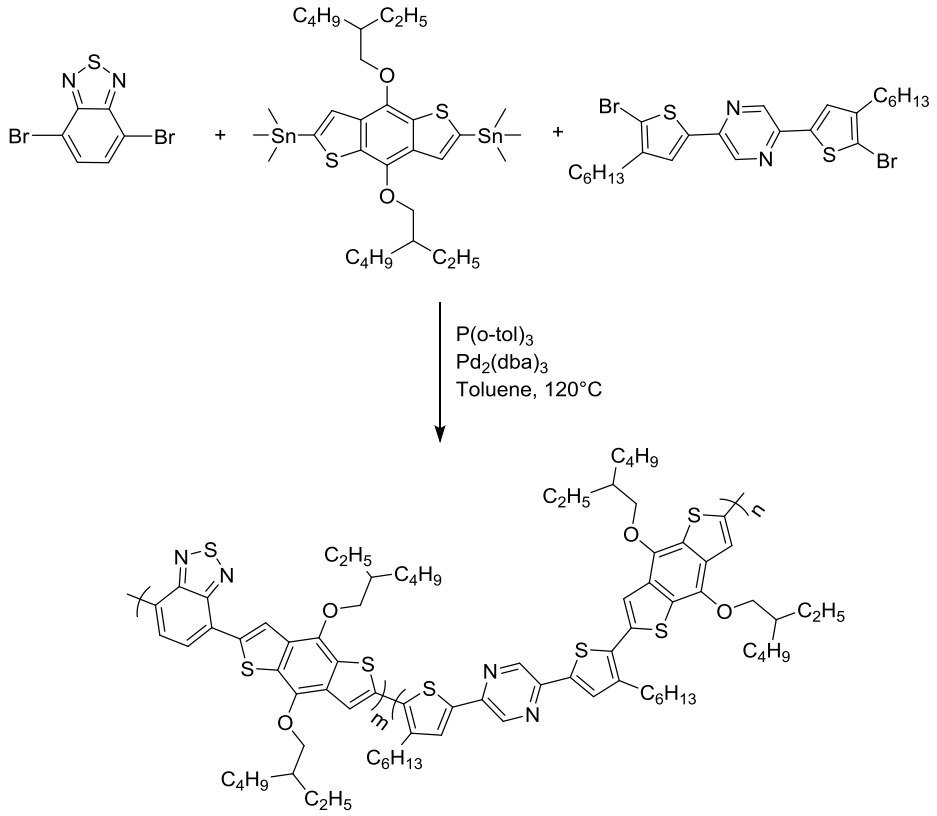


**Figure 2.10.** Synthesis of **RP2**

Benzothiadiazole acceptor (BT) (150 mg, 510 µmol), pyrazine (Pz) acceptor (291 mg, 510 µmol) and benzodithiophene (BDT) donor (788 mg, 1.02 mmol) were placed in a 100 mL Schlenk tube and dissolved in a freshly distilled toluene (10 mL). P(o-tolyl)$_3$ (15%) and $Pd_2(dba)_3$ (5%) were added to the reaction mixture followed by degassing 10 minutes under nitrogen atmosphere. The temperature was raised to 110 ℃, and the reaction was monitored by TLC. After stirring for 48 hours, 2-(tributylstannyl)thiophene (381 mg, 1.02 mmol) and 2-bromo thiophene (333 mg, 2.04 mmol) were added to the reaction intermediate as first and second end-cappers, respectively, at 3-hour intervals. The reaction was stirred overnight, and the polymerization reaction was complete after a total of 72 hours. Reaction mixture was cooled to room temperature, and the solution was slowly poured into cold methanol (100 mL). The precipitated polymer was collected by filtration and subjected to

Soxhlet extractor in methanol, acetone, and hexane respectively to remove monomers, oligomers, and other soluble organics. At the end, $CHCl_3$ was used to extract the polymer. To remove remaining catalysts, Pd scavenger was added to the solution and stirred for one hour. Subsequently, further purification was carried out via silica gel column chromatography ($CHCl_3$) to remove residual quadrasil. Solvent was evaporated under vacuum, and the polymer was obtained as a dark purple solid (382 mg, 75% yield).

GPC results of **RP2** were obtained as; $M_n$ = 5 kDa, $M_w$ = 7 kDa, PDI = 1.27.

### 2.3.3 Synthesis of RP3

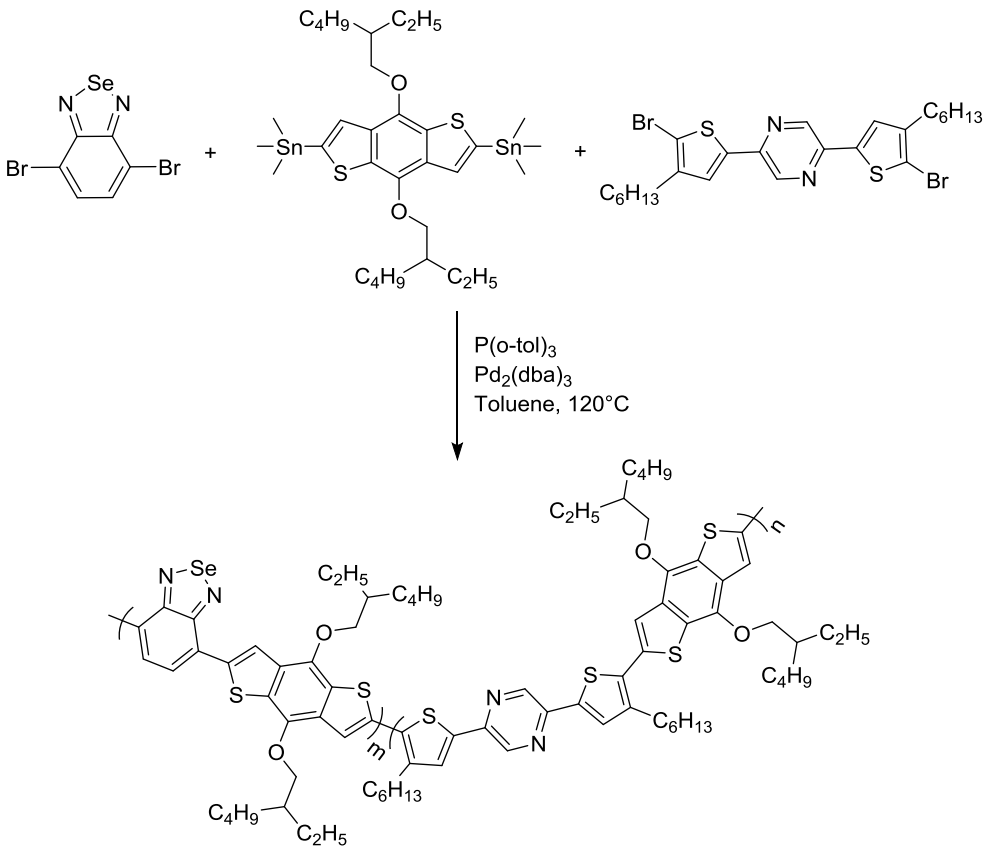


**Figure 2.11.** Synthesis of **RP3**

Benzoselenadiazole (BSe) acceptor (150 mg, 510.27 μmol), pyrazine (Pz) acceptor (251 mg, 510.27 μmol) and benzodithiophene (BDT) donor (680 mg, 1.02 mmol) were placed in a 100 mL Schlenk tube and dissolved in a freshly distilled toluene (10 mL). P(o-tolyl)$_3$ (15%) and $Pd_2(dba)_3$ (5%) were added to the mixture after degassing for 10 minutes under nitrogen gas. The reaction was heated to 110 ℃ and monitored by TLC. After stirring for 48 hours, 2-(tributylstannyl)thiophene (328 mg, 1.02 mmol) and 2-bromo thiophene (287 mg, 2.04 mmol) were added as first and second end-cappers respectively, and reaction was stirred overnight. The reaction mixture was cooled to room temperature after a total time of 72 hours. The solution was slowly poured into cold methanol (100 mL), and the polymer was precipitated. Polymer was obtained by filtration and purified by Soxhlet extraction method in various solvents. Methanol, acetone, and hexane solvents were used respectively to remove monomers, oligomers, and other soluble organics. $CHCl_3$ was used to extract the desired polymer, and Pd scavenger was added to the solution to remove catalysts. After stirring for 1 hour, further purification was carried out via silica gel column chromatography ($CHCl_3$) to remove quadrasile. Chloroform was removed under reducing pressure using a rotary evaporator. The polymer was obtained as a purple solid (374 mg, 85% yield).

GPC results of **RP3** were obtained as; $M_n$ = 6 kDa, $M_w$ = 8 kDa, PDI = 1.30.

### 2.3.4 Synthesis of P1A

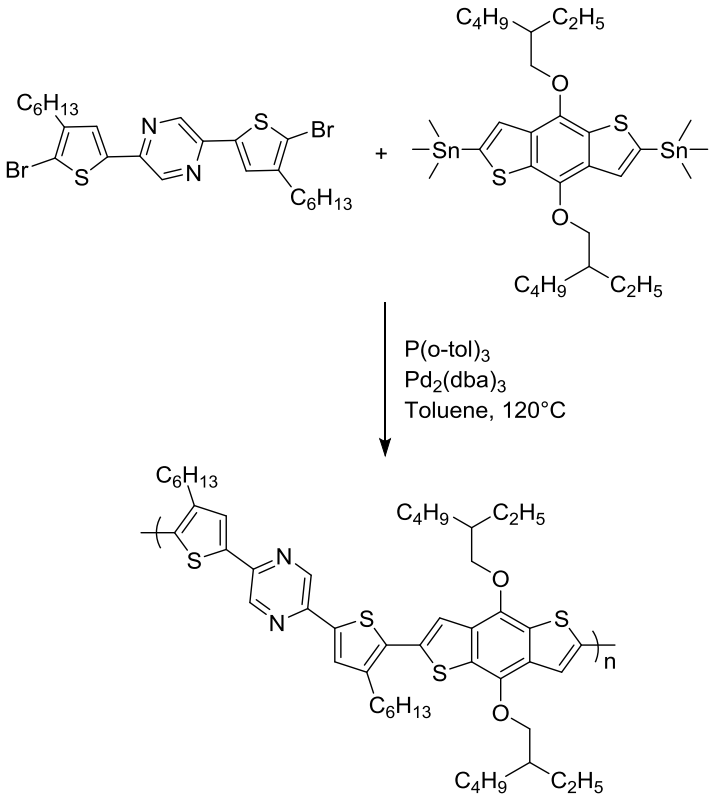


**Figure 2.12.** Synthesis of **P1A**

Pyrazine (Pz) acceptor and commercially available BDT moiety were used to carry out the Stille cross-coupling reaction for polymerization. 2,5-bis-(5-bromo-4-hexylthiophen-2-yl)pyrazine (500 mg, 877 µmol) and BDT donor unit (677 mg, 877 µmol) were placed in a 100 mL Schlenk tube and degassed under nitrogen atmosphere for 30 minutes. 10 mL of freshly distilled toluene was added and stirred. When the temperature reached up to 110 ℃, P(o-tolyl)$_3$ (15%) and $Pd_2(dba)_3$ (5%) were added as catalysts. TLC was used to monitor the reaction. After about 48 hours, 2-(tributylstannyl)thiophene and 2-bromo thiophene were added as first and second end-cappers, respectively, and the reaction continued overnight. The reaction was allowed to cool to room temperature at the end of a total of 72 hours, and the solution was slowly poured into cold methanol (100 mL). Precipitated polymer was collected on a filter paper and purified by Soxhlet extraction method using methanol, acetone,

and hexane solvents respectively to remove monomers, oligomers and other soluble organics. $CHCl_3$ was used to extract the desired polymer, and Pd scavenger was added to the solution to remove catalysts. After stirring for one hour, further purification was performed via silica gel column chromatography ($CHCl_3$) to remove quadrasils. Chloroform was removed under reducing pressure by using a rotary evaporator. The polymer was obtained as a purple solid (495 mg, 64% yield).

GPC results of **P1A** were obtained as; Mn = 6 kDa, Mw = 8 kDa, PDI = 1.39.

### 2.3.5 Synthesis of P1B

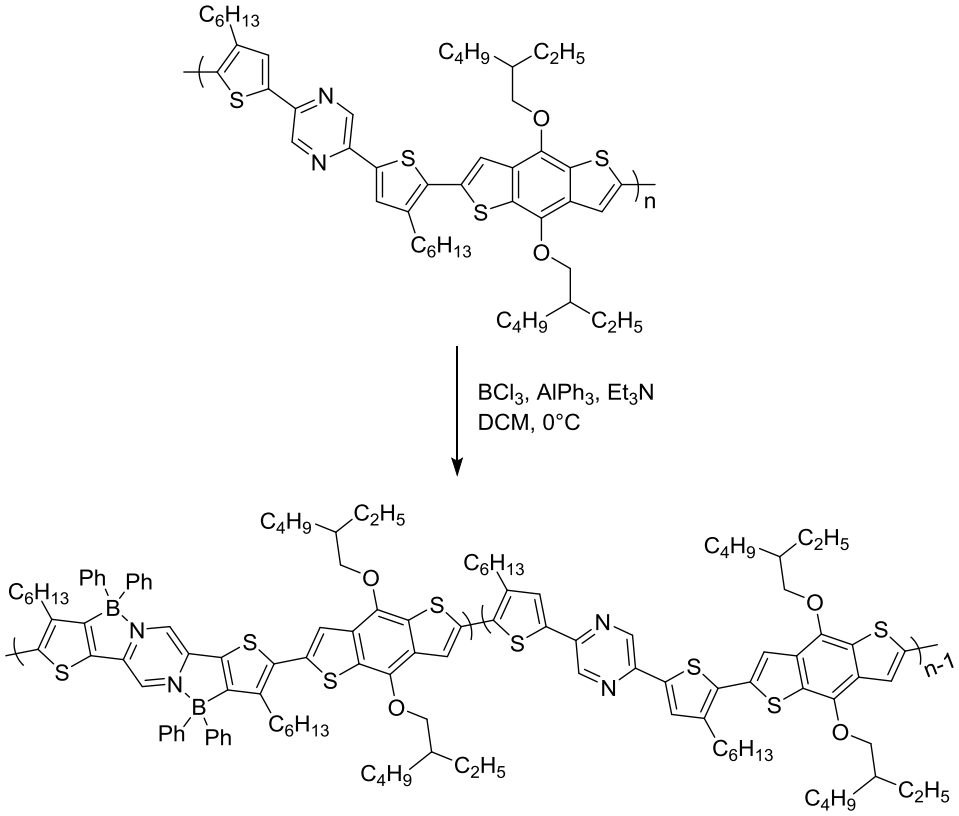


**Figure 2.13.** Synthesis of **P1B**

Polymer **P1A** (0.25 g, 0.3 mmol) was dissolved in 30 mL of anhydrous DCM solvent at room temperature after being degassed in a 100 mL Schlenk tube under the nitrogen atmosphere for 10 minutes. After the reaction temperature cooled to 0 ℃,

triethylamine ($Et_3N$) (57.0 mg 0.6 μmol) was added slowly. After 10 minutes, $BCl_3$ (1.8 mL of 1.8 mmol in 1 M hexane) was slowly added and it was observed that the color of the reaction mixture changed from dark red to dark blue. After 24 hours, triphenyl aluminum ($AlPh_3$) (1.8 mL, 1.8 mmol in 1 M dibutyl ether) was added dropwise to the reaction, which was stirred overnight at room temperature. After addition, the color of the reaction mixture changed from dark blue to wine red. 3 hours later, the reaction was completed and the reaction solution was concentrated under reduced pressure. It was then washed with cold methanol and the inorganic by-products formed by $AlPh_3$ were dissolved in methanol and the solution was filtered to give the boron-containing polymer **P1B** as a dark red solid (134.0 mg, 40% yield).

GPC results of **P1B** were obtained as; Mn = 8 kDa, Mw = 11 kDa, PDI = 1.45.

# CHAPTER 3

# RESULTS AND DISCUSSION

## 3.1 Optical Studies

As mentioned previously, absorption of the fraction of sunlight varies for different materials, and the differences can be attributed to the chemical structures of the polymers. In general, absorption of the incident light by the photoactive material is significantly related to the absorption characteristics and the range of the absorbed light by the polymer. In this direction, optical studies provide an outcome about the optical characteristics of polymers which are important for device performance. Accordingly, with the studies presented in this section, the optical properties of polymers were investigated both as thin films and in dilute chloroform solution using UV-Vis Spectrophotometry. The spectra of polymers can be seen in Figure 3.1. for random conjugated polymers, and in Figure 3.2. for borylated and non-borylated polymers. Maximum absorption wavelength values for both solution and thin-film were recorded. Optical band gap ($E_g^{op}$) values were obtained from the maximum absorption onset of the thin film spectra of polymers, which is calculated by the formula below. The resulting data are shown in Table 3-1 and Table 3-2 for random polymers **RP1**, **RP2** and **RP3**, and for **P1A** and **P1B**, respectively.

$$E_g^{op} = \frac{1241}{\lambda_{max}^{onset}}$$

According to the normalized UV-Vis absorption spectra of polymers **RP1**, **RP2** and **RP3**, shown in Figure 3.1., maximum absorption wavelengths ($\lambda_{max}$) of polymers in dilute $CHCl_3$ solution were obtained as 489, 485 and 483 nm respectively for **RP1**, **RP2** and **RP3**. As compared with the solution $\lambda_{max}$ values, thin-film $\lambda_{max}$ of polymers

were red-shifted values of 526, 517, 515 nm respectively for **RP1**, **RP2** and **RP3**, correspondingly. The resulting bathochromically-shifted absorptions in thin-film forms indicate great aggregation, and stronger intermolecular interactions in the thin-film of polymers.

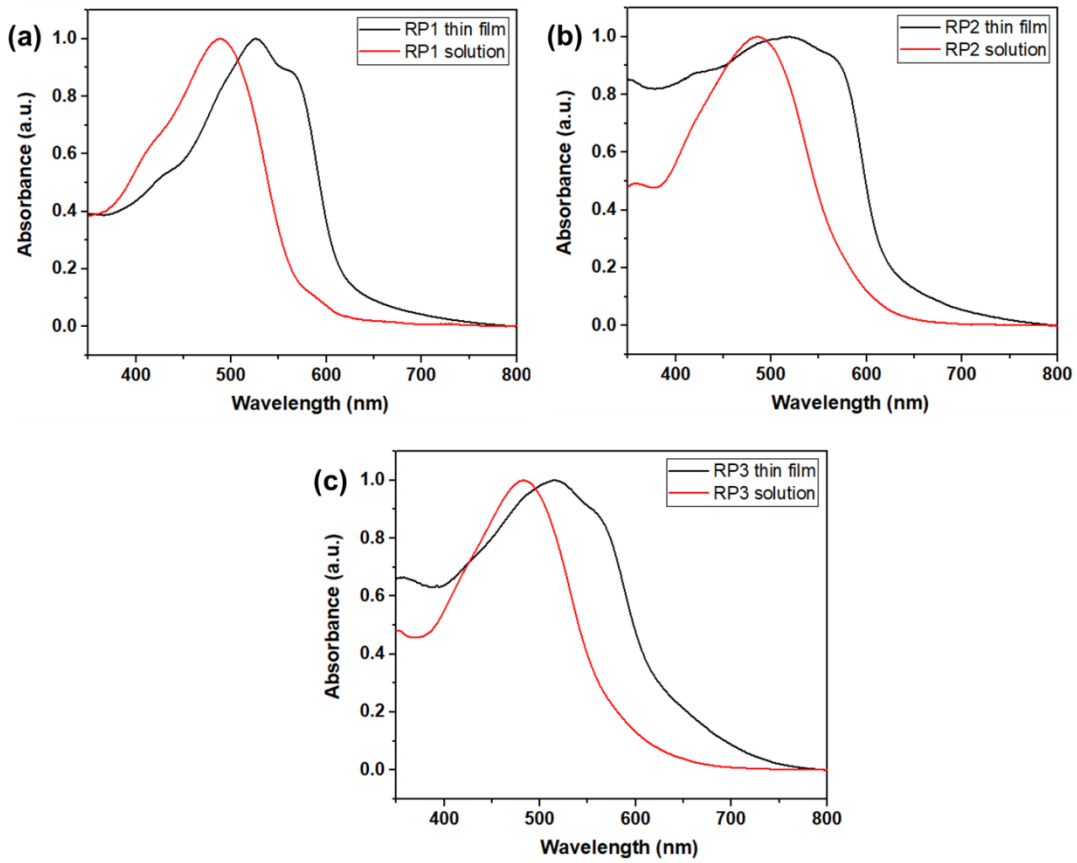


**Figure 3.1.** UV-Vis absorption spectra of polymers (a) **RP1**, (b) **RP2**, (c) **RP3** in dilute $CHCl_3$ solution (red) and as thin film (black)

The $E_g^{op}$ results of polymers, shown in Table 3-1, were found to be 1.99 eV for **RP1**, 1.97 eV for **RP2**, and 1.92 eV for **RP3**. Thus, the lowest optical band gap was obtained for **RP3** containing benzoselenadiazole unit. Due to the heavy Se atom, the bathochromic shift led to a decrease in $E_g^{op}$ as expected. This behavior can be explained by the reduced electronegativity and larger size of Se atom. The insertion of a larger Se atom compared to N and S atoms leads to a lower aromaticity due to poor overlap of the Se orbitals with the π-system. Moreover, formation of inter-chain Se-Se interactions provide higher charge carrier mobility for **RP3**.

**Table 3-1** The recorded values of $\lambda_{max}$, $\lambda_{max}^{onset}$, and $E_g^{op}$ of **RP1**, **RP2** and **RP3**

| Polymer | Solution $\lambda_{max}$ (nm) | Thin-film $\lambda_{max}$ (nm) | $\lambda_{max}^{onset}$ (nm) | $E_g^{op}$ (eV) |
|---|---|---|---|---|
| **RP1** | 489 | 526 | 624 | 1.99 |
| **RP2** | 485 | 517 | 630 | 1.97 |
| **RP3** | 483 | 515 | 646 | 1.92 |

As shown in Figure 3.2., normalized UV-Vis absorption spectra of polymers **P1A** (non-boylated) and **P1B** (borylated) were presented both in dilute $CHCl_3$ solution and as thin-films. $\lambda_{max}$ values for absorption spectra of **P1A** and **P1B** in dilute chloroform solution were recorded as 479 and 573 nm, respectively. For the thin film absorption spectra of polymers, $\lambda_{max}$ values were found as 518 nm for **P1A** and 555 nm for **P1B**. Thus, for both polymers, red-shifted absorption profile to longer wavelengths was observed for the thin-film form of **P1A** and **P1B**, as expected. This may again due to an increasing intramolecular charge transfer interactions and aggregation in thin-film forms.

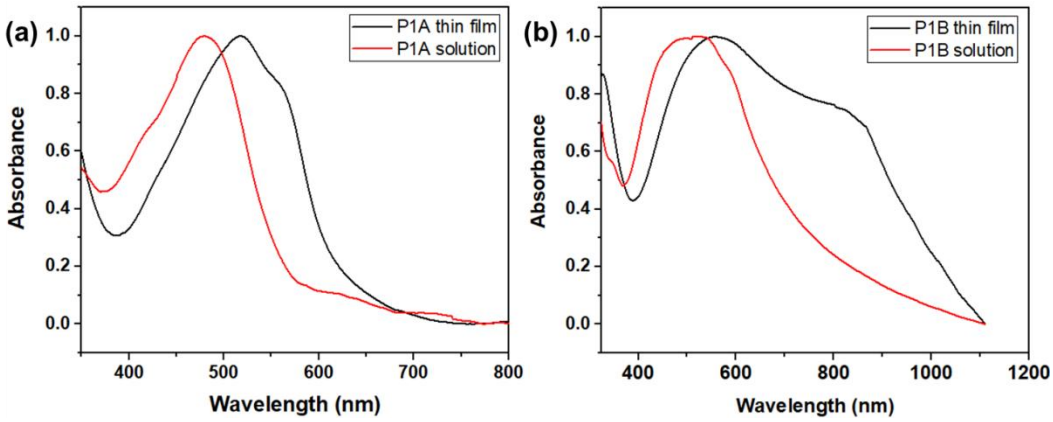


**Figure 3.2.** UV-Vis absorption spectra of polymers (a) **P1A** and (b) **P1B** in dilute $CHCl_3$ solution (red) and as thin film (black)

It should be noted that, a red-shift observation is one of the methods that signalize successfully achieved borylation. By referring to the article of Dailey and Turner et al. in the context of post-polymerization method, in which bathochromic shift was reported as a proof of borylation, in this study, similar profile observed when

polymers are compared for both solution and thin-film forms. However, here the shift was observed less than the recorded value of approximately 100 nm and above. In this study, the resulting bathochromic shift is recorded as approximately 30-40 nm. The reason for this lower shift may be caused from the borylation of only one repeating unit of the polymer. In the referred article, as the amount of borylated unit increases a larger red shift in the emission spectra was recorded. As a result, amount of units where boron is incorporated through partially borylation of the polymer may be the explanation of this recorded value of red shift observed in this study.

**Table 3-2** Recorded values of $\lambda_{max}$, $\lambda_{max}^{onset}$ and $E_g^{op}$ of **P1A** and **P1B**

| Polymer | Solution $\lambda_{max}$ (nm) | Thin-film $\lambda_{max}$ (nm) | $\lambda_{max}^{onset}$ (nm) | $E_g^{op}$ (eV) |
|---|---|---|---|---|
| **P1A** | 479 | 518 | 645 | 1.92 |
| **P1B** | 523 | 555 | 1098 | 1.13 |

Table 3-2 also gives the onset absorption maxima of the thin film spectra of polymers and resulting optical band gap values. From the absorption spectra of **P1A**, the onset of the thin-film absorption spectrum corresponds to the $\lambda_{max}$ value of 645 nm. Accordingly, the optical band gap of **P1A** was calculated to be 1.97 eV. On the other hand, the $\lambda_{max}$ and $E_g^{op}$ values of polymer **P1B** were found to be 1098 nm and 1.13 eV, respectively. Both the red-shifted absorption and the decrease in the optical band gap for **P1B** can be attributed to the incorporation of B-N units, which resulted in an extended absorption up to about 1000 nm in the NIR region.

## 3.2 Electrochemical Studies

To investigate the electronic properties, cyclic voltammogram consisting of a three-electrode system, in which Ag wire is the reference electrode (RE), platinum wire is the counter electrode (CE), and ITO coated glass is the working electrode (WE), is used. Polymers **RP1**, **RP2**, **RP3**, **P1A** and **P1B** were first dissolved in chloroform solvent, and then these solutions were spray coated onto ITO/glass. Three-electrode

system was immersed in a 0.1 M tetrabutylammonium hexafluorophosphate ($TBAPF_6$)/ acetonitrile (ACN) electrolyte solution. Single scan cyclic voltammograms were recorded at a scan rate of 100 mV/s and are shown in Figure 3.3. and Figure 3.4. Recorded oxidation and reduction onset potentials were used to estimate the HOMO and LUMO energy levels of polymers. Calculations of the frontier orbital levels were done by using the following equations:

$$E_{HOMO} = -(4.75 + E_{ox}^{onset})$$

$$E_{LUMO} = -(4.75 + E_{red}^{onset})$$

The above formulas can be used to determine the energy levels, HOMO and LUMO, and onset oxidation and reduction potentials are obtained with respect to ferrocene. This is due to calibration of CV by taking ferrocene/ferrocenium redox couple, abbreviated as Fc/Fc+, as a standard reference.

The electronic band gap, $E_g^{el}$ can be calculated by taking the difference between HOMO and LUMO levels as introduced in the following equation:

$$E_g^{el} = |E_{HOMO} - E_{LUMO}|$$

The cyclic voltammograms shown in Figure 3.3. represents the electrochemical redox behavior of polymers, which demonstrate the ambipolar characteristics of polymers **RP1**, **RP2** and **RP3** due to their n-doping and p-doping potentials obtained from these studies. The resulting values of oxidation-reduction potentials, HOMO-LUMO levels which were calculated using these potentials, and electronic band gaps of random polymers are recorded in Table 3-3.

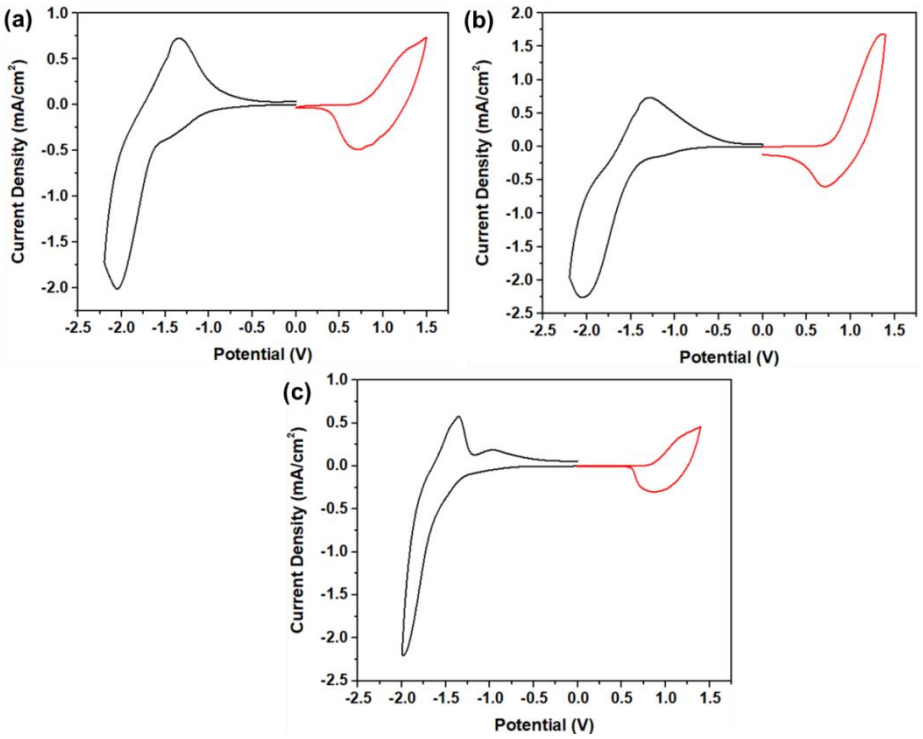


**Figure 3.3.** Single scan cyclic voltammograms of random polymers (a) **RP1**, (b) **RP2** and (c) **RP3** in 0.1 M $TBAPF_6$/ACN electrolyte solution

Using the above formulas, frontier orbital energy levels were calculated as show in Table 3-3. HOMO levels of **RP1**, **RP2** and **RP3** were obtained as -5.54, -5.56 and -5.57 eV, respectively. Similarly, LUMO levels were calculated and the results were obtained as -3.24, -3.31 and -3.25 eV for **RP1**, **RP2** and **RP3**, correspondingly. The differences between HOMO levels of polymers were found negligible. LUMO level was obtained as the lowest for **RP2**, whereas the difference between LUMO values of **RP1** and **RP3** were insignificant. As a result, lowest electronic band gap was obtained for **RP2** as 2.25 eV, and other $E_g^{el}$ values obtained for **RP1** and **RP3** were recorded as 2.30 and 2.32 eV, respectively.

**Table 3-3** Resulting oxidation-reduction potentials, HOMO-LUMO and $E_g^{el}$ values of polymers **RP1**, **RP2** and **RP3** extracted from cyclic voltammograms

| Polymer | $E_{p\text{-doping}}$ (V) | $E_{n\text{-doping}}$ (V) | $E_{ox}^{onset}$ (V) | $E_{red}^{onset}$ (V) | HOMO (eV) | LUMO (eV) | $E_g^{el}$ (eV) |
|---|---|---|---|---|---|---|---|
| **RP1** | 1.23 | -1.57 | 0.79 | -1.51 | -5.54 | -3.24 | 2.30 |
| **RP2** | 1.27 | -1.94 | 0.81 | -1.44 | -5.56 | -3.31 | 2.25 |
| **RP3** | 1.10 | -1.71 | 0.82 | -1.50 | -5.57 | -3.25 | 2.32 |

When comparing the band gap values obtained from optical and electrochemical studies of random polymers, $E_g^{el}$ values are found as greater than $E_g^{op}$ values, which is a general trend observed for these measurements in the literature. Moreover, as stated before, due to heavy Se atom insertion, the red-shifted absorption led to a decrease in the optical band gap for **RP3**, as predicted. However, electronic band gap of **RP3** was found as the largest value of 2.32 eV. This behavior can be attributed to the electrode-film interface charge barrier, in other words, an energy barrier generated at the interface between the polymer film surface and the electrode during the electrochemical oxidation-reduction process.

Cyclic voltammograms of **P1A** and **P1B** are shown in Figure 3.4. and the corresponding oxidation-reduction potentials, HOMO-LUMO levels and electronic band gap values are given in Table 3-4.

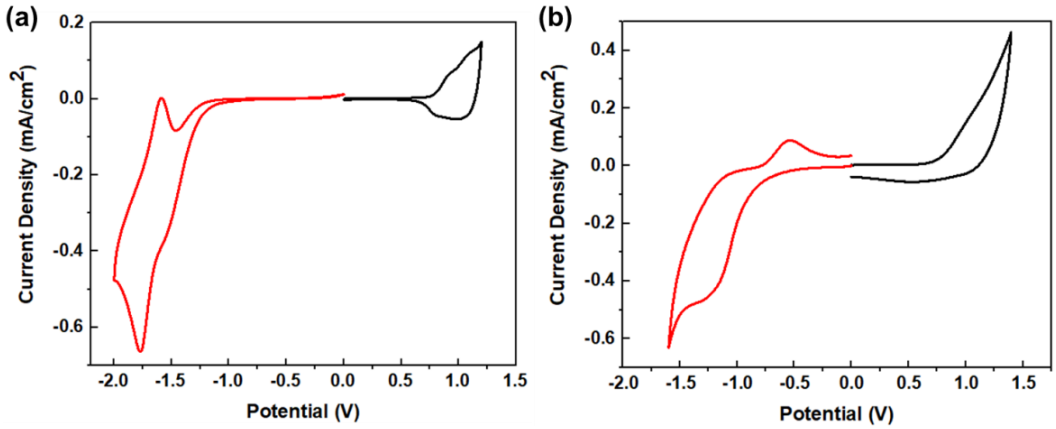


**Figure 3.4.** Single scan cyclic voltammograms of polymers (a) **P1A** and (b) **P1B** in 0.1 M $TBAPF_6$/ACN electrolyte solution

Initially, electrochemical studies were performed using the introduced three-electrode system and 0.1 M $TBAPF_6$/ACN electrolyte solution. To obtain clear oxidation-reduction peak observation different electrolyte solution was prepared with different salts. In this direction, sodium perchlorate ($NaClO_4$) and lithium perchlorate ($LiClO_4$) salts were dissolved in DCM and ACN solvent mixture, and electrodes were immersed in this 0.1 M of electrolyte solution. However, this enhancement procedure did not lead to a significant difference in cyclic voltammograms as compared with the resulting cyclic voltammograms obtained from previously performed procedure applied with 0.1 M $TBAPF_6$/ACN electrolyte solution. As a result of these studies, it was observed that polymers **P1A** and **P1B** possess p- and n-dopable features, and thus, ambipolar materials. Resulting data extracted from electrochemical studies of these polymers are reported in Table 3-4.

**Table 3-4** Resulting oxidation-reduction potentials, HOMO-LUMO and $E_g^{el}$ values of polymers **P1A** and **P1B** extracted from cyclic voltammograms

| Polymer | $E_{p\text{-doping}}$ (V) | $E_{n\text{-doping}}$ (V) | $E_{ox}^{onset}$ (V) | $E_{red}^{onset}$ (V) | HOMO (eV) | LUMO (eV) | $E_g^{el}$ (eV) |
|---|---|---|---|---|---|---|---|
| **P1A** | 0.87 | -1.53 | 0.75 | -1.23 | -5.50 | -3.52 | 1.98 |
| **P1B** | 1.03 | -1.15 | 0.77 | -0.46 | -5.52 | -4.29 | 1.23 |

The resulting values of onset oxidation and reduction potentials were used to calculate HOMO and LUMO levels of the polymers. As a result, HOMO and LUMO of **P1A** were recorded as -5.50 eV and -3.52 eV, while for **P1B** these values were found as -5.52 eV and -4.29 eV, respectively. By incorporation of B-N units, **P1B** displays lowered HOMO and LUMO levels. However, it should be noted that very large decrease in the LUMO level was observed, and as compared to the LUMO of the fullerene-based acceptor, this value is even lower. This very low-lying LUMO of **P1B** causes problems during the charge separation stage of the OPV device operation. The $E_g^{el}$ values of **P1A** and **P1B** were found to be 1.98 and 1.23 eV, respectively, which are larger than the $E_g^{op}$ values of the corresponding polymers as expected. The narrowed band gap and decreased HOMO-LUMO energy levels of **P1B** can be originated due to the electron-withdrawing property of B in the polymer backbone.

### 3.3 Thermal Studies

Thermal characteristics of polymers were investigated by TGA and DSC with heating rate of 10 °C/min under nitrogen atmosphere, and with differing temperature ranges between 25 °C to 600 °C and 25°C to 300 °C, respectively. In these analyses of polymers **P1A**, **P1B**, **RP1**, **RP2** and **RP3**, the weight of polymers over temperature were observed to indicate when polymers exhibit a weight loss with an increasing temperature conditions. According to the results obtained from TGA analyses, polymers **RP1** and **RP2** shows great thermal stabilities up to 200 °C. On the other hand, **RP3** exhibits thermal stability up to much higher temperature of 300 °C. For polymer **P1A**, the thermal stability started to decrease from 100 °C, and even much lower thermal stability was observed for boron-containing polymer **P1B**, which starts to loses weight above 60 °C. The recorded weight losses of polymer **RP1**, **RP2**, **RP3**, **P1A** and **P1B** were 62 %, 56 %, 49 %, 60 % and 54 %, respectively. DSC analyses of all polymers, which were carried out up to the maximum decomposition temperature, also indicates thermal features of materials upon heating and cooling.

These results, which are shown along with TGA analyses results in the appendices section, demonstrate correlation with results extracted from TGA analyses.

## 3.4 Photovoltaic Studies

### 3.4.1 Photovoltaic Studies of P1A and P1B

Photovoltaic characterizations of **P1A** and **P1B** polymers started with the examination of the fabricated cells by dissolving polymer:$PC_{71}BM$ mixtures in 1,2-dichlorobenzene ($C_6H_4Cl_2$) and chlorobenzene ($C_6H_5Cl$) and coating the prepared solutions without being filtered. Due to the solubility problems of the polymers and the thin films they form on the ITO substrates, these prepared solutions were coated without filtration in order to avoid material loss and to obtain thicker polymer films. As a result of three trials, it was determined that the solar cells consisting of active layers formed by the solutions coated without filtration did not work and showed short-circuit characteristics. Later, the same solutions were covered by filtration through polytetrafluoroethylene (PET) filters with a pore size of 0.45 μm, but it was understood that, although it showed photovoltaic properties in terms of current-voltage trend, it performed very poorly. Thereupon, it was decided to prepare the active layer solutions with a different solvent. In this direction, chloroform-based solutions were prepared and optimizations were made for both polymers. In the first stage, cells were tried to be produced with filtered solutions, but it was observed that the solutions prepared in chloroform were not filtered through PET filters. Therefore, solar cell fabrication and characterization were carried out by coating the same solutions without filtering. The results of this characterization are reported in Table 3-5.

**Table 3-5** Photovoltaic properties of **P1A** and **P1B** containing solar cells fabricated using chloroform-based active layer solutions

| Polymers | Polymer:$PC_{71}BM$ (w:w) | Rpm | $J_{SC}$ ($mA/cm^2$) | $V_{OC}$ (V) | FF (%) | PCE (%) |
|---|---|---|---|---|---|---|
| **P1A** | 1:3, 20 mg/mL | 1500 | 0.58 | 0.61 | 0.48 | 0.17 |
| **P1A** | 1:3, 20 mg/mL | 3000 | 1.08 | 0.62 | 0.45 | 0.30 |
| **P1B** | 1:3, 20 mg/mL | 3000 | 0.23 | 0.55 | 0.29 | 0.04 |

As a result of the first characterizations made in Table 3-5, it was observed that the polymers performed better in the active layer solutions obtained by dissolving in chloroform. This can be explained by the better solubility of polymers in solvents, the ability to form thicker films or the improved morphology. However, it was decided to try 1,2-dichlorobenzene and chlorobenzene chloroform solvent systems, as observed in the previous studies that polymer solutions performed better by filtration. In these systems, it is aimed to benefit from the increase of chloroform on the photovoltaic performance of polymers and the effect of the other solvents mentioned on the polymer-based mixtures to form leachable solutions. Photovoltaic performances of **P1A**-based solar cells prepared using these solvent systems are summarized in Table 3-6. The photovoltaic properties of the active layer solution containing **P1B** dissolved in 1,2-dichlorobenzene are also shown in Table 3-6.

**Table 3-6** Photovoltaic performances of **P1A** and **P1B** based organic solar cells using different solvent systems

| Polymers | Polymer:$PC_{71}BM$ (w:w) | Solvent System | $J_{SC}$ ($mA/cm^2$) | $V_{OC}$ (V) | FF (%) | PCE (%) |
|---|---|---|---|---|---|---|
| **P1A** | 1:3, 20 mg/mL | $C_6H_4Cl_2$:$CHCl_3$ | 0.25 | 0.48 | 0.28 | 0.03 |
| **P1A** | 1:3, 20 mg/mL | $C_6H_5Cl$: $CHCl_3$ | 0.67 | 0.46 | 0.36 | 0.11 |
| **P1B** | 1:3, 20 mg/mL | $C_6H_4Cl_2$ | 0.35 | 0.56 | 0.31 | 0.06 |

Corresponding J-V curves representing the photovoltaic performances of polymers **P1A** and **P1B** are given in Figure 3.5., Figure 3.6. and Figure 3.7..

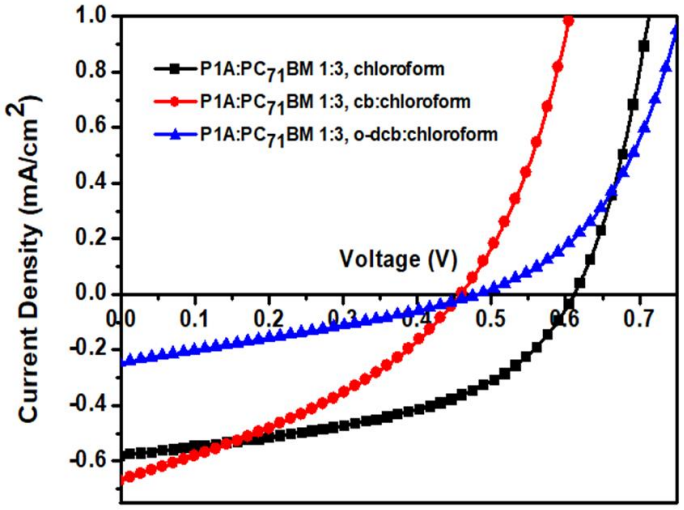


**Figure 3.5**. J-V curve summarizing the solvent optimization of **P1A**-based OPVs

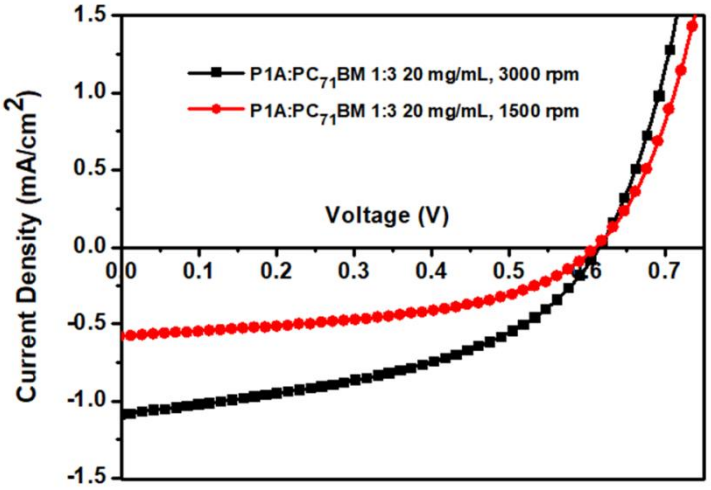


**Figure 3.6.** J-V curve summarizing the thickness optimization of **P1A**-based OPVs prepared using chloroform

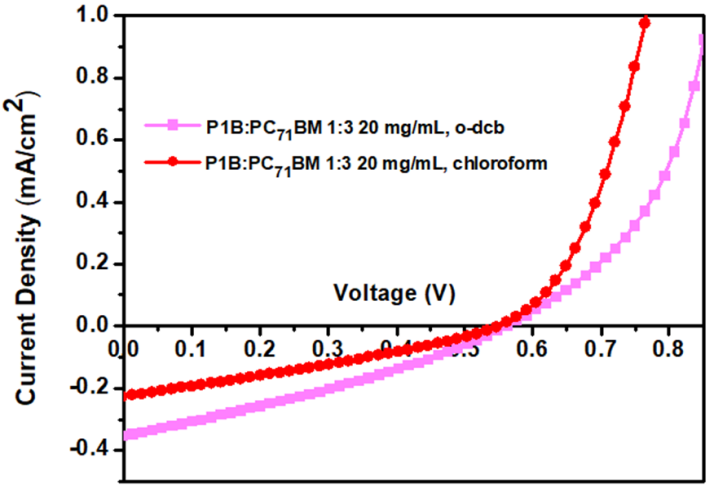


**Figure 3.7.** J-V curve summarizing the solvent optimization of **P1B**-based OPVs

Considering the photovoltaic performances of organic solar cells fabricated using different solvent systems, it was observed that the optimum conditions were obtained for **P1A** using chloroform, and for **P1B** using 1,2-dichlorobenzene. The energy level diagram of the solar cells created using the mixture of polymers **P1A** and **P1B** with $PC_{71}BM$ is given in Figure 3.8.

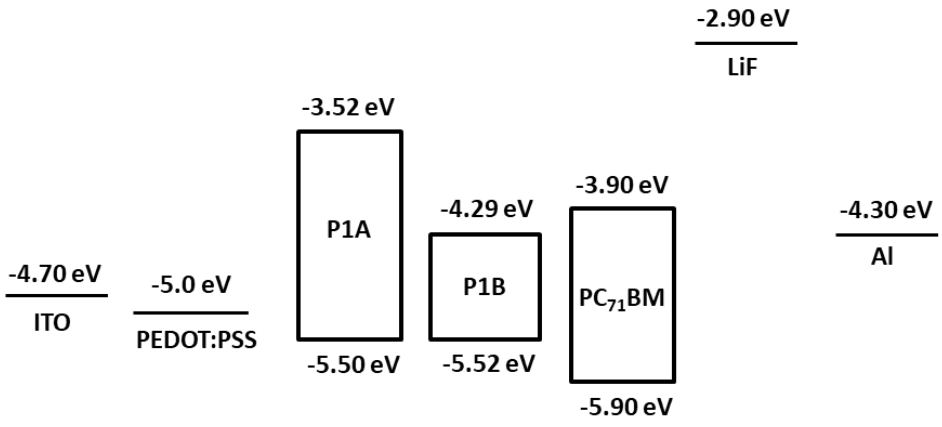


**Figure 3.8.** Energy level diagrams of **P1A** and **P1B** based organic solar cells

The relatively low photovoltaic performance of the **P1A** polymer can be explained by the low solubility that the polymer exhibits. As observed in the experimental stage, the polymers showed the highest solubility in chloroform among the solvent systems used. For this reason, it is an expected result that among the non-filtered

solutions, results can be achieved using a chloroform-based system. However, the problem that occurred with other non-filtered systems also occurred with chloroform-based systems prepared for highly concentrated mixtures. When the concentration of chloroform-based solutions was increased in order to increase the current values, it was observed that the fabricated solar cells lost their photovoltaic features. In the filtered solvent systems, some filtration problems were experienced, and although the solubility increased, it is understood that the majority of the molecules had solubility problems in the mixture. Very thin films of the active layers coated on the substrates also highlights that the filtered solutions are poor in polymers. This indicates that insoluble molecules remained in the filter during filtration. Thus, thin films obtained caused a decrease in currents, resulting in these systems to exhibit lower photovoltaic properties than chloroform-based systems.

The energy level diagram in Figure 3.8. shows that **P1B** is not suitable for OPV applications. The LUMO level of the polymer is -4.29 eV, which is incompatible with $PC_{71}BM$. Excited electrons are not expected to carry out transition from a more stable energy level to a more unstable one. The high LUMO level of $PC_{71}BM$ relative to the polymer makes charge separation difficult and results in poor performance of the polymer.

### 3.4.2 Photovoltaic Studies of RP1, RP2 and RP3

Initially, photovoltaic characterizations of polymers **RP1**, **RP2** and **RP3** were based on the study of fabricated OPVs by dissolving polymer:$PC_{71}BM$ mixtures in 1,2-dichlorobenzene ($C_6H_4Cl_2$) and chlorobenzene ($C_6H_5Cl$) solvents and coating after filtration. However, due to much thinner and poorer film formations on the ITO substrates, these prepared solutions are coated without filtration. This was performed to avoid loss of material as most of the polymers remained in the filter during filtration, and also to obtain thicker polymer films. Due to the poor thin-films obtained with these solvents, active layer solutions of the polymers were prepared using chloroform solvent. However, it is known that the solvents chlorobenzene and

1,2-dichlorobenzene are usually preferred to observe better thin-film forms of the active layer. Moreover, they can be used as co-solvents which have an impact on the morphology and efficiency of OPVs. Unfortunately, the use of chlorobenzene and 1,2-dichlorobenzene as co-solvents did not lead to the formation of better thin-films due to the higher volatility of $CHCl_3$. As a result, it was decided to use these solvents as an additive again with $CHCl_3$ solvent, which resulted in poor thin-film observations as before. Finally, $CHCl_3$ solvent was used to prepare the active layer solutions, which resulted in better thin-film surfaces.

Proper selection of the solvent was followed by several optimizations that were carried out to achieve desired values of the solar cell parameters. First optimizations were based on the polymer:$PC_{71}BM$ blend ratios. Subsequently, concentration of the blended polymer:$PC_{71}BM$ and thickness of the active layer were optimized with various spin coating rates. Finally, additive treatments were performed to achieve higher device performances. In the following, all optimizations were presented for the devices based on **RP1**, **RP2** and **RP3** in the Table 3-7, Table 3-8 and Table 3-9, respectively.

**Table 3-7** Device parameters of **RP1**-based OPVs

| **RP1**:$PC_{71}BM$ (w:w) | Additive Treatment | Rpm | $J_{SC}$ ($mA/cm^2$) | $V_{OC}$ (V) | FF (%) | PCE (%) |
|---|---|---|---|---|---|---|
| 1:1, 20 mg/mL | - | 2000 | 3.08 | 0.69 | 43 | 0.92 |
| 1:2, 20 mg/mL | - | 2000 | 3.69 | 0.72 | 46 | 1.23 |
| 1:3, 20 mg/mL | - | 2000 | 3.92 | 0.74 | 47 | 1.36 |
| 1:4, 20 mg/mL | - | 2000 | 2.96 | 0.74 | 50 | 1.10 |
| 1:3, 30 mg/mL | - | 2000 | 1.30 | 0.73 | 39 | 0.36 |
| 1:3, 35 mg/mL | - | 2000 | 1.08 | 0.73 | 43 | 0.34 |
| 1:1, 20 mg/mL | - | 2000 | 3.08 | 0.69 | 43 | 0.92 |
| 1:3, 20 mg/mL | - | 1500 | 3.19 | 0.74 | 50 | 1.18 |
| 1:3, 20 mg/mL | - | 2500 | 4.21 | 0.76 | 49 | 1.53 |

**Table 3-7** Device parameters of **RP1**-based OPVs (continued)

| | | | | | | |
|---|---|---|---|---|---|---|
| 1:3, 20 mg/mL | 2% DIO | 2500 | 4.09 | 0.72 | 53 | 1.56 |
| **1:3, 20 mg/mL** | **3% DPE** | **2500** | **4.51** | **0.68** | **55** | **1.68** |
| 1:3, 20 mg/mL | 6% DPE | 2500 | 3.55 | 0.70 | 56 | 1.40 |

**Table 3-8** Device parameters of **RP2**-based OPVs

| **RP2**:$PC_{71}BM$ (w:w) | Additive Treatment | Rpm | $J_{SC}$ ($mA/cm^2$) | $V_{OC}$ (V) | FF (%) | PCE (%) |
|---|---|---|---|---|---|---|
| 1:2, 20 mg/mL | - | 2500 | 3.07 | 0.65 | 37 | 0.76 |
| **1:3, 20 mg/mL** | **-** | **2500** | **3.79** | **0.69** | **44** | **1.15** |
| 1:4, 20 mg/mL | - | 2500 | 3.21 | 0.68 | 43 | 0.96 |
| 1:3, 30 mg/Ml | - | 2500 | 2.16 | 0.67 | 43 | 0.63 |
| 1:3, 20 mg/mL | - | 3500 | 1.51 | 0.65 | 32 | 0.32 |
| 1:3, 20 mg/mL | 3% DPE | 2500 | 4.28 | 0.63 | 35 | 0.98 |

**Table 3-9** Device parameters of **RP3**-based OPVs

| **RP3**:$PC_{71}BM$ (w:w) | Rpm | $J_{SC}$ ($mA/cm^2$) | $V_{OC}$ (V) | FF (%) | PCE (%) |
|---|---|---|---|---|---|
| 1:1, 20 mg/mL | 2500 | 3.44 | 0.65 | 37 | 0.76 |
| 1:2, 20 mg/mL | 2500 | 3.89 | 0.69 | 44 | 1.15 |
| **1:3, 20 mg/mL** | **2500** | **5.24** | **0.81** | **51** | **2.14** |
| 1:4, 30 mg/Ml | 2500 | 3.54 | 0.81 | 52 | 1.49 |
| 1:3, 20 mg/mL | 2000 | 5.24 | 0.77 | 43 | 0.61 |
| 1:3, 20 mg/mL | 3000 | 3.70 | 0.81 | 50 | 1.49 |
| 1:3, 15 mg/mL | 2500 | 4.17 | 0.84 | 56 | 1.99 |
| 1:3, 30 mg/mL | 3500 | 3.13 | 0.81 | 53 | 1.52 |

Energy level representation of the polymers with $PC_{71}BM$ was given in Figure 3.9., below. Corresponding J-V curves indicate the photovoltaic performances of the OPV devices based on polymers **RP1**, **RP2** and **RP3** are presented in Figure 3.10., Figure 3.11. and Figure 3.12., respectively.

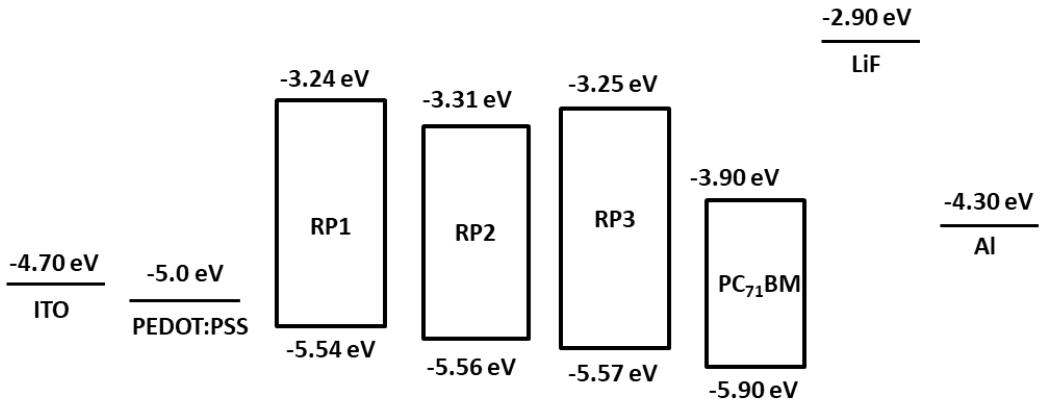


**Figure 3.9.** Energy level representation of the polymers **RP1**, **RP2** and **RP3** with materials used in fabricating OPVs

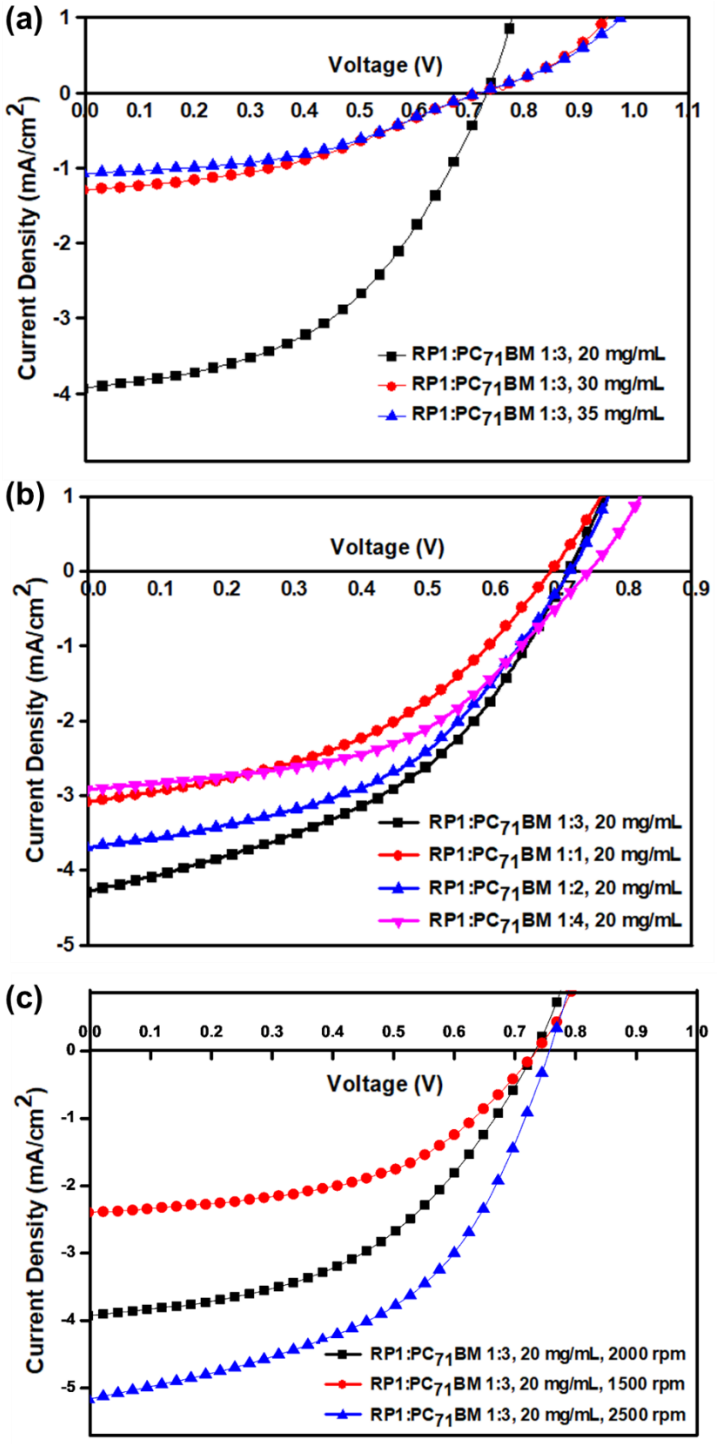


**Figure 3.10.** J-V curves of the OPV devices based on **RP1**:$PC_{71}BM$ summarizing optimization of (a) blend concentrations, (b) D/A ratios, (c) spin coating rates

By the optimization studies of the OPV devices based on **RP1**: $PC_{71}BM$ given in Figure 3.10. and Table 3-7, the current density of the device increased with an optimized polymer concentration of 20 mg/mL. In addition, both $V_{OC}$ and $J_{SC}$ increased when D/A blend ratio was adjusted as 1:3 **RP1**:$PC_{71}BM$. For **RP1**-containing OPV device, thickness of the active layer had an impact on the photovoltaic performances. Normally, decrease in the spin coating rates result in thicker active layer forms, which results in better photovoltaic performances. However, since chloroform solvent was used to prepare active layer solutions, spin coating of the active layer was applied with higher rpm values due to high volatility of $CHCl_3$. Among the introduced values, spin coating of the active layer solution with a 2500 rpm was observed with better device parameters. Moreover, additive treatments were performed using diphenyl ether (DPE) and diiodooctane (DIO), and with the help of these treatments, the best result was achieved with 3% DPE addition to the active layer. This can be addressed to better thin-film formation, which can be stated as the morphological enhancement of the active layer, due to additive effect, and also to the remarkable increase in FF value. As a result, **RP1**-containing device was observed with the best PCE (%) of 1.68, with 4.51 $mA/cm^2$ of $J_{SC}$ value, 0.68 V of $V_{OC}$ and FF (%) value of 55.

The following figure, Figure 3.11., represents the optimizations of the OPV devices based on **RP2**:$PC_{71}BM$, which was also given in Table 3-8 in detail. Here, 20 mg/mL blend concentration of **RP1**:$PC_{71}BM$ were resulted in better performances as compared with the resulting device parameters with 30 mg/mL blend concentration, which can be attributed to the increase in current density and FF of the device. For the D/A ratio optimization studies, with 1:3 blend ratio of **RP2**: $PC_{71}BM$, the best PCE (%) was achieved as 1.15. For the best resulting device performance, $J_{SC}$, $V_{OC}$ and FF (%) values were achieved as 3.79 $mA/cm^2$, 0.69 V and 44, respectively. On the other hand, spin coating rate of the active layer and additive treatment were found as ineffective to enhance device performances of **RP2**-based OPVs, which can be seen in Table 3-8 containing all the data of device parameters with corresponding optimizations.

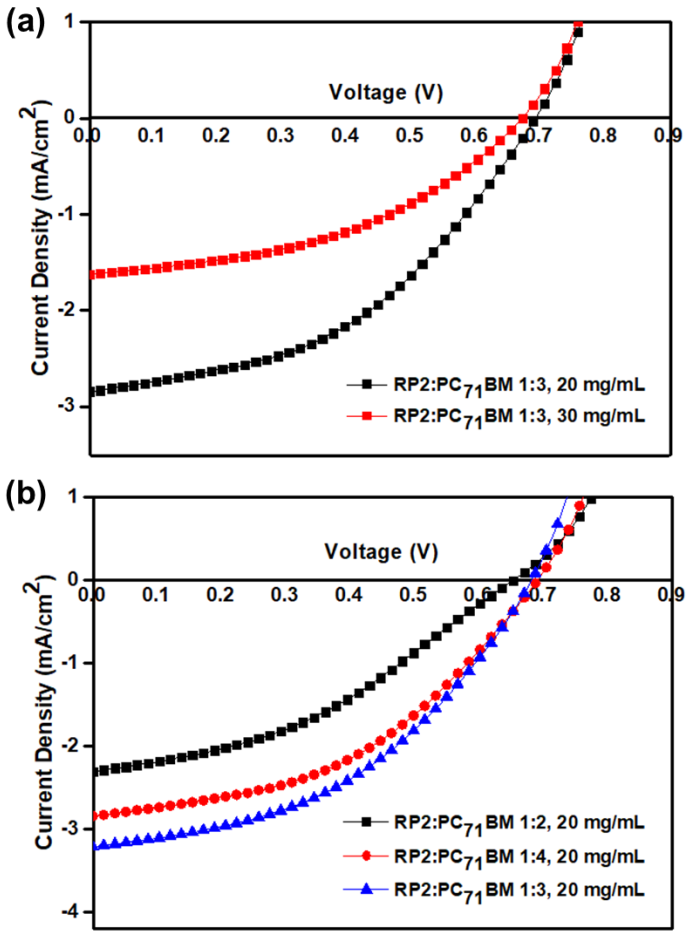


**Figure 3.11.** J-V curves of the OPV devices based on **RP2**:$PC_{71}BM$ summarizing optimization of (a) blend concentrations and (b) D/A ratios

Lastly, device applications of **RP3** were performed and the resulting data for performed optimizations were given in the following figure, Figure 3.12. and Table 3-9. With 20 mg/mL blend concentration of the polymer **RP3** and $PC_{71}BM$, a significant increase in current density has been noticed. The optimization studies of D/A ratio resulted in lower FF values for 1:1 and 1:2 ratio of polymer and fullerene-based acceptor. However, when two other D/A ratio was examined, FF values were significantly increased up to 51 for 1:3 ratio, and 52 for 1:4 ratio of **RP3**: $PC_{71}BM$. Although 1:4 ratio has a higher FF value, with 1:3 D/A ratio, a remarkably high current density was obtained as 5.24 $mA/cm^2$ due to increase in polymer concentration with 1:3 ratio, which is important for the absorption ability. An optimum spin coating rate of 2500 rpm was determined for the coating of the active

layer. Additive treatments were also performed, but negative effect on the device performances was unfortunately obtained. As a result, after all the optimizations were completed, the best efficiency was obtained among all devices fabricated with **RP1**, **RP2** and **RP3**. As mentioned before, this great efficiency can be attributed to the formation of inter-chain Se-Se interactions to provide higher charge carrier mobility and lower aromaticity of benzoselenadiazole for **RP3**. The best PCE (%) was obtained as 2.14 for the device fabricated with **RP3**: $PC_{71}BM$ (1:3, 20 mg/mL), of which active layer was spin coated with 2500 rpm. $J_{SC}$, $V_{OC}$ and FF values were also found to be 5.24 mA/cm$^2$, 0.81 V and 51, respectively.

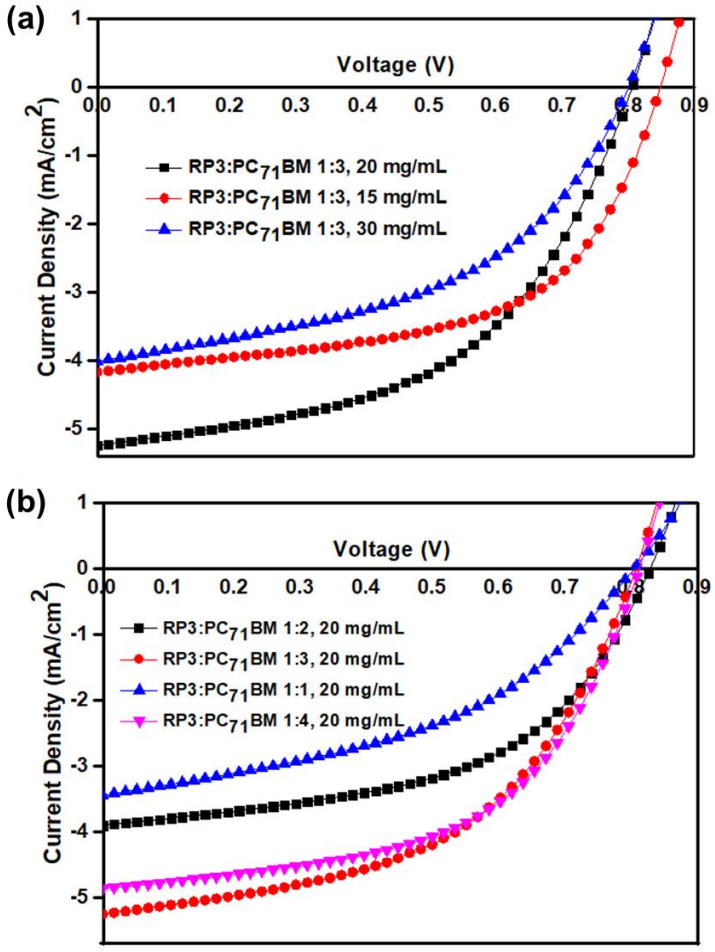


**Figure 3.12.** J-V curves of the OPV devices based on **RP3**:$PC_{71}BM$ summarizing optimization of (a) blend concentrations and (b) D/A ratios

## 3.5 Morphology

In general, high performances obtained from the OPV devices are significantly rely on the optimized BHJ morphology to achieve extraordinary photovoltaic properties due to charge separation and charge transport features. To achieve the final active layer morphology of these devices, several different optimization and enhancement techniques were applied. Atomic Force Microscopy (AFM) and Transmission Electron Microscopy (TEM) were utilized to gain information about the morphology of the fabricated devices based on polymers **RP1**, **RP2** and **RP3**. Unfortunately, due to very poor PCE values of OPVs containing non-borylated and borylated polymers, **P1A** and **P1B**, morphology results could not be obtained for these polymers. Figure 3.13. and Figure 3.14. represents, AFM and TEM images of the devices based on all random polymers with the best efficiency, respectively.

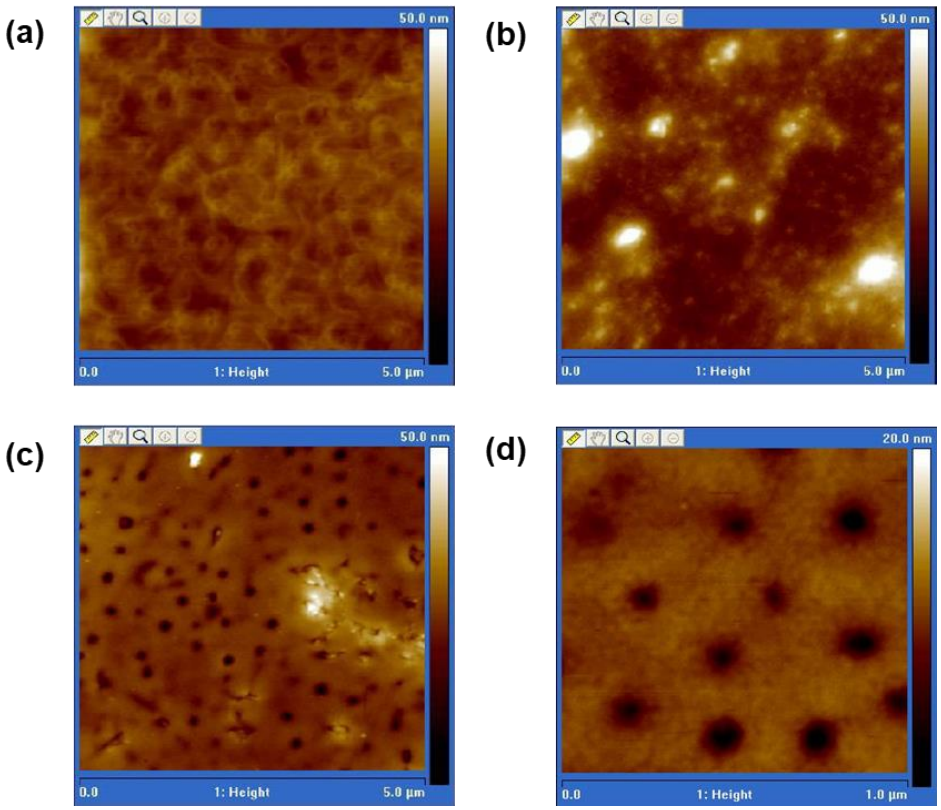


**Figure 3.13.** AFM images of the best performed devices (a) **RP1**:$PC_{71}BM$ (1:3, w:w), (b) **RP1**: $PC_{71}BM$ (1:3, w:w) with the additive DPE, (c) **RP2**:$PC_{71}BM$ (1:3, w:w) and (d) **RP3**:$PC_{71}BM$ (1:3, w:w)

According to the results of AFM analyses, surface roughness values of 2.41 nm, 6.09 nm, 7.72 nm and 1.59 nm were obtained for the OPVs based on **RP1**:$PC_{71}BM$ (1:3, w:w), **RP1**:$PC_{71}BM$ (1:3, w:w) with the additive DPE, **RP2**:$PC_{71}BM$ (1:3, w:w) and **RP3**:$PC_{71}BM$ (1:3, w:w), respectively. Active layer thicknesses of the best devices containing **RP1**, **RP1** with the additive DPE, **RP2** and **RP3** were measured and reported as 84 nm, 101 nm, 129 nm and 97 nm correspondingly. Figure 3.14. presents TEM images of the best performed devices to provide a detailed explanation of the surface morphologies.

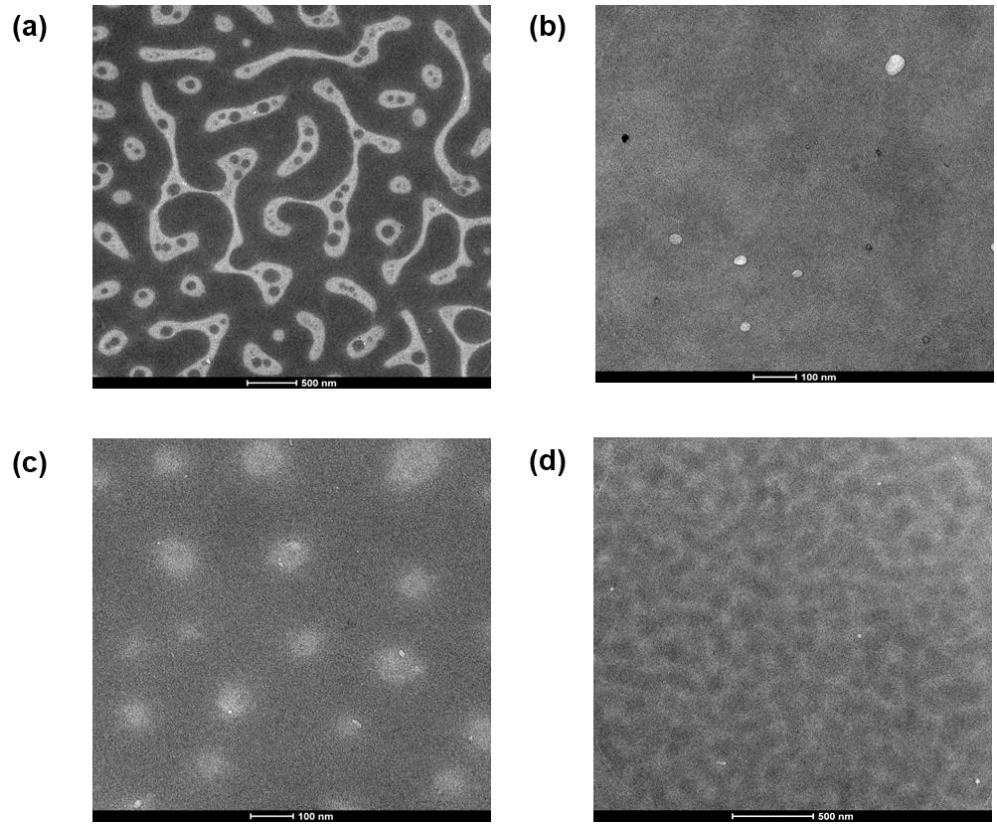


**Figure 3.14.** TEM images of the best performed devices (a) **RP1**:$PC_{71}BM$ (1:3, w:w), (b) **RP1**: $PC_{71}BM$ (1:3, w:w) with the additive DPE, (c) **RP2**:$PC_{71}BM$ (1:3, w:w) and (d) **RP3**:$PC_{71}BM$ (1:3, w:w)

The photoactive layer of the device containing **RP1**:$PC_{71}BM$ (1:3, w:w) was introduced with 3% DPE additive, which led to the enhancement of the photovoltaic performance. Compared to the non-additive analogue of the **RP1** containing device, a significant morphological enhancement can be observed, which correlates with an

increase in PCE (%) from 1.53 to 1.68. In the presence of 3% DPE, a homogeneous distribution of polymer and fullerene acceptor in the active layer was achieved. Moreover, nanofibrillar networks and efficient charge transport pathways were possibly achieved using the 3% DPE treatment as a solvent additive. On the other hand, AFM and TEM images of **RP2**:$PC_{71}BM$ (1:3, w:w) show that poor thin-film morphology and inhomogeneous distribution of the active layer were obtained, which correlates with the low PCE (%) of 1.15. According to TEM image shown in Figure 3.14., in which brighter areas are polymer rich and darker areas are $PC_{71}BM$ rich, active layer consisting of **RP2**:$PC_{71}BM$ (1:3, w:w) created a less interpenetrated donor acceptor network. Bicontinuous network is more obvious for the blend morphology of **RP3**:$PC_{71}BM$ (1:3, w:w), which might have provided an enhanced charge separation and ease of charge transportation to the electrodes. As a result, this morphology explains the high efficiency of 2.14% for the device containing **RP3**.

# CHAPTER 4

# CONCLUSIONS

In this thesis, the effect of two different subjects were investigated for the photovoltaic applications of organic conjugated polymers. The effect of boron was investigated by incorporating boron units into the conjugated system, which aimed to provide unique properties such as tunable optoelectronic features, enhanced charge transport characteristics and finally improved performance in OPV devices. This study was investigated using a recently reported post-polymerization borylation method applied to BDT and Py containing non-borylated **P1A**, resulting in a partially borylated polymer **P1B**. GPC analyzes and optical studies revealed an increase in the molecular weight and red-shifted absorption for **P1B** compared to **P1A**, which signilizes the successful borylation. Based on the results of the electrochemical and optical studies, it can be said that very low-lying LUMO of **P1B** leads to incompatibility with $PC_{71}BM$ and indicates that this polymer is not suitable for photovoltaic applications. Although the integration of the boron moiety is expected to improve the photovoltaic properties of the system according to the literature review, an efficiency of 0.06% was obtained for borylated polymer **P1B**, which correlates with the mismatched energy levels. Very poor efficiency was also determined for the non-borylated polymer **P1A** as 0.30%, which can be attributed to the poor thin-film formation of the active layer. Moreover, thermal analyzes of **P1B** demonstrate a lower thermal stability as compared to the non-borylated analogue. In the study of heteroatom effect, **RP1**, **RP2** and **RP3** random polymers containing BDT, Py and benzazole acceptors of benzotriazole, benzothiadiazole and benzoselenadiazole, respectively, were synthesized based on the one donor-two acceptor $(D\text{-}A_1)$-$(D\text{-}A_2)$ system. This study was carried out to investigate the effect of altering a single heteroatom of the benzazole acceptor units on the optical, electronic and photovoltaic properties of the synthesized polymers. The optical

studies revealed red-shifted absorptions from solution form to thin-film, which is expectedly due to great aggregation and stronger intramolecular interactions in the thin film forms. On the other hand, results of the electrochemical studies reveal their ambipolar characteristics and suitable HOMO-LUMO and electronic band gap values for solar cell applications. Thermal analyzes of polymers from DSC and TGA show that all three polymers exhibit high thermal stability. As a result of photovoltaic studies, PCE (%) of the best efficient devices were found to be 1.68 for **RP1**, 1.15 for **RP2** and 2.14 for **RP3**. These efficiencies, which are lower than expected, can be attributed to the low molecular weights of these polymers, since molecular weights can affect the effective conjugated chain length and change the optoelectronic properties of polymers, in general. Thus, with higher molecular weight polymers, the efficiencies of OPVs would be much higher. On the other hand, morphological analyzes indicate a correlation of the obtained efficiencies, which can be reported as morphological enhancement for **RP1** with 3% DPE additive treatment, poor thin-film morphology of the active layer containing **RP2**, and bicontinuous interpenetrating D-A network of the blend morphology of the active layer containing **RP3**. According to these observations, polymers **P1A** and **P1B** are incompatible materials for solar cell applications; however, random polymers **RP1**, **RP2** and **RP3** are promising materials that can be used to achieve promising and efficient OPV devices.

## REFERENCES


[1] T. M. Razykov, C. S. Ferekides, D. Morel, E. Stefanakos, H. S. Ullal, and H. M. Upadhyaya, "Solar photovoltaic electricity: Current status and future prospects," *Sol. Energy*, vol. 85, no. 8, pp. 1580–1608, 2011, doi: 10.1016/j.solener.2010.12.002.

[2] P. G. V. Sampaio and M. O. A. González, "Photovoltaic solar energy: Conceptual framework," *Renew. Sustain. Energy Rev.*, vol. 74, no. March, pp. 590–601, 2017, doi: 10.1016/j.rser.2017.02.081.

[3] S. Shauddin, "Comparison among Various Emerging PV Cells with History, Current Status and Future Challenges," *Energy and Power*, vol. 3, no. 6, pp. 91–105, 2013, doi: 10.5923/j.ep.20130306.01.

[4] S. Sinha, D. K. Nandi, P. S. Pawar, S. H. Kim, and J. Heo, "A review on atomic layer deposited buffer layers for Cu(In,Ga)Se2 (CIGS) thin film solar cells: Past, present, and future," *Sol. Energy*, vol. 209, no. August, pp. 515–537, 2020, doi: 10.1016/j.solener.2020.09.022.

[5] E. Kabir, P. Kumar, S. Kumar, A. A. Adelodun, and K. H. Kim, "Solar energy: Potential and future prospects," *Renew. Sustain. Energy Rev.*, vol. 82, no. September 2016, pp. 894–900, 2018, doi: 10.1016/j.rser.2017.09.094.

[6] K. Fukuda, K. Yu, and T. Someya, "The Future of Flexible Organic Solar Cells," *Adv. Energy Mater.*, vol. 10, no. 25, pp. 1–10, 2020, doi: 10.1002/aenm.202000765.

[7] H. Machrafi, *Green Energy and Technology*. 2012.

[8] "Champion-Module-Efficiencies.20200708.Pdf." 2020.

[9] M. C. Scharber and N. S. Sariciftci, "Efficiency of bulk-heterojunction organic solar cells," *Prog. Polym. Sci.*, vol. 38, no. 12, pp. 1929–1940, 2013, doi: 10.1016/j.progpolymsci.2013.05.001.

[10] G. Dennler, M. C. Scharber, and C. J. Brabec, "Polymer-fullerene bulk-heterojunction solar cells," *Adv. Mater.*, vol. 21, no. 13, pp. 1323–1338, 2009, doi: 10.1002/adma.200801283.

[11] A. J. Heeger, "25th anniversary article: Bulk heterojunction solar cells: Understanding the mechanism of operation," *Adv. Mater.*, vol. 26, no. 1, pp. 10–28, 2014, doi: 10.1002/adma.201304373.

[12] T. H. Lai, S. W. Tsang, J. R. Manders, S. Chen, and F. So, "Properties of interlayer for organic photovoltaics," *Mater. Today*, vol. 16, no. 11, pp. 424–432, 2013, doi: 10.1016/j.mattod.2013.10.001.

[13] A. J. Breeze, “Next generation thin -film solar cells,” pp. 168–171, 2008.

[14] N. K. Elumalai and A. Uddin, “Open circuit voltage of organic solar cells: An in-depth review,” *Energy Environ. Sci.*, vol. 9, no. 2, pp. 391–410, 2016, doi: 10.1039/c5ee02871j.

[15] B. Qi and J. Wang, “Open-circuit voltage in organic solar cells,” *J. Mater. Chem.*, vol. 22, no. 46, pp. 24315–24325, 2012, doi: 10.1039/c2jm33719c.

[16] S. R. Cowan, A. Roy, and A. J. Heeger, “Recombination in polymer-fullerene bulk heterojunction solar cells,” *Phys. Rev. B - Condens. Matter Mater. Phys.*, vol. 82, no. 24, pp. 1–10, 2010, doi: 10.1103/PhysRevB.82.245207.

[17] U. Rau and H. W. Schock, *Cu(In,Ga)Se2 thin-film solar cells*. Elsevier Ltd, 2018.

[18] M. S. Kim, B. G. Kim, and J. Kim, “Effective variables to control the fill factor of organic photovoltaic cells,” *ACS Appl. Mater. Interfaces*, vol. 1, no. 6, pp. 1264–1269, 2009, doi: 10.1021/am900155y.

[19] Y. Gao, M. Liu, Y. Zhang, Z. Liu, Y. Yang, and L. Zhao, “Recent development on narrow bandgap conjugated polymers for polymer solar cells,” *Polymers (Basel).*, vol. 9, no. 2, 2017, doi: 10.3390/polym9020039.

[20] A. Armin, M. Velusamy, P. Wolfer, Y. Zhang, P. L. Burn, and P. Meredith, “Quantum E ffi ciency of Organic Solar Cells: Electro-Optical Cavity Considerations,” 2014.

[21] O. Amargos Reyes, M. D. Barreiro-Arguelles, Á. D. Romero-Borja, J.-L. Maldonado, and J. A. Gaspar Armenta, “Active thin film variation in OPV cells and analysis through external and internal quantum efficiency,” no. September 2018, p. 101, 2018, doi: 10.1117/12.2322638.

[22] M. Audenaert, G. Gusman, and R. Deltour, “Electrical conductivity of I2-doped polyacetylene,” *Phys. Rev. B*, vol. 24, no. 12, pp. 7380–7382, 1981, doi: 10.1103/PhysRevB.24.7380.

[23] Z. Zhang, M. Liao, H. Lou, Y. Hu, X. Sun, and H. Peng, “Conjugated Polymers for Flexible Energy Harvesting and Storage,” *Adv. Mater.*, vol. 30, no. 13, pp. 1–19, 2018, doi: 10.1002/adma.201704261.

[24] D. Khokhar, S. Jadoun, R. Arif, and S. Jabin, “Functionalization of conducting polymers and their applications in optoelectronics,” *Polym. Technol. Mater.*, vol. 60, no. 5, pp. 463–485, 2021, doi: 10.1080/25740881.2020.1819312.

[25] C. M. So and F. Y. Kwong, “Palladium-catalyzed cross-coupling reactions of aryl mesylates,” *Chem. Soc. Rev.*, vol. 40, no. 10, pp. 4963–4972, 2011, doi: 10.1039/c1cs15114b.

[26] A. Perveen and M. Qaiser, “Pollen Flora of Pakistan-Lix. linaceae,” *Pakistan J. Bot.*, vol. 40, no. 5, pp. 1819–1822, 2008.

[27] L. G. Mercier and M. Leclerc, “Direct (hetero)arylation: A new tool for polymer chemists,” *Acc. Chem. Res.*, vol. 46, no. 7, pp. 1597–1605, 2013, doi: 10.1021/ar3003305.

[28] C. Cordovilla, C. Bartolomé, J. M. Martínez-Ilarduya, and P. Espinet, “The stille reaction, 38 years later,” *ACS Catal.*, vol. 5, no. 5, pp. 3040–3053, 2015, doi: 10.1021/acscatal.5b00448.

[29] P. Espinet and A. M. Echavarren, “The mechanisms of the Stille reaction,” *Angew. Chemie - Int. Ed.*, vol. 43, no. 36, pp. 4704–4734, 2004, doi: 10.1002/anie.200300638.

[30] G. Anguera and D. Sánchez-García, “Applications in Optoelectronics,” *Afinidad*, vol. 71, no. 568, pp. 8–20, 2014.

[31] E. Bundgaard and F. C. Krebs, “Low band gap polymers for organic photovoltaics,” *Sol. Energy Mater. Sol. Cells*, vol. 91, no. 11, pp. 954–985, 2007, doi: 10.1016/j.solmat.2007.01.015.

[32] B. G. Kim *et al.*, “Energy level modulation of HOMO, LUMO, and band-gap in conjugated polymers for organic photovoltaic applications,” *Adv. Funct. Mater.*, vol. 23, no. 4, pp. 439–445, 2013, doi: 10.1002/adfm.201201385.

[33] E. E. Havinga, W. ten Hoeve, and H. Wynberg, “Alternate donor-acceptor small-band-gap semiconducting polymers; Polysquaraines and polycroconaines,” *Synth. Met.*, vol. 55, no. 1, pp. 299–306, 1993, doi: 10.1016/0379-6779(93)90949-W.

[34] N. Co-investigator, “Donor-Acceptor Methods for Band Gap Reduction in Conjugated Polymers: the Role of Electron Rich Donor Heterocycles,” *J. Chem. Inf. Model.*, vol. 53, pp. 1689–1699, 2013.

[35] L. M. Kozycz, D. Gao, A. J. Tilley, and D. S. Seferos, “One donor-two acceptor (D-A1)-(D-A2) random terpolymers containing perylene diimide, naphthalene diimide, and carbazole units,” *J. Polym. Sci. Part A Polym. Chem.*, vol. 52, no. 23, pp. 3337–3345, 2014, doi: 10.1002/pola.27395.

[36] G. L. Gibson, T. M. McCormick, and D. S. Seferos, “Atomistic band gap engineering in donor-acceptor polymers,” *J. Am. Chem. Soc.*, vol. 134, no. 1, pp. 539–547, 2012, doi: 10.1021/ja208917m.

[37] J. Dhar, K. Swathi, D. P. Karothu, K. S. Narayan, and S. Patil, “Modulation of electronic and self-assembly properties of a donor-acceptor-donor-based molecular materials via atomistic approach,” *ACS Appl. Mater. Interfaces*, vol. 7, no. 1, pp. 670–681, 2015, doi: 10.1021/am506905b.

[38] S. C. Cevher *et al.*, "A comprehensive study: Theoretical and experimental investigation of heteroatom and substituent effects on frontier orbitals and polymer solar cell performances," *J. Polym. Sci.*, vol. 58, no. 19, pp. 2792–2806, 2020, doi: 10.1002/pol.20200513.

[39] Ö. Azeri *et al.*, "Efficient benzodithiophene and thienopyrroledione containing random polymers as components for organic solar cells," *Polymer (Guildf).*, vol. 133, pp. 60–67, 2017, doi: 10.1016/j.polymer.2017.11.024.

[40] S. Ghosh, P. B. Pati, and S. S. Zade, "Effect of the change of heteroatom on phenyl capped benzazole: Photophysical and electrochemical properties from the structural viewpoint," *J. Lumin.*, vol. 194, no. October 2017, pp. 164–169, 2018, doi: 10.1016/j.jlumin.2017.10.029.

[41] J. Hou *et al.*, "Bandgap and molecular energy level control of conjugated polymer photovoltaic materials based on benzo[l,2-b:4,5-b′]dithiophene," *Macromolecules*, vol. 41, no. 16, pp. 6012–6018, 2008, doi: 10.1021/ma800820r.

[42] X. L. Wong, M. L. Rahman, and M. S. Sarjadi, "Benzodichalcogenophene-based conjugated polymers as photo-voltaic materials," *Int. J. Electrochem. Sci.*, vol. 12, no. 7, pp. 6315–6339, 2017, doi: 10.20964/2017.07.76.

[43] P. Meti, H. H. Park, and Y. D. Gong, "Recent developments in pyrazine functionalized π-conjugated materials for optoelectronic applications," *J. Mater. Chem. C*, vol. 8, no. 2, pp. 352–379, 2020, doi: 10.1039/c9tc05014k.

[44] P. Meti, J. W. Yang, S. H. Jung, and Y. D. Gong, "Synthesis, characterization and optoelectronic properties of pyrrolopyrazine based Y-shaped color-tunable dipolar molecules," *Dye. Pigment.*, vol. 161, no. September 2018, pp. 470–481, 2019, doi: 10.1016/j.dyepig.2018.09.082.

[45] P. B. Pati, "Benzazole (B, N, O, S, Se and Te) based D-A-D type oligomers: Switch from electropolymerization to structural aspect," *Org. Electron.*, vol. 38, pp. 97–106, 2016, doi: 10.1016/j.orgel.2016.07.035.

[46] E. Lee, W. Shin, O. Bae, F. S. Kim, and Y. J. Hwang, "Synthesis and Characterization of a highly crystalline benzotriazole-selenophene copolymer semiconductor," *Polymer (Guildf).*, vol. 184, no. July, p. 121856, 2019, doi: 10.1016/j.polymer.2019.121856.

[47] S. Kutkan, S. Goker, S. O. Hacioglu, and L. Toppare, "Syntheses, electrochemical and spectroelectrochemical characterization of benzothiadiazole and benzoselenadiazole based random copolymers," *J. Macromol. Sci. Part A Pure Appl. Chem.*, vol. 53, no. 8, pp. 475–483, 2016, doi: 10.1080/10601325.2016.1189280.

[48] Z. Huang, S. Wang, R. D. Dewhurst, N. V. Ignat'ev, M. Finze, and H. Braunschweig, "Boron: Its Role in Energy-Related Processes and

Applications," *Angew. Chemie - Int. Ed.*, vol. 59, no. 23, pp. 8800–8816, 2020, doi: 10.1002/anie.201911108.

[49] T. Baumgartner and F. Jäkle, *Main Group Strategies towards Functional Hybrid Materials*. 2017.

[50] A. Fukazawa and S. Yamaguchi, "Ladder π-conjugated materials containing main-group elements," *Chem. - An Asian J.*, vol. 4, no. 9, pp. 1386–1400, 2009, doi: 10.1002/asia.200900179.

[51] S. K. Mellerup and S. Wang, "Boron-Doped Molecules for Optoelectronics," *Trends Chem.*, vol. 1, no. 1, pp. 77–89, 2019, doi: 10.1016/j.trechm.2019.01.003.

[52] F. Liu, Z. Ding, J. Liu, and L. Wang, "An organoboron compound with a wide absorption spectrum for solar cell applications," *Chem. Commun.*, vol. 53, no. 90, pp. 12213–12216, 2017, doi: 10.1039/c7cc07494h.

[53] C. Dou, J. Liu, and L. Wang, "Conjugated polymers containing B←N unit as electron acceptors for all-polymer solar cells," *Sci. China Chem.*, vol. 60, no. 4, pp. 450–459, 2017, doi: 10.1007/s11426-016-0503-x.

[54] H. Kobayashi, *Encyclopedia of Polymeric Nanomaterials*. 2015.

[55] M. Miyata and Y. Chujo, "π-Conjugated organoboron polymer as an anion sensor," *Polym. J.*, vol. 34, no. 12, pp. 967–969, 2002, doi: 10.1295/polymj.34.967.

[56] F. Jäkle, "Advances in the synthesis of organoborane polymers for optical, electronic, and sensory applications," *Chem. Rev.*, vol. 110, no. 7, pp. 3985–4022, 2010, doi: 10.1021/cr100026f.

[57] J. Huang and Y. Li, "BN embedded polycyclic π-conjugated systems: Synthesis, optoelectronic properties, and photovoltaic applications," *Front. Chem.*, vol. 6, no. AUG, pp. 1–22, 2018, doi: 10.3389/fchem.2018.00341.

[58] D. L. Crossley *et al.*, "Enhancing electron affinity and tuning band gap in donor-acceptor organic semiconductors by benzothiadiazole directed C-H borylation," *Chem. Sci.*, vol. 6, no. 9, pp. 5144–5151, 2015, doi: 10.1039/c5sc01800e.

[59] D. L. Crossley *et al.*, "Post-polymerization C-H Borylation of Donor-Acceptor Materials Gives Highly Efficient Solid State Near-Infrared Emitters for Near-IR-OLEDs and Effective Biological Imaging," *ACS Appl. Mater. Interfaces*, vol. 9, no. 34, pp. 28243–28249, 2017, doi: 10.1021/acsami.7b08473.

[60] C. Y. Kuo *et al.*, "Effect of side-chain architecture on the optical and crystalline properties of two-dimensional polythiophenes," *Macromolecules*, vol. 46, no. 15, pp. 5985–5997, 2013, doi: 10.1021/ma4007945.

[61] Y. Li *et al.*, “Synthesis of B←N embedded indacenodithiophene chromophores and effects of bromine atoms on photophysical properties and energy levels,” *Tetrahedron*, vol. 74, no. 32, pp. 4308–4314, 2018, doi: 10.1016/j.tet.2018.06.035.

[62] H. Akpinar, A. Balan, D. Baran, E. K. Ünver, and L. Toppare, “Donor-acceptor-donor type conjugated polymers for electrochromic applications: Benzimidazole as the acceptor unit,” *Polymer (Guildf).*, vol. 51, no. 26, pp. 6123–6131, 2010, doi: 10.1016/j.polymer.2010.10.045.

[63] H. Yu *et al.*, “Side-chain engineering of green color electrochromic polymer materials: Toward adaptive camouflage application,” *J. Mater. Chem. C*, vol. 4, no. 12, pp. 2269–2273, 2016, doi: 10.1039/c6tc00197a.

[64] X. Song, M. Wang, L. Kong, and J. Zhao, “Effects of the acceptor pattern and substitution position on the properties of N-phenyl-carbazolyl based donor-acceptor-donor molecules,” *RSC Adv.*, vol. 7, no. 30, pp. 18189–18198, 2017, doi: 10.1039/c7ra01449j.

[65] A. Tanimoto and T. Yamamoto, “Nickel-2,2′-bipyridyl and palladium-triphenylphosphine complex promoted synthesis of new π-conjugated poly(2-hexylbenzotriazole)s and characterization of the polymers,” *Adv. Synth. Catal.*, vol. 346, no. 13–15, pp. 1818–1823, 2004, doi: 10.1002/adsc.200404227.

# APPENDICES

## A. NMR Data

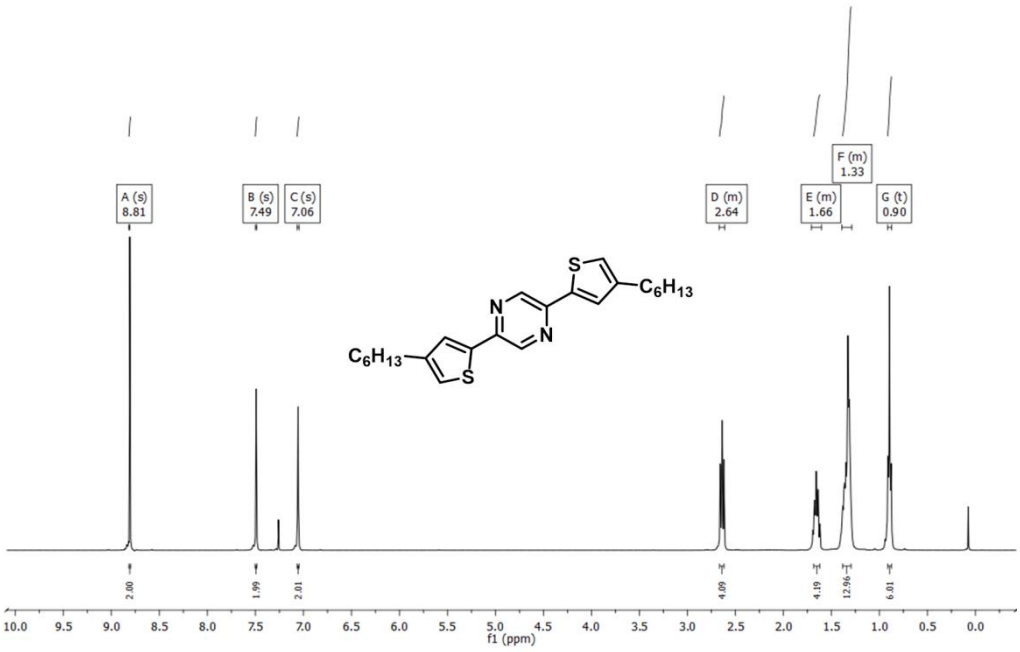


**Figure A..1.** $^{1}$H NMR of 2,5-di(3-hexylthiophen-2-yl)pyrazine

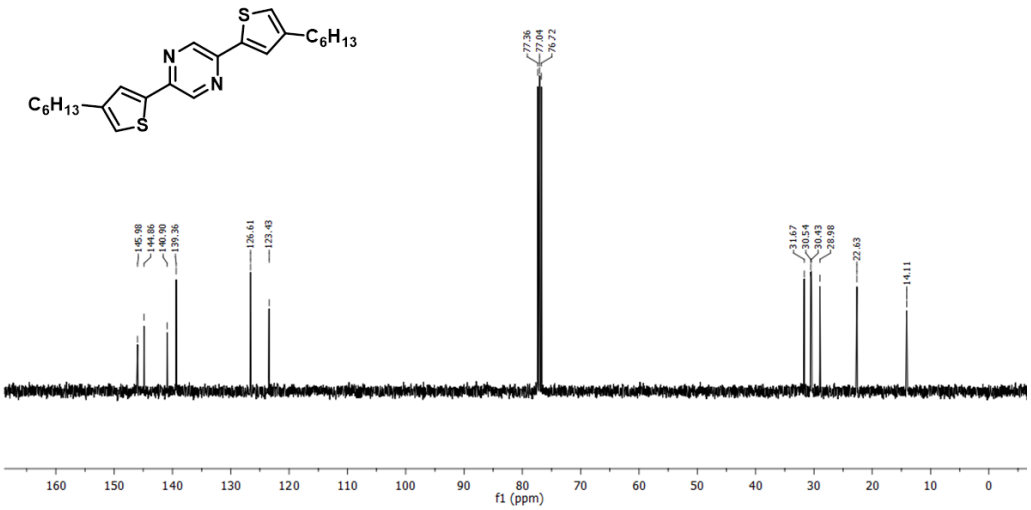


**Figure A.2.** $^{13}$C NMR of 2,5-di(3-hexylthiophen-2-yl)pyrazine

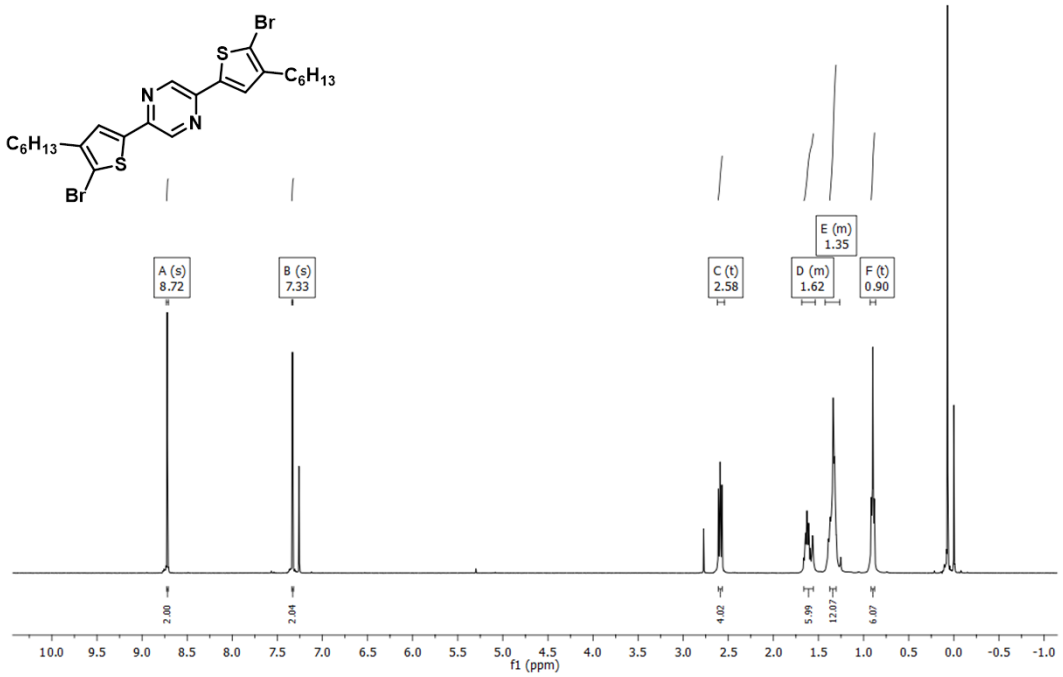


**Figure A.3.** $^{1}$H NMR of 2,5-bis-(5-bromo-4-hexylthiophen-2-yl)pyrazine

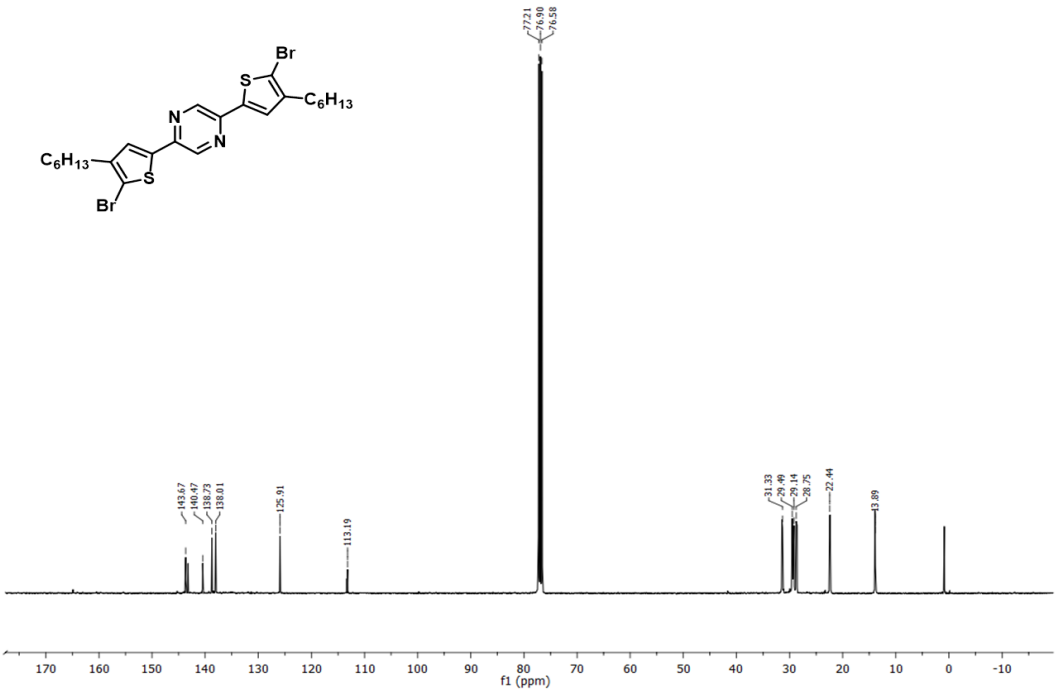


**Figure A.4.** $^{13}$C NMR of 2,5-bis-(5-bromo-4-hexylthiophen-2-yl)pyrazine

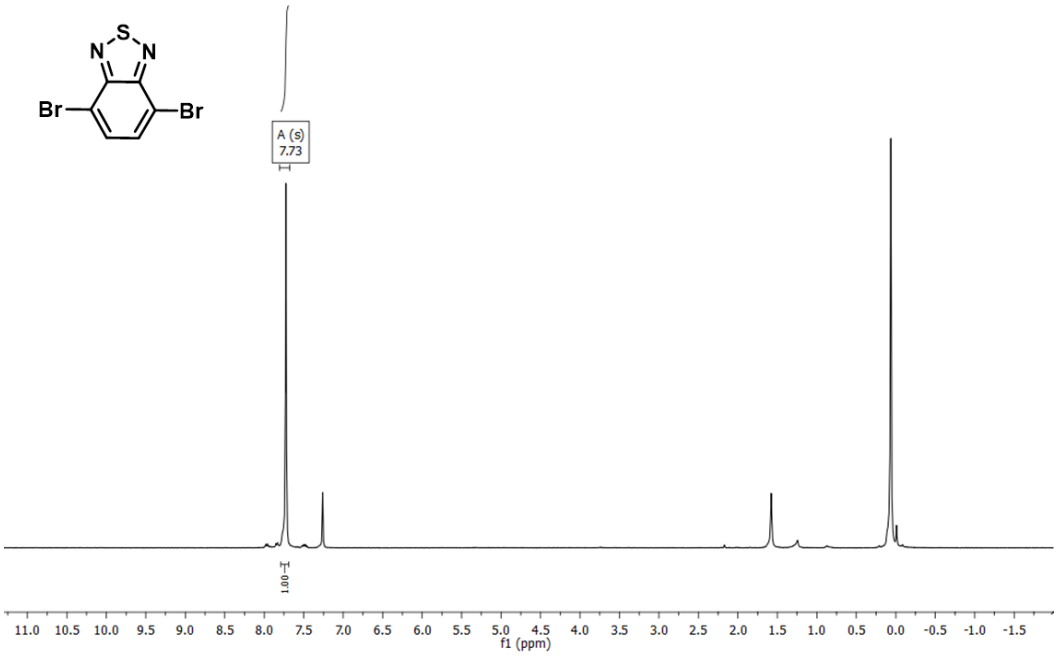


**Figure A.5.** $^{1}$H NMR of 4,7-dibromobenzo[*c*][1,2,5]thiadiazole

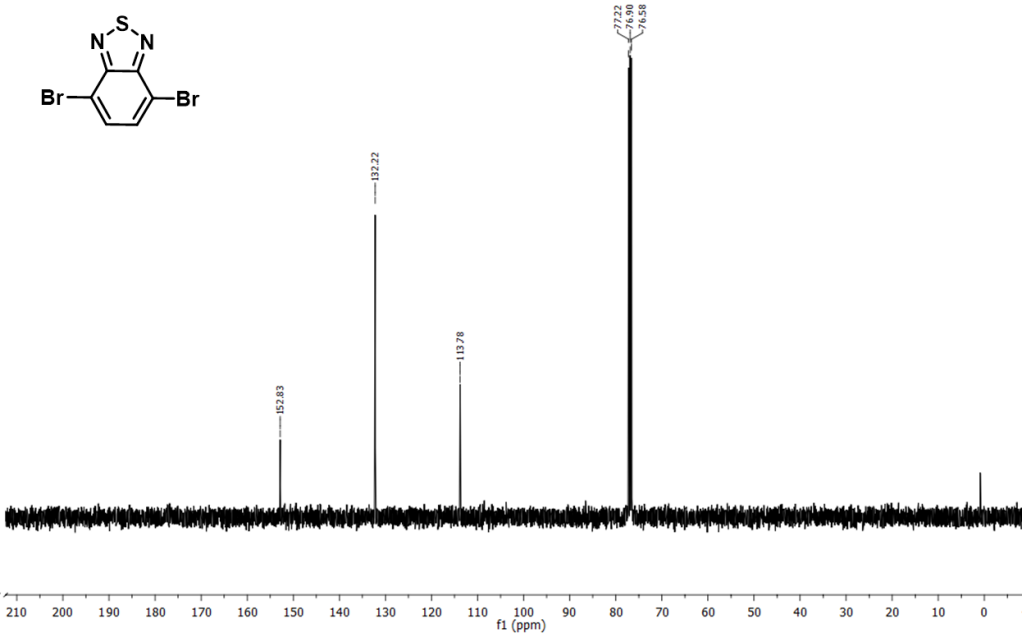


**Figure A.6.** $^{13}$C NMR of 4,7-dibromobenzo[*c*][1,2,5]thiadiazole

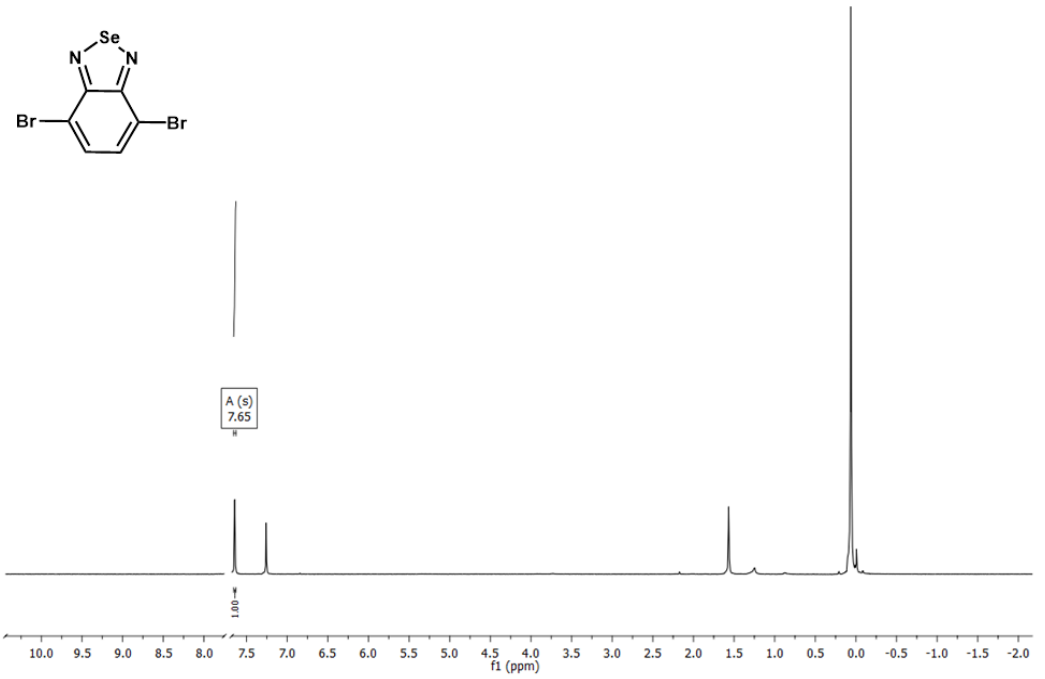


**Figure A.7.** $^{1}$H NMR of 4,7-dibromobenzo[*c*][1,2,5]selenadiazole

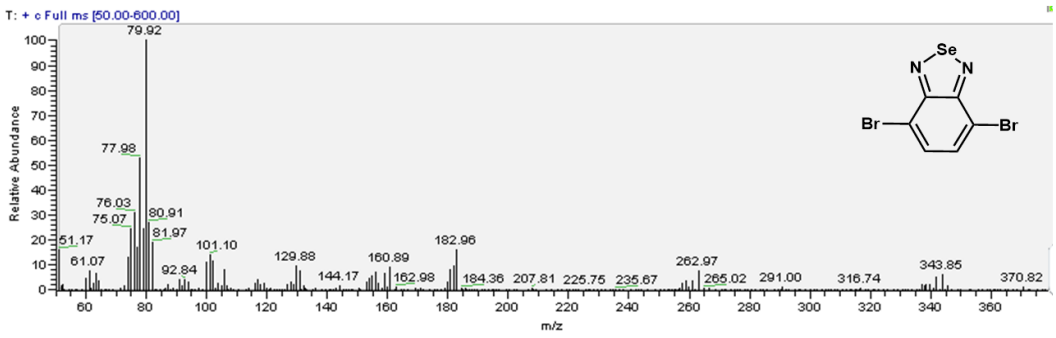


**Figure A.8.** GC-MS result of 4,7-dibromobenzo[*c*][1,2,5]selenadiazole

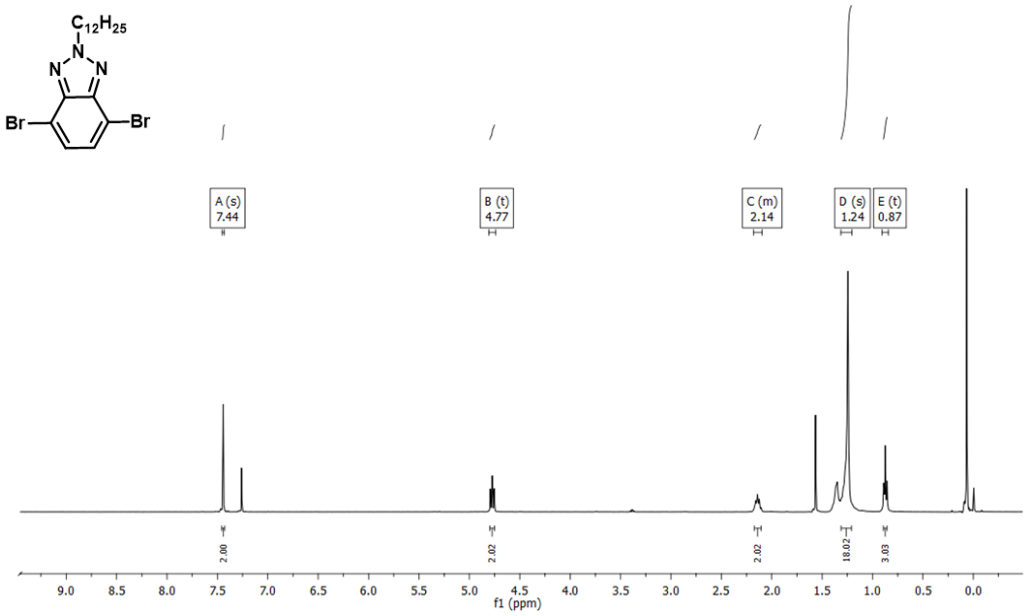


**Figure A.9.** [1]H NMR of 4,7-dibromo-2-dodecyl-2H-benzo[*d*][1,2,3]triazole

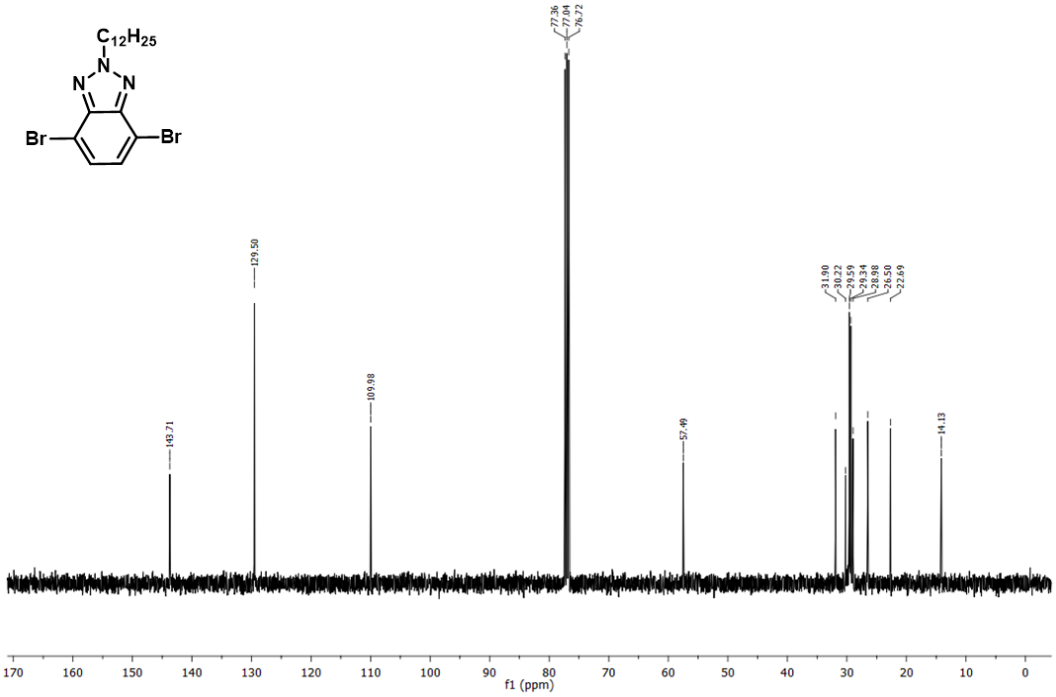


**Figure A.10.** [13]C NMR of 4,7-dibromo-2-dodecyl-2H-benzo[*d*][1,2,3]triazole

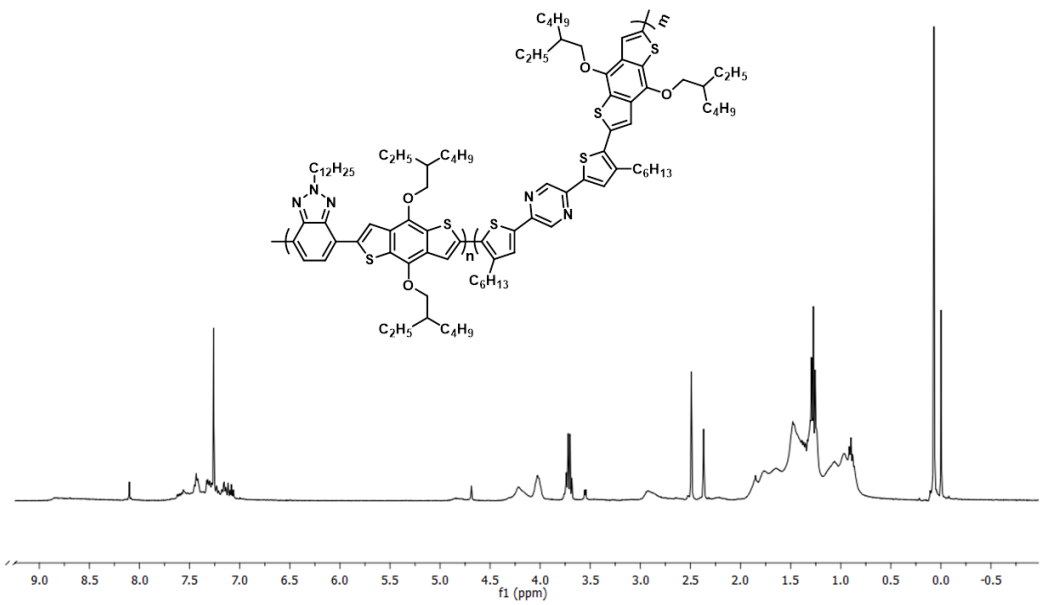


**Figure A.11.** $^{1}$H NMR of **RP1**

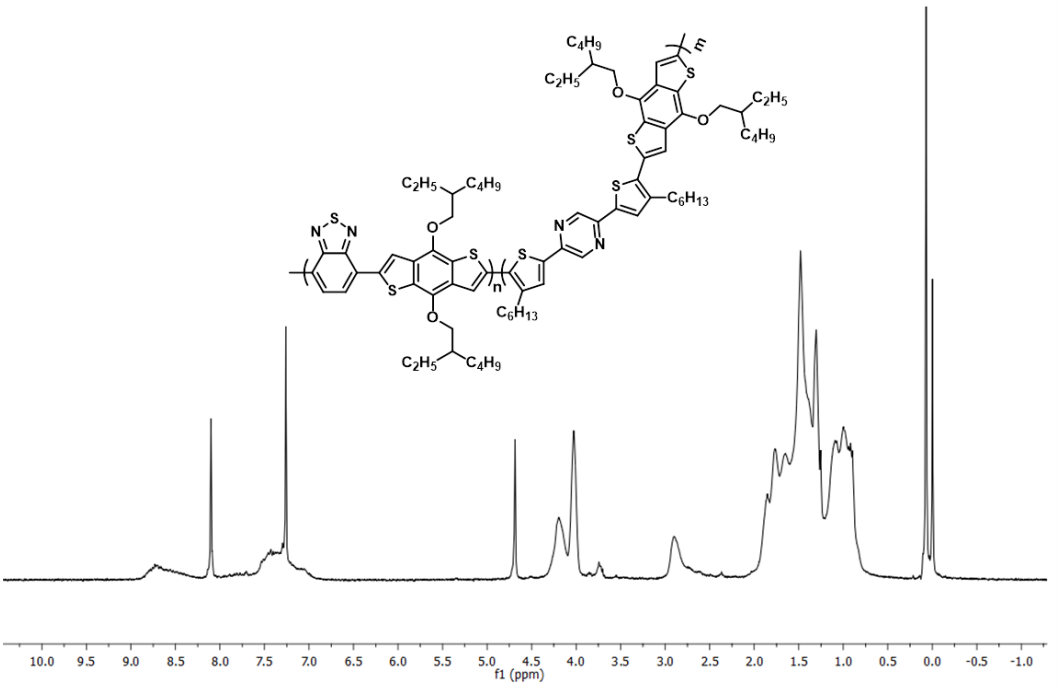


**Figure A.12.** $^{1}$H NMR of **RP2**

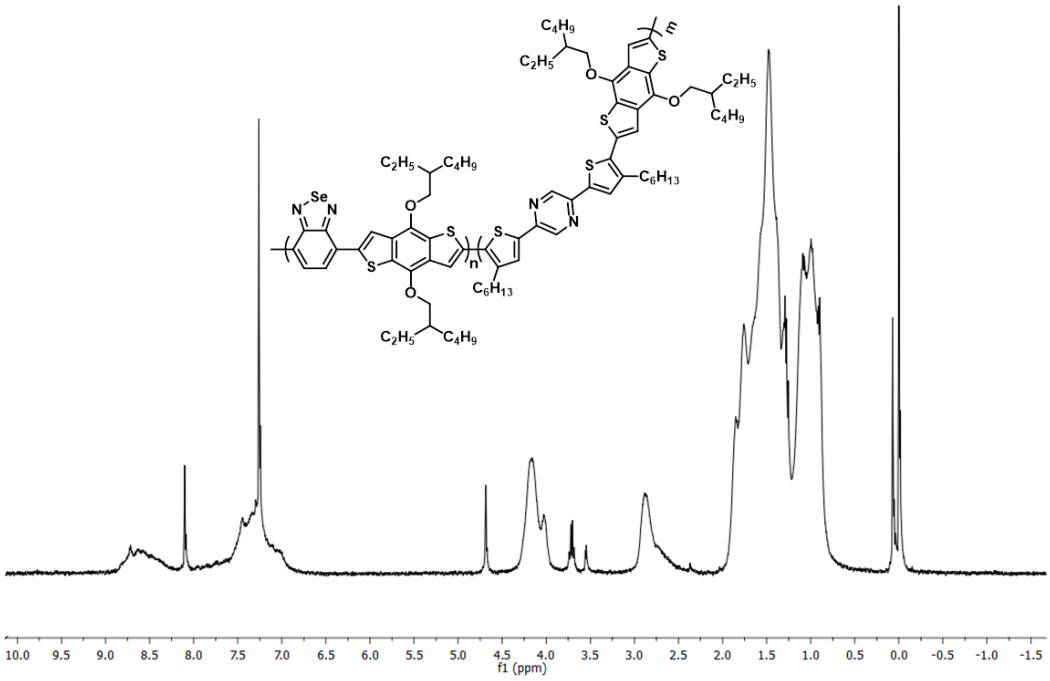


**Figure A.13.** $^{1}$H NMR of **RP3**

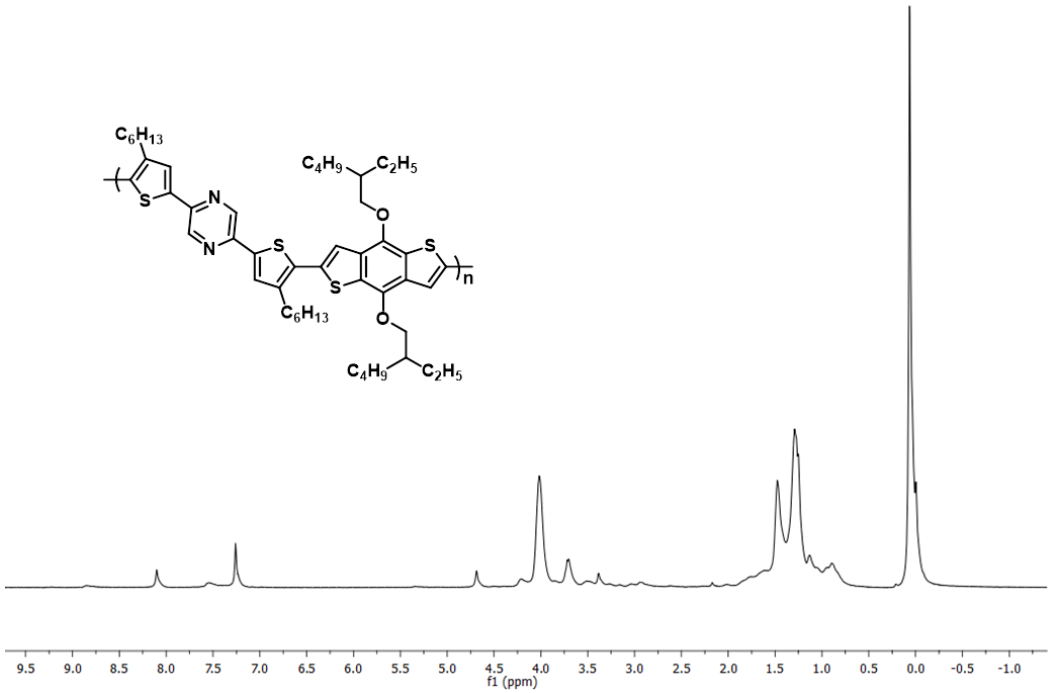


**Figure A.14.** $^{1}$H NMR of **P1A**

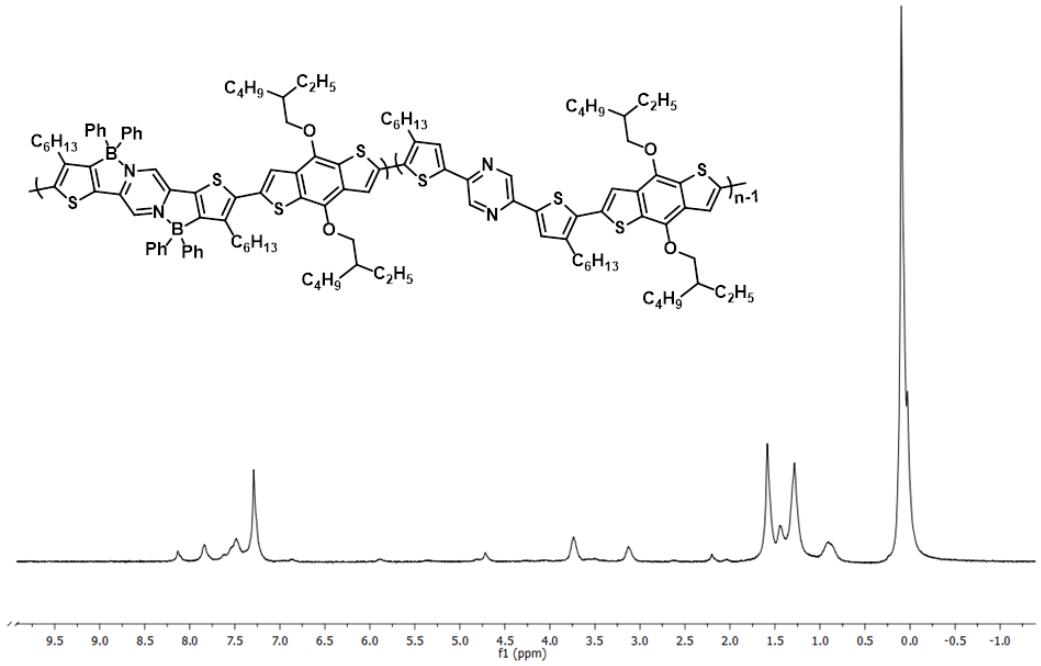


**Figure A.15.** $^{1}$H NMR of **P1B**

## B. Thermal Analyses Results

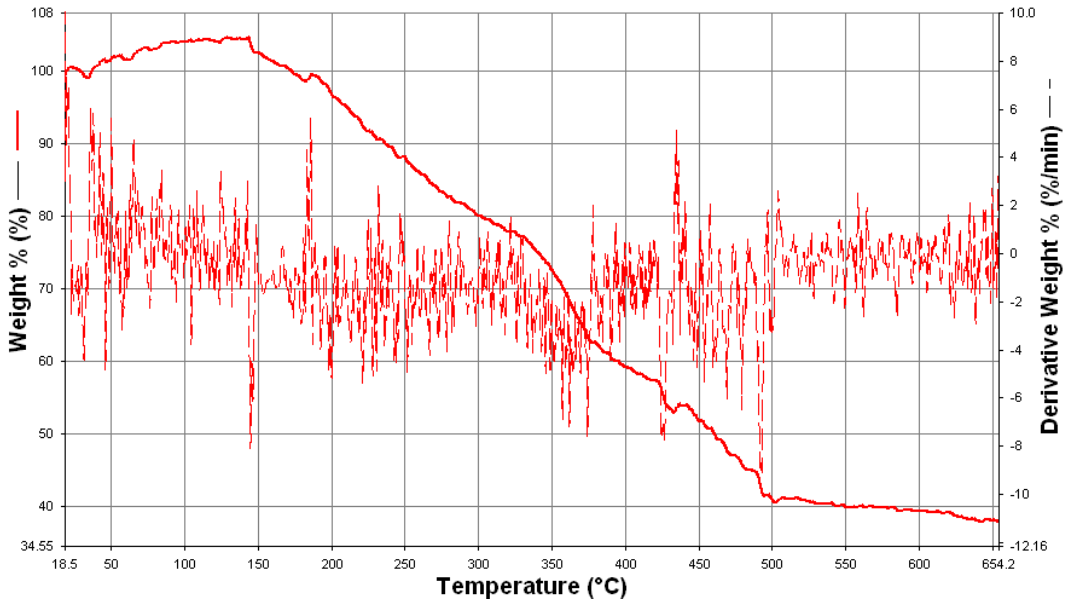


**Figure B.1.** Thermal analysis result obtained from TGA for **RP1**

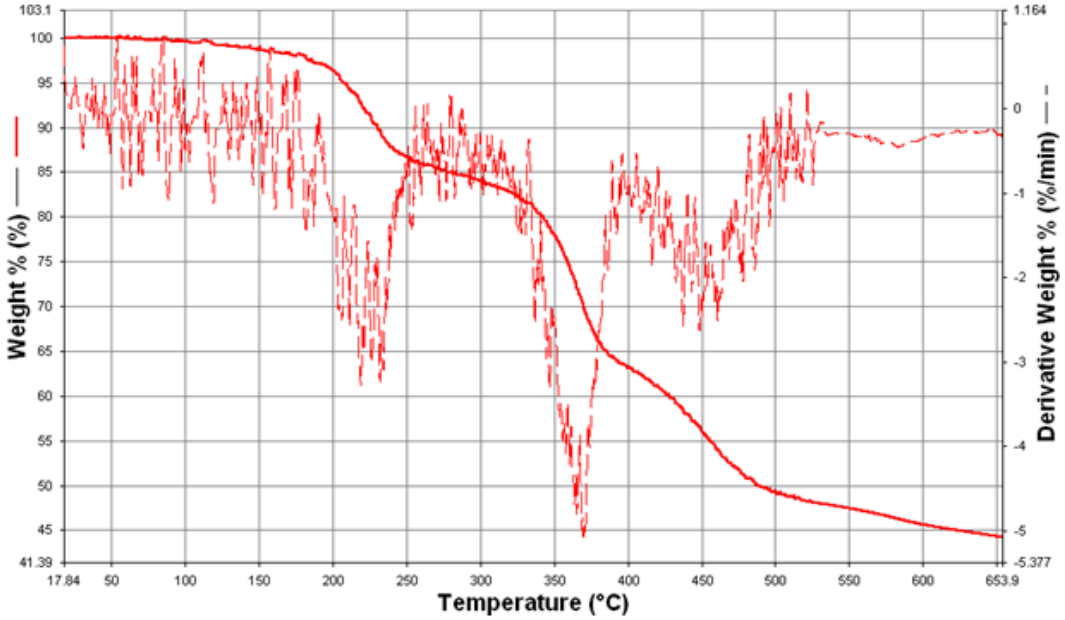


**Figure B.2.** Thermal analysis result obtained from TGA for **RP2**

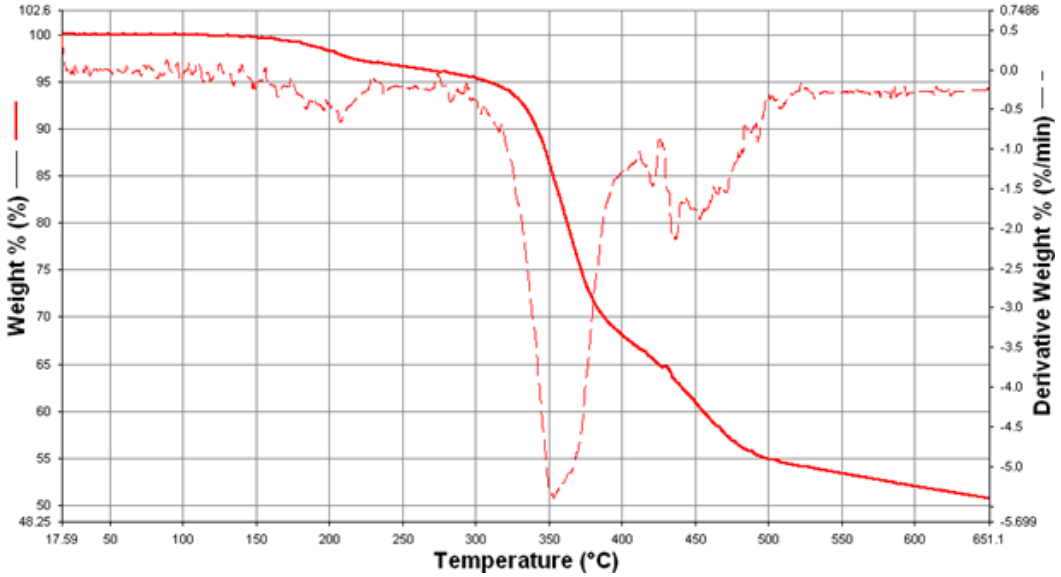


**Figure B.3.** Thermal analysis result obtained from TGA for **RP3**

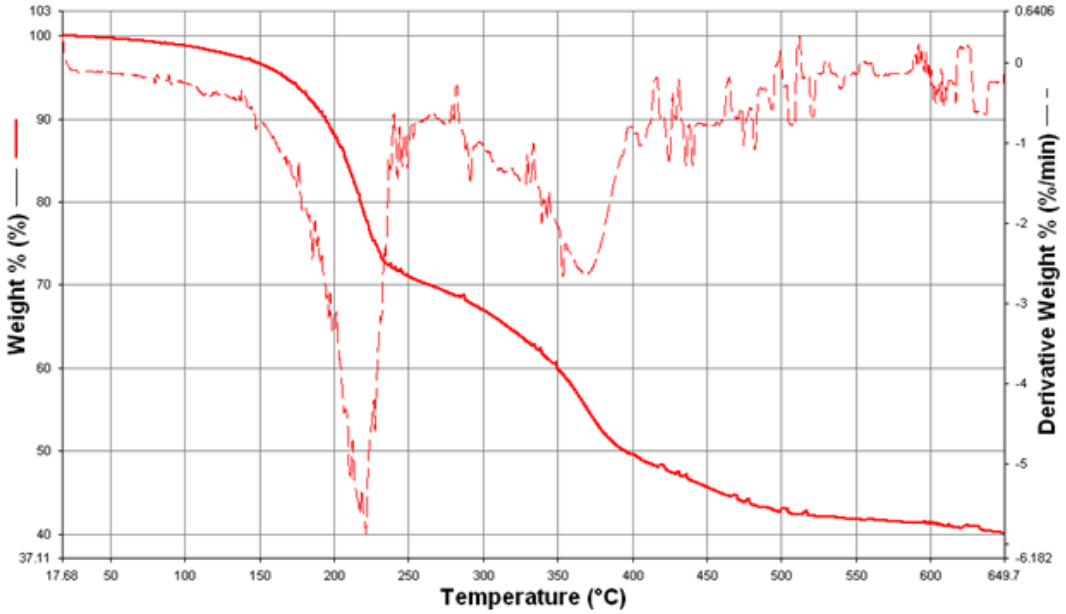


**Figure B.4.** Thermal analysis result obtained from TGA for **P1A**

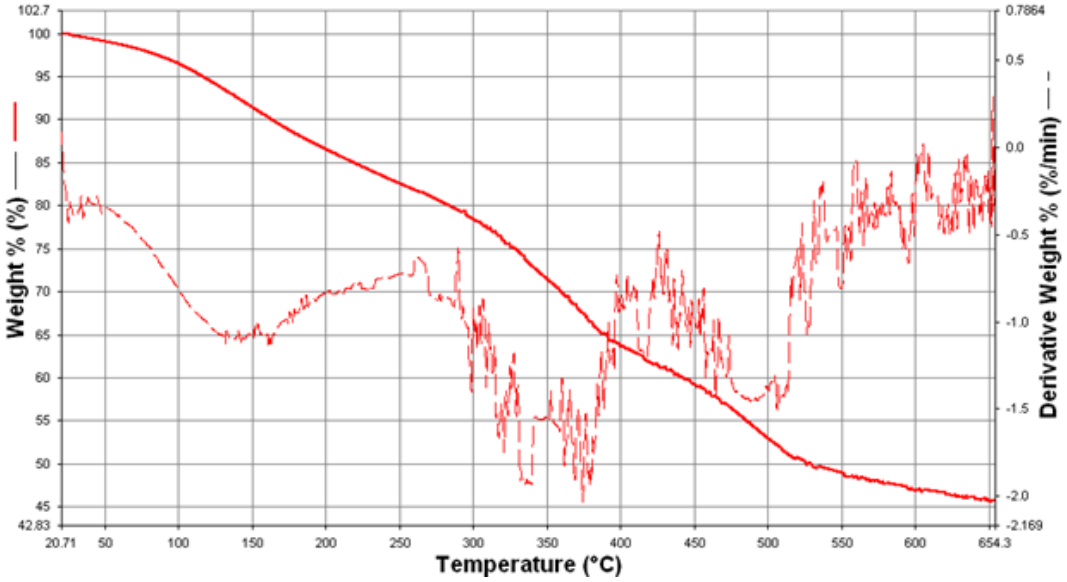


**Figure B.5.** Thermal analysis result obtained from TGA for **P1B**

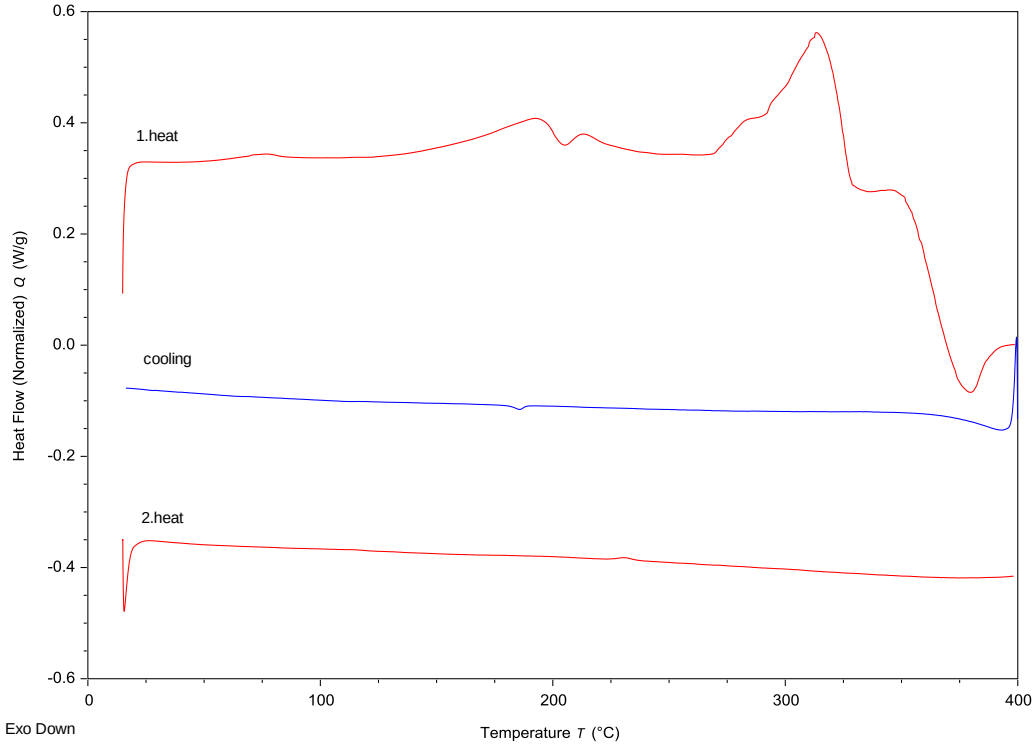


**Figure B.6.** Thermal analysis result obtained from DSC for **RP1**

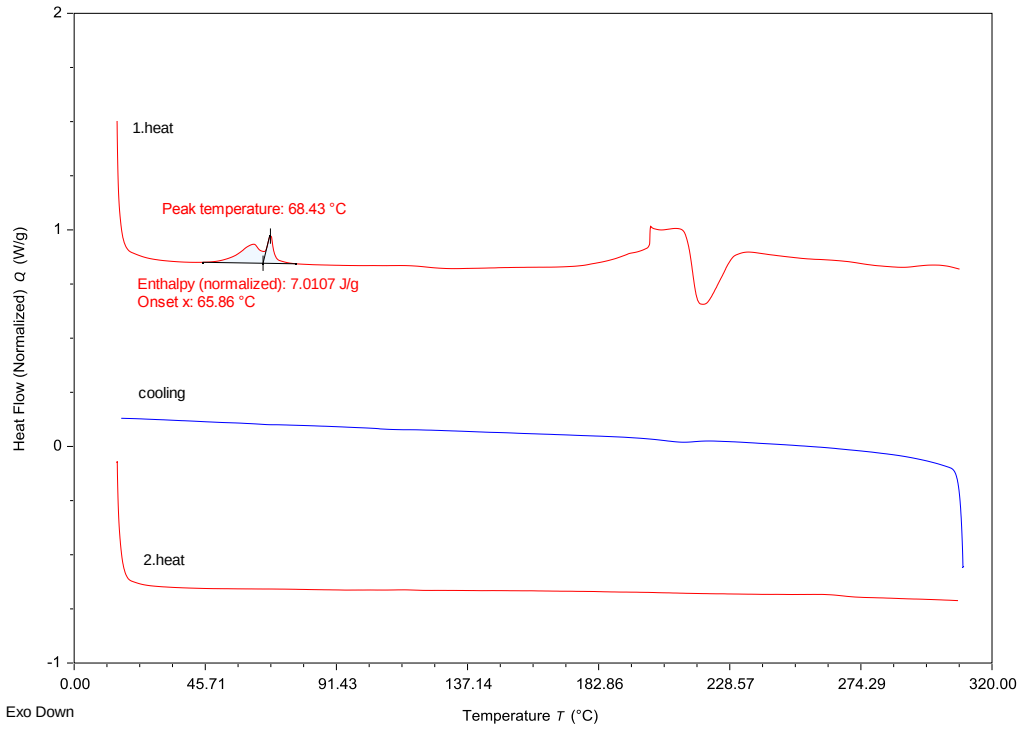


**Figure B.7.** Thermal analysis result obtained from DSC for **RP2**

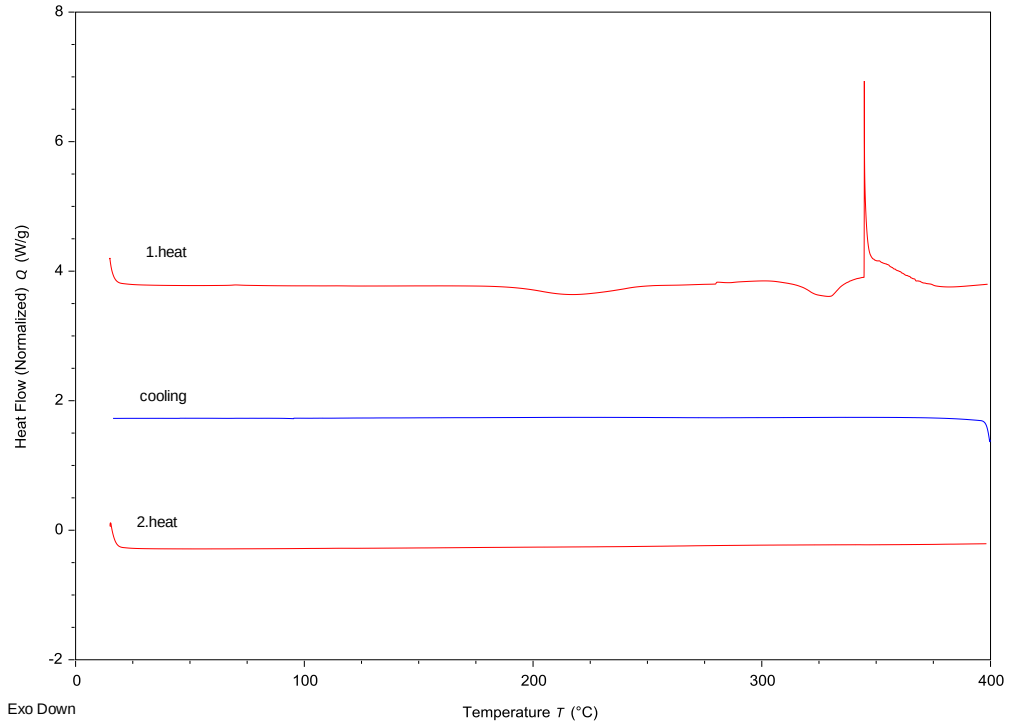


**Figure B.8.** Thermal analysis result obtained from DSC for **RP3**

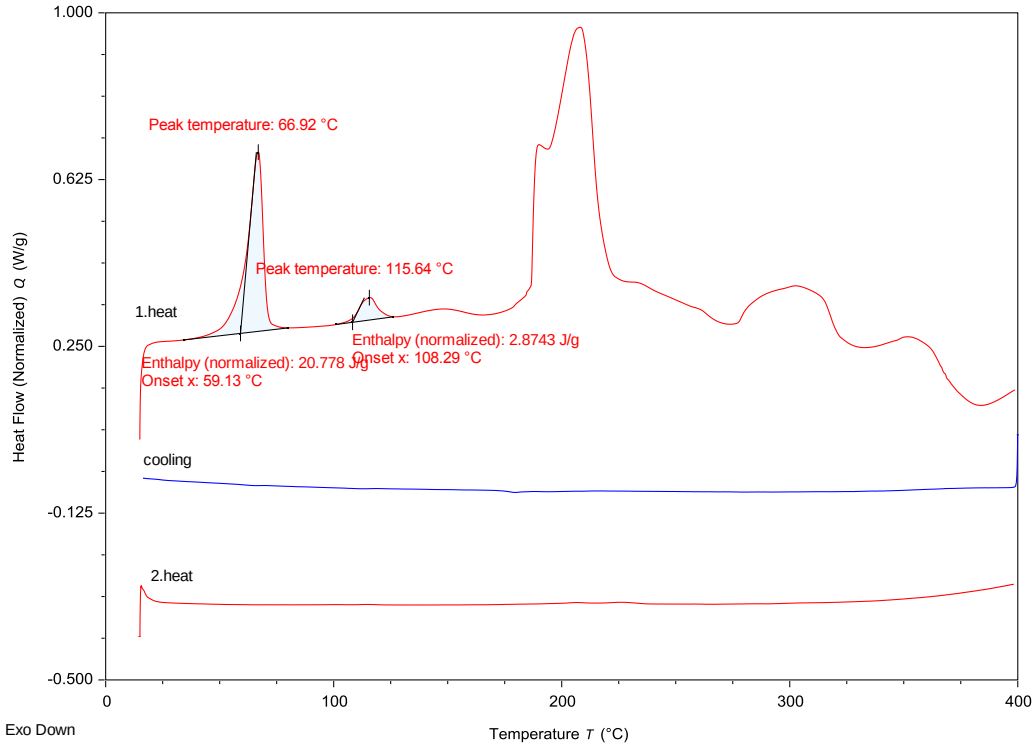


**Figure B.9.** Thermal analysis result obtained from DSC for **P1A**

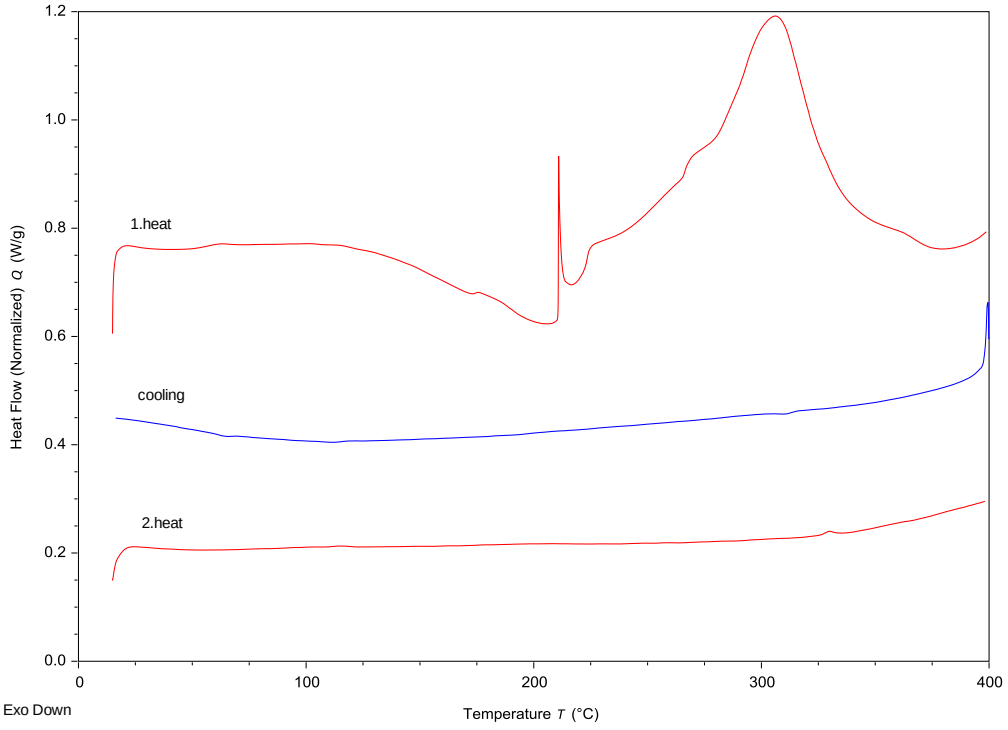


**Figure B.10.** Thermal analysis result obtained from DSC for **P1B**